Synthesis and characterization of metallic and functionalized nanoparticles of copper, zinc, silver and iron and their polymer composites for biomedical applications

Ummul Khair Fatema

September 2016

Synthesis and characterization of metallic and functionalized nanoparticles of copper, zinc, silver and iron and their polymer composites for biomedical applications

A Dissertation Submitted to University of Dhaka for the Partial Fulfillment of the Requirements of the Degree of Doctor of Philosophy in Chemistry

Submitted by

Ummul Khair Fatema

Registration No. 187

Session: 2009-2010

Re-registration No. 67

Session: 2014-2015

DEPARTMENT OF CHEMISTRY

PHYSICAL CHEMISTRY RESEARCH LABORATORY

University of Dhaka

Dhaka-1000, Bangladesh

September 2016

Dedicated

to

My son – my life– cosmos in the miniature

My husband– for always being there for me

My parents – for providing me with the opportunity to pursue my research and support me always

My supervisors – for their continuous dedication and valuable discussionthroughout

Acknowledgements

I would like to express my sincere gratitude and appreciation to my supervisor **Professor Dr. Md. Abu Bin Hasan Susan**, Department of Chemistry, University of Dhaka, for his scholastic supervision, keen interest, constructive suggestions and continual guidance throughout the research work and his emendation of the manuscript without which the present research work might not have been completed. I sincerely owe to him for giving me an opportunity to work in close association with him.

I am also grateful to my respected supervisor **Professor Dr. M. MuhiburRahman**, Academic Innovation Fund Management Specialist, University Grants Commission of Bangladeshfor his valuable comments, advice and kind assistance during experiments. Hispositive interest, guidance, encouragementwere true inspiration for me.

I am indebted to **Professor Dr. M. Yousuf Ali Mollah**, Member, University Grants Commission of Bangladesh for his valuable and sagacious advice and kind assistance for solving various problems related to research experiments. His patience, guidance, encouragement were like a tonic, inspiration and moral support throughout this work.

I sincerely express my gratitude to **Associate ProfessorDr. Md. Mominul Islam** and **Associate ProfessorDr.Muhammed Shah Miran**,Department of Chemistry, University of Dhaka for their valuable comments, friendly collaboration, invaluable suggestions which helped me to resolve critical points related to this research work. Special thank goes to **Dr. Saika Ahmed**, Lecturer, Department of Chemistry, University of Dhaka for her vivid and friendly helpful attitude to my research work.I am also grateful to **Associate Professor Dr. Md. Rakibul Islam,** Department of Biochemistry and Molecular Biology, University of Dhaka for hiscollaboration, prompt response and friendly suggestions.

I sincerely acknowledge friendly and invaluable helpsof the members of Material Chemistry Research Laboratory. My efforts would have been fruitless without their relentless help towards me whenever I required them. I wish to express my heartfelt thanks to all the teachers and students of Physical Chemistry section of the Department for their cooperation.

I gratefully acknowledge support from the sub project (CP-231) of the Higher Education Quality Enhancement Project of the University Grants Commission of Bangladesh financed by World Bank and the Government of Bangladesh.I gratefully express my sincere thanks to the Ministry of Science and Technology, Bangladesh for Bangabandhu Ph.D. Fellowship.

I am thankful to my husband Md. Mominur Rahman and son Aayan Muhtasim Rahman for their continuous moral support. I am grateful to my parents without whose support this work could not be done at all. My keen gratitude is also for all the other family members and well-wishers for their encouragement.

(Ummul Khair Fatema)

Declaration

Experiments described in this thesis were carried out by the author of this thesis in the Department of Chemistry, University of Dhaka, Dhaka-1000, Bangladesh. This work has not been presented, and will not be presented for any other degree.

Prof. Dr. Md. Abu Bin Hasan Susan
Department of Chemistry
University of Dhaka
Dhaka-1000
Bangladesh
Ph.D. Supervisor

Prof. Dr. M. MuhiburRahman
AIF Management Specialist
(HEQEP)
University Grants Commission
ofBangladesh, 29/1 Agargaon,
Sher-E-Bangla Nagar, Dhaka-
1207, Bangladesh
Ph.D. Co-Supervisor

Ummul Khair Fatema
Department of Chemistry
University of Dhaka
Dhaka-1000
Bangladesh
Author (Ph.D. Student)

Abstract

Series of water in oil (w/o) microemulsions of cationic, anionic and nonionic surfactants were prepared in a wide range of compositions by varying different parameters related to the preparation of microemulsionsincluding nature and concentration of surfactant, water to surfactant molar ratio andamount and chain length of cosurfactant. The influence of these parameters on the formation of microemulsionsand the size of microemulsion droplets have been discussed in detail. The potentials of these microemulsion droplets as nanoreactors for reactions within restricted geometries have been explored. Themicroemulsions have been used for preparation of different metal and functionalized metal nanoparticlesand metal nano/polymer composites with controllable size. Efforts have been made to correlatedifferent parameters with the sizes of microemulsion droplets andalso the sizes of nanoparticles prepared in these systems.Special emphasis has been given onthe understanding of the template role of microemulsion droplets to control over the size of nanoparticles.Finally, the antibacterial activity of different metallic and functionalized nanoparticles and their polymer composites has been investigated.

The size and size distributions of microemulsion droplets have been studied by dynamic light scattering (DLS) measurements. The size of the microemulsion droplets has been found to be dependent on the nature of the surfactant.The average size is affected by water to surfactant ratio and surfactant concentration. Addition of cosurfactant couldalso modulate the dimensions of microemulsion droplets. Increasing the amount and chain length of cosurfactant resulted in relatively smaller microemulsions.

Four metallic nanoparticles, copper (Cu), zinc (Zn), silver(Ag) and iron(Fe)were synthesized by reduction of corresponding metal salts in different microemulsions.Nanoparticles with varyingsize could be synthesized by the manipulation of different components of microemulsions. DLS results showed that nanoparticles of varying size could be prepared in microemulsions of different surfactants with the same composition. The size of nanoparticles was governed by the hydrophilic–lipophilic balance(HLB) and rigidity of the surfactant. The average size of nanoparticles was affected by water to surfactant ratio and surfactant concentration. Cosurfactant acted as a key factor in regulating the dimensions of nanoparticles. Increasing the concentration and

chain length of cosurfactant resulted in relatively smaller nanoparticles. In most of these cases there was a concomitant relation between the size of nanoparticles and microemulsion droplets. Antibacterial activity of the nanoparticles against Gram-negative *Escherichia coli* (*E. coli*) and Gram-positive *Staphylococcus aureus* (*S. aureus*) were tested by zone of inhibition method. The nanoparticles showed antibacterial activity against *E. coli* and *S. aureus* at very low concentrations. Ag nanoparticles showed higher antibacterial activities compared to other nanoparticles. At high concentrations, Ag and Cu nanoparticles showed sensitivity comparable to conventional antibiotics against *E. coli*. However the concentration dependence on antibacterial activity has been less pronounced.

Functionalized nanoparticles, Fe_3O_4@Ag were prepared by reducing silver nitrate on the surface of Fe_3O_4 nanoparticles inw/omicroemulsions. Two polymer composites, Ag/polyaniline (Ag/PAni) nanocomposite and Ag/poly(vinyl alcohol) (Ag/PVA) nanocomposite film were also successfully prepared using w/o microemulsion. For the preparation of Ag/PAninanocompositesin w/o microemulsion, chemical oxidative polymerization of aniline monomer by ammonium peroxydisulfate in preformed Ag nanoparticles (prepared by the reduction of metal salts in microemulsion) was carried out. For a comparative studypure PAni was also prepared by using w/o microemulsionand aqueous solution method.For the preparation of Ag/PVA nanocomposite film reduction of metal salt was carried out in the core of w/o microemulsion droplet containing PVA polymeric matrix. Ag/PVA nanocomposite film was then prepared by solution casting method after separation from the microemulsion. For a comparison Ag/PVA film was also prepared through *in situ* generation of Ag nanoparticles by chemical reduction process on PVA host without using microemulsion. For optical, structural and morphological characterization of these nanoparticles and composites UV-visible spectra, Fourier transform infrared spectra andscanning electron microscopic (SEM) images were taken.DLS measurements gave size and size distribution of nanoparticles. Thermogravimetric analysis was carried out to study the thermal stability of nanocomposites. Finally, the antibacterial activity of these functionalized nanoparticles and polymer composites was evaluated by zone of inhibition method.

DLS showed that Fe_3O_4@Ag particles innanodimensionwas formed.SEM images revealed spherical morphology of the functionalized nanoparticles and showed uniform coating of Ag around Fe_3O_4. The antibacterial testresults showed pronounced antibacterial performance ofFe_3O_4@Ag nanoparticles against *E. coli* and *S. aureus* because of synergistic antibacterial effect of Fe_3O_4 and Ag nanoparticles.

In w/o microemulsion it was possible to prepare PAninanoparticles which was smaller in size compared to that obtained from bulk.But thermal stability of thesePAni from microemulsionwas lower than PAni from bulk synthesis because of less conjugation in PAni chain prepared in microemulsion. In comparison with PAni from microemulsion,Ag/PAninanocomposites showed somewhat better thermal stability which is attributed to interactions of Ag nanoparticles with PAni chain. The antibacterial test resultsdemonstrated that Ag/PAninanocomposites have enhanced antibacterial efficiency compared to PAni generated in microemulsion which is more efficient than PAni from aqueous synthesis.

Ag/PVA nanocomposite film with high concentration of Ag nanoparticles wassuccessfully prepared using w/omicroemulsion.In this approach the presence of polymeric matrix in the droplets of microemulsion ensured uniform and homogeneous distribution with smaller Ag nanoparticles which also prevented aggregation of nanoparticles even after separation from microemulsion. The uniform dispersity could be achieved at high Ag content whereas conventional *in situ*generation of Ag nanoparticles by chemical reduction process on PVA host gave agglomerated particles. As prepared Ag/PVA nanocomposite film has higher thermal stability than that prepared from bulk synthesis. The antibacterial properties of Ag/PVA films against *E. coli* and *S. aureus* showed that the as synthesized Ag/PVA nanocomposite film has enhanced antibacterial efficacy compared to that generated through *in situ* synthesis without using microemulsion under the same test condition.This methodology is advantageous than *in situ*approach of Ag/PVA film formationwithout using microemulsionsince the template role of microemulsion in combination with PVA nanoreactor provide homogeneous and

uniform distribution of Ag nanoparticles which enable controlled leaching of nanoparticles making the film effective bactericide.

Thusitis possible to fine-tune the droplet-size in the microemulsionsby the proper selection of composition of microemulsionsand hencethismicroemulsion method iseffective and advantageous to synthesize metallic nanoparticles, functionalizednanoparticles and metal nano/polymer composites of precisely controlled sizefor efficiently use as antibacterial agents.

Title of the thesis:

Synthesis and characterization of metallic and functionalized nanoparticles of copper, zinc, silver and iron and their polymer composites for biomedical applications

Submitted by:

UmmulKhairFatema, Ph.D. Student, Department of Chemistry, University of Dhaka

The General description and outline of this thesis are given below:

Chapter 1: Introduction

Chapter 1 describes the necessity and objective of the present research.

Chapter 2:Droplet sizes in water in oil microemulsions and their correlation with microemulsion variables

Chapter 2 presents the roles of different parameters of water in oil (w/o) microemulsions such as surfactant, water content and cosurfactant on the formation of microemulsions and their effects on the size of microemulsion droplets.The size and size distribution of microemulsion droplets have been measured by dynamic light scattering (DLS) measurements. It has been observed that different surfactants result in the formation of microemulsions of varying size. The average size is affected by water to surfactant ratio and surfactant concentration. Addition of cosurfactant can modulate the dimensions of microemulsion droplets. Concentration and chain length of cosurfactanthave also impact on the size of microemulsion droplets. Thus it is possible to fine-tune the composition of microemulsions to obtain microemulsion droplets of desirable dimension.

Chapter 3: Preparation of metal nanoparticles in water in oil microemulsions with controllable dimension and their antibacterial properties

Chapter 3 discusses aboutthe correlation between the sizes of microemulsion droplets and nanoparticles prepared in microemulsions. The effects of various size controlling parameters (surfactant, water content and cosurfactant)of microemulsions on the size of metal nanoparticles, copper (Cu), zinc (Zn), silver(Ag) and iron(Fe) prepared in these systems have been discussed. It could beclearly shown that the size of nanoparticles were dependent upon the types of surfactantand the surfactant and cosurfactant concentration as well as the molar ratio ofwater to surfactant. Nanoparticles of varying size could be prepared by using microemulsions of different surfactants. Water to surfactant ratio and surfactant concentration affected the average size of nanoparticles. Cosurfactant acted as a key factor in regulating the dimensions of nanoparticles. In most of these cases there was a concomitant relation between the size of nanoparticles and microemulsion droplets and this study focuses on understanding the template role of microemulsion droplets to control over the size of nanoparticles. The antibacterial activities of these nanoparticles

against Gram-negative *Escherichia coli*(*E. coli*) and Gram-positive *Staphylococcus aureus* (*S. aureus*) were tested by zone of inhibition method. All the four nanoparticles showed antibacterial activity against *E. coli* and *S. aureus* at very low concentration. Ag nanoparticles showed higher antibacterial activities among others. At high concentration, the sensitivities of*E. coli*to Ag and Cu nanoparticles were as good as conventional antibiotics. In this case, the concentration dependence on antibacterial activity has been less pronounced.

Chapter 4: Synthesis and antibacterial activities of Ag functionalized Fe_3O_4 nanoparticles prepared using water in oil microemulsion

In Chapter 4,preparation of functionalized nanoparticles, Fe_3O_4@Ag with antibacterial properties is reported.Ag functionalized Fe_3O_4nanoparticles was prepared by reducing silver nitrate on the surface of Fe_3O_4 nanoparticles in w/omicroemulsion. The nanoparticles were characterized by Fourier transform infrared (FTIR) spectroscopy, UV-visible spectroscopy, DLS measurementsand scanning electron microscopy (SEM). FTIR spectrum confirmed the presence of Fe-O in Fe_3O_4 nanoparticles.UV–visible absorption spectra confirmed the presence of both Fe_3O_4 and Ag nanoparticles. DLS showed that particles in nanodimensions were formed. SEM images revealed spherical morphology of the functionalized nanoparticles and showed uniform coating of Ag around Fe_3O_4. The antibacterial activity was evaluated by zone of inhibition method. The results showed antibacterial performance of Fe_3O_4@Ag nanoparticles against *E. coli* and *S. aureus*.

Chapter 5: Preparation of silver/polyanilinenanocomposites using water in oil microemulsion for synergistic antibacterial effects

Chapter 5 presentsthe synthesis ofpolyaniline (PAni) and Ag/PAninanocompositesin w/omicroemulsion. PAniwas prepared by chemical oxidative polymerization of aniline monomer by ammonium peroxydisulfatein microemulsion. Ag/PAninanocomposites were then prepared usingmicroemulsion by the same polymerization method in preformed Ag nanoparticles prepared by the reduction of metal salts in microemulsion.For a comparative study PAni was also prepared using aqueous solution method.Pure PAni and Ag/PAninanocomposites were characterized by UV-visiblespectroscopy, FTIRspectroscopy, DLS measurements, SEM imagesand thermogravimetric analysis (TGA). Both UV-visible and FTIR spectra revealed the formation of PAni and Ag/PAni composite. DLS results and SEM images showed that PAni synthesized in microemulsionswere of smaller size than that obtained from bulk synthesis. From TGA results it was observed that PAni from microemulsion has a lower thermal stability thanPAni from bulk. But in comparison with PAni from microemulsion, Ag/PAninanocomposites showed somewhat better thermal stability.The antibacterial propertiesof PAni and Ag/PAninanocompositeswere tested by zone of inhibition methodagainst *E. coli* and *S. aureus*.The results demonstrated that

Ag/PAninanocompositespossessed enhanced antibacterialefficiency compared to PAni generated in microemulsions which is more efficient than PAni from bulk.

Chapter 6: Preparation of silver/poly(vinyl alcohol)nanocomposite film using water in oil microemulsion for antibacterial applications

Chapter 6 describes the preparation ofSilver/poly(vinyl alcohol) (Ag/PVA) nanocomposite film usingw/o microemulsion. For the preparation, reduction of metal salt was carried in the core of w/omicroemulsion droplets containing PVA polymeric matrix. Ag/PVA nanocomposite film was then prepared by solution casting method after separation from the microemulsion. The nanocomposite film was characterized by FTIR spectroscopy, specular reflectance spectroscopy, SEM images and TGA. DLS measurements gave the average size and size distribution of Ag nanoparticles. It was observed that PVA could effectively prevent the aggregation of Ag nanoparticles whereas in the absence of PVA the nanoparticles agglomerated when separated from microemulsion. SEM images of the film prepared using microemulsionshowed homogeneous and uniformdistributionof Ag nanoparticles on PVA surface, whereas the film prepared through *in situ* generation of Ag nanoparticles by chemical reduction process on PVA host showed bunches of small but non-uniform and aggregated Ag nanoparticles. The thermal stability of as prepared Ag/PVA nanocomposite film wasalso higher than that prepared from bulk synthesis. The antibacterial properties of Ag/PVA films against *E. coli* and *S. aureus* tested by zone of inhibition method demonstrated that the as synthesized Ag/PVA nanocomposite film has enhanced antibacterial efficacy compared to that generated through *in situ* synthesis without using microemulsion under the same test condition.

Chapter 7: General conclusions

Chapter 7 summarizes the results for a general conclusion and discusses the future prospect of w/omicroemulsionsystems as suitable media to control over the size, morphology and structure of metallic and functionalized nanoparticles and their polymer composites for manifold applications.

CONTENTS

LIST OF FIGURES

LIST OF TABLES

1.1. General introduction

Nanoparticles are entities some billionths of a meter which is limited conventionally to about 100 nm in size in any direction.[1] Nanoparticles exhibit unique characteristics, which *inter alia* include unusual electronic, optical, magnetic[2] and chemical properties[3] that can hardly be obtained from individual atoms or molecules or conventional bulk materials.[2,4] Their extremely small sizes and large specific surface areas[5] associated with the ease of synthesis[6] and chemical modification[7] have made them most fascinating materials of current research[5] for potential application in diverse areas, e.g. chemistry, physics, material science, medical sciences, biology, and the corresponding engineerings. Various applications so far found to be promising are catalysis, electronic, optical, and mechanic devices, magnetic recording media, superconductors, high-performance engineering materials, dyes, pigments, adhesives, photographic suspensions and drug delivery.[8-12] In particular, there has been an upsurge of interest for application of metallic and functionalized nanoparticles and metal nano/polymer composites for biomedical applications.[13-15]

With the outbreaks of infectious diseases caused by pathogenic bacteria, viruses and micro-organisms much attention in pharmaceutical and medical fields has been focused on creating new antibacterial, antiviral, and other antimicrobial agents.[14] Metallic and their funtionalized nanoparticles have proved to be very promising candidates for such applications owing to their high surface-to-volume ratio and their novel physical and chemical properties on the nanoscale level.[14,16,17] Metallic nanoparticles of silver,[18,19] copper,[20] zinc[21] and iron[22] possess antibacterial properties. In a recent study, metal nanoparticles have been reported to interact with HIV-1, and Ag nanoparticles of sizes 1-10 nm attached to HIV-1 have prevented the virus from bonding to host cells.[23] Various medical products and industrial devices such as urinary catheters, suture rings, wood flooring and packaging material have nanocrystalline Ag as an antiseptic component. Bifunctional Fe_3O_4@Ag nanoparticles with both superparamagnetic and antibacterial properties were proved to have excellent antibacterial ability against *Escherichia coli*, *Staphylococcus epidermidis* and *Bacillus subtilis*.[14] Copper nanoparticles functionalized with an acrylate group has been found to be biocidal against biofilm formation.[24]

High reactivity of metal nanoparticles due to the large surface to volume ratio play a crucial role in inhibiting bacterial growth in aqueous and solid media.[25] Their small size and high surface to volume ratio allows them to interact closely with microbial membranes.[26] Copper nanoparticles with a larger surface to volume ratio thus may provide more efficient means for antibacterial activity.[20] The antimicrobial activity of colloidal silver particles is influenced by the dimensions of the particles, the smaller the particle size is, the greater is the antimicrobial effect.[27] Therefore, development of novel routes for synthesis of antibacterial nanoparticles with tunable dimension has become a fascinating domain of current research.

Research to-date includes numerous attempts to prepare nanosized materials. The techniques used are gas-evaporation, sputtering, coprecipitation, sol-gel method, hydrothermal, microemulsion, and so on.[25] Water in oil (w/o) microemulsions or reverse micelles are a particularly attractive reaction medium for preparing nanoparticles,[28,29] especially of metals by reduction from their salts. These microemulsions are transparent, isotropic liquid media with nanosized water droplets that are dispersed in a continuous oil phase and stabilized by surfactants and cosurfactants accumulated at the oil/water interface.[25,28,30] These highly dispersed surfactant-covered water pools offer a unique nanoenvironment which can solubilize inorganic reagents (metal salt and reducing agent) and act as nanoreactors for processing reactions. Reduction, nucleation and growth take place within these confined environment.[31] They also inhibit the excess aggregation of particles because the surfactants could adsorb on the particle surface when the particle size approaches to that of water pool. The steric barrier by the surfactant monolayer restricts the growth of precipitated particles and hinders intergrain coagulation.[25,32] As a result, the particles obtained in such a medium are generally very fine and monodispersed. Most importantly, the particle size and the morphology of the particles can be easily controlled by varying the nanoreactor size which can be tuned by changing different parameters of microemulsions such as water content, surfactant, cosurfactant, oil phase and temperature. Tailor-made nanoparticles can thus be prepared by using w/o microemulsions as size and shape of the dispersed nanodroplets can be controlled by changing different parameters of microemulsions. As nanoparticles are templated by the size and shape of the nanodroplets of microemulsions, nanoparticles with desirable size can be prepared using w/o microemulsions.

W/o microemulsions have been widely used to synthesize nanoparticles and the factors affecting the size and shape of nanostructured materials obtained by microemulsion synthesis have also been studied. Khilar et al.[33] and Cason et al.[34] investigated the role of aqueous content on the size of AgCl nanoparticles and copper nanoparticles respectively. Marchand et al. studied the influence of cosurfactants on size of molybdenum sulfide nanoparticles.[35] Charinpanitkul et al. studied the size and shape of ZnS nanoparticles with variation in the chain length of cosurfactant along with aqueous content.[36] Many researcher synthesized silver nanoparticles in different microemulsions and studied the effect of different controlling parameters on the size and size distribution of nanoparticles.[32] Ranjan et al. determined how the surfactant, cosurfactant, and aqueous content control the size, shape, aspect ratio, and growth of nanostructures of copper oxalate monohydrate.[28] However, the role of the different dominant parameters of microemulsions on the size of droplets and the finally formed nanoparticles is not still clear. The relationship between droplet size and particle size is not also yet well understood. So it is interesting to investigate how surfactant, cosurfactant and water change microenvironment i.e., the droplet size of miroemulsion and the size of metallic and functionalized nanoparticles prepared in these systems.

To realize biomedical applications of nanoparticles, it is necessary to prepare nanoparticle/polymer composites, which would still have small size and large surface area, but the presence of a polymeric matrix would prevent aggregation to stabilize nanoparticles within a matrix[37] even after separation from microemulsion and ensure slow and controlled leaching of nanoparticles. To utilize antibacterial properties of metal nanoparticles it is required to prepare composites with suitable polymers which can be widely used for the design of materials for biomedical devices and hospital equipments.

1.1.1. Outline of the research

In this work, metallic (Cu, Zn, Ag, Fe) and functionalized (Fe_3O_4@Ag) nanoparticles have been prepared using w/o microemulsion. Microemulsions were prepared with variation of the surfactant, cosurfactant and water content. Average size and size distribution of microemulsion droplets were measured and the effect of these different variables of microemulsion on the microemulsion-droplet size and also on the size of

prepared nanoparticles were investigated. The antibacterial activities of different metallic and functionalized nanoparticles have been studied. Metal nano/polymer composites (silver/polyaniline nanocomposite and silver/poly(vinyl alcohol) nanocomposite film) using w/o microemulsions were also prepared and their antibacterial activities were studied.

1.2. Introduction to nanoscience and nanotechnology

Nanoscience is the study of phenomena on a nanometer scale (generally 1–100 nm).[38,39] Since the 1980s, the field nanoscience has rapidly expanded.[40] Nanoscience are science concerning objects of nanometer dimensions, which are atoms (on a scale of tenths of nanometers) and molecules (on a scale of nanometers). Since everything is made of atoms and molecules, nanoscience could, in principle, be thought to cover all the branches of science[8] from fundamental sciences (physics, chemistry, biology) to applied sciences (electronics, engineering, medicine and materials).[9] Nanoscience considers a large number of important issues which have the potential for novel technical applications and when it deals with impacts and applications on different disciplines the term nanotechnology become appropriate.[39] Actually nanoscience is the study of the properties of materials and structures at the nanoscale[41] ranging from 1 to 100 nanometers which generally contain 20–15,000 of atoms and exist in a realm that straddles the quantum and Newtonian scales.[9] In particular, nanoscience focuses on the unique, size-dependent properties of solid-state materials.[41] Nanotechnology creates, controls and manipulates objects on the nanometer scale with the aim of producing novel materials that have specific properties (functionalized materials).[39] Nanoscience comprises basic research and development that is happening in laboratories all over the world. Nanotechnology produces gradually improved products where some form of nanotechnology enabled material (such as carbon nanotubes, nanocomposite structures or nanoparticles of a particular substance) or nanotechnology process is used during the manufacturing course that are in the market today. The ultimate aim of developing such technologies is to make them affordable for common people. The major quest, therefore, is to improve existing products by creating smaller components and better performance materials at lower cost.

Therefore the main goals of nanoscience and nanotechnology are the creation of functional materials, devices, and systems through control of matter on the nanometer length scale and exploitation of novel phenomena and properties (physical, chemical, and biological) at that scale.[37]

1.3. Early history

The concept of nanotechnology though considered to be a modern science has a long history dating back for millennia. Noble metal colloidal suspension in therapeutics has been used since ancient time. In different forms, gold has a long history of uses for therapeutic purposes.[42] In ancient times silver was considered to be more valuable than gold. Alchemists used it to cure ailments related to the brain. They considered Aurum potable (drinking gold) and Luna potable (drinking silver) as elixirs since 1570.[43]

Colloidal gold and silver were used as colorant in earlier days.[44] Nanoparticles of gold and silver were used by the artisans of Mesopotamia to generate a glittering effect to pots. The Lycurgus cup that was manufactured in the 5th to 4th century B.C. possesses the unique feature of changing color depending upon the light in which it is viewed. It appears green when viewed in reflected light, but looks ruby red when a light is shone from inside and is transmitted through the glass. Presence of a very small amount of tiny (~70 nm) metal crystals containing Ag and Au in an approximate molar ratio of 14:1 gives the Lycurgus cup its special color display. A colloid with heterocoagulation of gold nanoparticles and tin oxide is the colorant in glasses, "Purple of Cassius" which was popular in the 17th century. In 1857, Faraday reported the formation of deep-red solutions of colloidal gold by reduction of an aqueous solution of chloroaurate $[AuCl_4]^-$ using phosphorus in CS_2 (a two-phase system) in a well-known work. This probably was the first rationalized report on the purposeful synthesis of colloidal gold nanoparticles. Faraday investigated the optical properties of thin films prepared from dried colloidal solutions and observed reversible color changes of the films upon mechanical compression (from bluish-purple to green upon pressurizing).[45,46] Faraday called this colloided gold, "the divided metal". The term "colloid" (from the French, colle) was coined shortly thereafter by Graham, in 1861[45] for suspended particles in liquid medium and was categorized to be in the size range 1 nm to few μm. In 1857, Faraday first recognized

the existence of metallic nanoparticles in solution and in 1908 Mie gave a quantitative explanation of their color. In 1950's and 1960's the nanoparticles were used in the drug delivery system. Paul and co-workers investigated polyacrylic beads for oral administration, then focused on microcapsules and in the late 1960s developed the first nanoparticles for drug delivery purposes and for vaccines.[47] In 1974, Norio Taniguchi used the term 'nanotechnology' [48] for the colloidal particles, which have at least one dimension of the length scale of 1-100 nm. He approached nanotechnology from the 'top-down' standpoint. However in 1986, K. Eric Drexler studied the idea more to depth and then introduced the term 'nanotechnology' more precisely. This was the time when nano-revolution conceptually started.[49]

All these inventions were followed by the discovery of carbon nanotubes, preparation of quantum dots, first DNA made motor and fuel cells with the help of nanotube. The work has reached such heights that now scientists are even able to visualize mobility of nanoparticles and their therapeutic behaviors such as engulfment of nanoparticles by cells during cancer treatment.[50]

1.4 Importance of being nano

Nanoscale materials with at least one dimension between 1 and 100 nm serve as the fundamental building blocks for various nanotechnological applications. Within this size range, different properties of the nanoparticles such as physical, chemical and biological properties change in fundamental ways from the properties of both individual atoms or molecules and of the corresponding bulk material.[51] Properties change radically as the size of particles reduces from macro/micro scale to nanoscale.[52] Increased relative surface area and quantum effects are the two principal factors that make nanomaterials to differ significantly from other materials. These factors can change or enhance properties such as reactivity, strength and electrical characteristics. As the size of a particle decreases, greater will be the surface atoms compared to those inside. As a result nanoparticles have a much greater surface area per unit mass compared to larger one[38] which alters the physical and chemical properties of a material. This large fraction of surface atoms and high surface energy may affect the thermal stability and catalytic, mechanical, electronic and magnetic properties of such materials. Thus the melting points of small metal particles are below the melting temperature of the bulk metal and particles exhibit size-dependent

melting. Melting points decrease with decreasing particle size.[53] Catalytic activity of material in nanoparticulate form is higher than larger particles. Smaller the particles larger the surface area per unit mass compared with larger particles. Since chemical reactions occur at surfaces, so larger surface area makes nanoparticles much more reactive than the same mass of material made up of larger particles.[38] Nanocrystalline materials also show higher mechanical strength than their bulk counterpart because of the reduction of crystal defects.[54] Strength, stiffness, and ductility of nanometer scale metallic wires are extraordinarily high relative to bulk materials which also show favorable functional properties.[55]

Quantum size effect observed due to quantum confinement can dominate the behaviour of matter at the nanoscale and affect the optical, electrical and magnetic behaviour of materials that differ drastically from their bulk counterparts. For example, gold is non-magnetic yellow metal in the bulk form while gold nanospheres of dimension of ~100 nm or less appear red when suspended in transparent media. When size become much more smaller (<3 nm), gold nanoparticles act as excellent catalysts[55] and exhibit considerable magnetism. Gold nanoparticles of smaller than 2 nm turn into insulator.[56]

1.5. Metallic and functionalized nanoparticles for biomedical applications

Nanoparticles exist with great chemical diversity in the form of metals, metal oxides, semiconductors, polymers, carbon materials, organics or biological.[51] Among them metallic nanoparticles are more diverse and wide-spread types.[57] Metallic nanoparticles have become a fascinating domain of research for over a century because of their huge potential in biomedical sciences and engineering.[7] A recent upsurge of interest on metallic nanoparticles is due to their immense alteration in physical and chemical properties for nanodimension. The intense interest in the metallic nanoparticles derives from their unique chemical, electronic and optical properties arising from the small volume to big surface area ratio and the separation in the electronic energy level. Optical properties of metal nanoparticles distinguish themselves from other nanoplatforms by their unique surface plasmon resonance as nonmetallic particles do not show this photophysical response.[58] Upon exposure to light metallic nanoparticles exhibit coherent but confined oscillations of the quasi-free electrons in the conduction bands. When the characteristic frequency of these

oscillations coincides with that of the light excitation, the response of the metallic nanoparticles becomes resonant and strong absorption in the visible and near-infrared range occurs which is called surface plasmon resonance, SPR.[59] Plasmonic nanoparticles (noble metal, especially gold and silver) show much more stronger SPR band than other metals.[58] After absorption, the surface plasmon can decay radiatively which results in light scattering or nonradiatively which converts the absorbed light into heat.[7] These radiative and nonradiative properties of the nanoparticles offer multiple modalities for biological and medical applicaitons. Due to the SPR oscillation, the light absorption and scattering are strongly enhanced.[58] This surface plasmon absorption and surface plasmon light scattering can be used for diagnostic and therapeutic applications and gold nanoparticles are relevant for such applications.[60] The surface plasmon resonance and large effective scattering cross-section of individual silver nanoparticles make them ideal candidates for molecular labeling.[23] In imaging, silver nanoparticles also have received considerable attention using surface-enhanced Raman imaging.[7] Another important application of metallic nanoparticles is their wide use for antimicrobial functionality. Different metallic nanoparticles, including titanium, copper, magnesium and particularly silver and gold, are known for their antimicrobial, antiviral and antifungal capabilities.[60] In fact, silver nanoparticles are now replacing silver sulfadiazine as an effective agent in the treatment of wounds.[7] Currently, there is also an effort to incorporate silver nanoparticles into a wide range of medical devices, including bone cement, surgical instruments, surgical masks, etc.[7] Silver nanoparticles due to their excellent biocompatibility and antibacterial property raise considerable interest for biomedical applications.[61]

Magnetic iron oxide nanoparticles have been applied in magnetic bioseparation and detection of biological entities (cell, protein, nucleic acids, enzyme, bacteria, virus, etc.), clinic diagnosis and therapy such as magnetic resonance image and magnetic fluid hyperthermia, targeted drug delivery and biological labels. However, the naked iron oxide nanoparticles have high chemical activity, and are easily oxidized in air (especially magnetite, Fe_3O_4), generally resulting in loss of magnetism and dispersibility. Therefore, proper surface coating/surface modification i.e., surface funcionalization is necessary for effective protection to keep the stability which ultimately gives dual functionalities from both materials. Surface functionalization by

the single-metal layer has a tremendous impact on the scope of applications of iron oxides, particularly to expand its scope of biomedical applications. Especially, silver-metal functionalization of magnetic iron oxide have enormous potential for biomedical applications such as hyperthermia treatment, magnetic resonance imaging contrast agents, and magnetic separation.[62,63] Another advantage of such functionalization is the modification of the surface of silver by other functional groups which might have great potential applications in biomedical sector.[64]

Some factors- size, shape and composition of nanoparticles have significant effect on their efficacy. Therefore extensive research is necessary on synthesizing and characterizing nanoparticles.

1.6. Techniques for synthesis of nanoparticles

All preparation methods of metallic nanoparticles fall into one of the two broad categories- top down or bottom-up approach (Figure 1.1) which can also be considered as physical and chemical method respectively. Top-down approaches are those in which nanoparticles or well-organized assemblies are directly generated from a bulk piece of a required materials via the generation of isolated atoms using various distribution techniques.[65] In this strategy nanomaterials are prepared from larger entities without atomic-level control. These methods mainly include photolithography, electron beam lithography, milling techniques, anodization, ion and plasma etching, sputtering, laser ablation, thermal decomposition.[66,67] In the bottom-up approach, molecular components as starting materials link with chemical reactions, nucleation and growth process which ultimately promote the formation of more complex clusters. Bottom-up strategies include sol-gel processes, supercritical fluid synthesis, chemical vapor deposition, laser pyrolysis, bio-assisted synthesis.[66,67] A wide variety of nanoparticles are prepared using physical methods. But there are some major problems with these methods compared to nanoparticles produced by chemical methods. These are usually high-energy methods and are not very well suitable for preparation of small and uniform nanoparticles, and stabilization of nanoparticles is a matter of some difficulty.[68] So physical methods produce poor quality product and usually require costly vacuum systems or equipments to prepare nanoparticles.

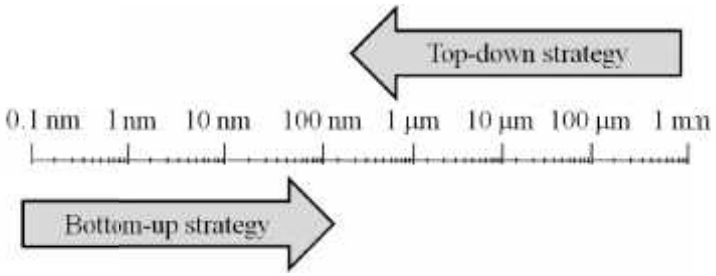

Figure 1.1. Top-down and bottom-up strategies.

Alternatively, the bottom-up approach is more preferable for the preparation of nanoparticles. For instance, chemical reduction method is the most common synthetic pathway for metal nanoparticles synthesis due to easy protocols.[66] Metal nanoparticles are prepared by the reduction of metal salts by reducing agents such as sodium borohydride, hydrazine, different reducing agents obtained from plant extracts and many more. The choice of reducing agent is an important factor for controlling rate as well as size of nanoparticles in the aqueous media. However, in aqueous media, size and distribution of nanoparticles are difficult to control only by controlling the concentration of reducing agents. Therefore different stabilizing agents are added [6865] to the reaction mixture to control the size of the prepared nanoparticles. The size of nanoparticles may be controlled if the synthesis is performed in a confined environment. This is the basis of the use of microemulsion as template and has been one of the most commonly used chemical methods for preparation of nanoparticles.

1.7. Microemulsion

Among the various methods used for the preparation of nanomaterials, chemical reactions in the colloidal solution in the presence of soft templates namely microemulsions have been widely used as an efficient route to control the particle size and shape. In 1959, Hoar and Schulman first introduced the concept of microemulsion. Accordingly, microemulsion can be defined as a multiphase system consisting of water, oil and amphiphile, which is a single optically isotropic and thermodynamically stable liquid solution.[69] In microemulsions large amounts of surfactant(s) frequently in combination with cosurfactant(s) are disposed at the hydrophilic liquid and lipophilic liquid (such as water and oil) interface thereby reducing the interfacial tension. Thus mixtures of two mutually insoluble liquids become thermodynamically stable and homogeneous and the system is formed spontaneously without requesting any additional external energy. Some characteristic

properties of microemulsions are ultralow interfacial tension, low viscosity, large interfacial area, capacity to solubilize both aqueous and oil-soluble compounds.[70] Microemulsions consist of monodispersed spherical droplets (diameter ranging from 600 nm to 8000 nm).[67] Microemulsion shows different organization due to the use of wide range of surfactant concentration, water-oil ratios, temperature etc.[71] Depending on the composition three types of microemulsion are most likely to be formed (Figure 1.2):

1. Oil in water (o/w) microemulsion where oil droplets are dispersed in the continuous aqueous phase.
2. Water in oil (w/o) microemulsion where water droplets are dispersed in the continuous oil phase;
3. Bicontinuous microemulsion where microdomains of oil and water are inter-dispersed within the system.

In all the three types of microemulsions, the interface is stabilized by an appropriate combination of surfactants and/or cosurfactants.[72]

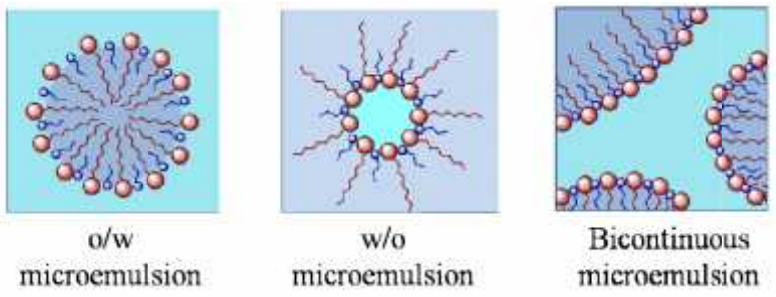

Figure 1.2. Different types of microemulsions.

1.7.1. Surfactant and cosurfactant for the formation of microemulsion

Microemulsions are formed due to the adsorption of surfactants at the interface of polar phase (generally water) and non-polar phase (generally hydrocarbon liquid or oil). These surfactants (derived from surface active agent, Figure 1.3.) are amphiphilic substances which contain two structurally distinct parts- a hydrophilic head group (water loving part) and hydrophobic tail group (oil loving part). Because of the presence of these two groups, at the oil-water interface surfactants are arranged in a such a way that their tail groups are directed toward oil phase and the polar head groups are heading for water. As a result, the interfacial tension is reduced.[73]

Surfactants can be classified by the presence of formally charged groups in its head. Nonionic surfactants have no charge groups in its head. The head of ionic surfactants carries a net charge. If the charge is negative, the surfactant is more specifically called anionic; if the charge is positive, it is called cationic. If a surfactant contains a head with two oppositely charged groups, it is termed zwitterionic[74] (Figure 1.3.).

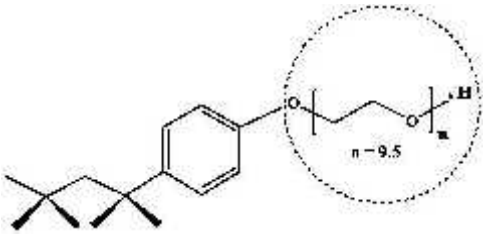

(a) Polyoxyethylene octyl phenyl ether (TX-100), non-ionic surfactant

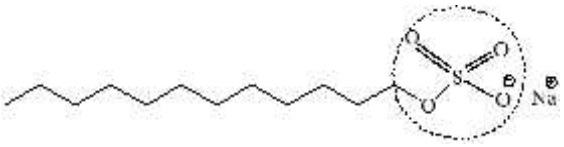

(b) Sodium dodecyl sulfate (SDS), anionic surfactant

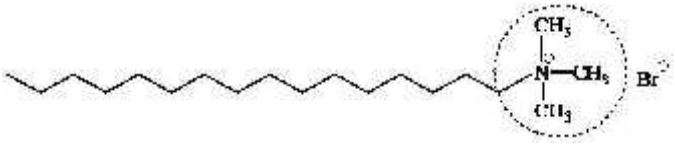

(c) Cetyltrimethyl ammonium bromide (CTAB), cationic surfactant

(d) Dodecyl betaine, zwitterionic surfactant

Figure 1.3. Different types of surfactants.

Hydrophilic – lipophilic balance (HLB) and packing parameter (PP) are the two vital aspects to understand the surfactant properties in terms of molecular parameters which can vary depending on the geometry and constituents of surfactants finally governing the type of self-assembled structure of surfactants aggregate. HLB is an empirical number which depends on the size of the two groups- polar head group and long alkyl chain. HLB of a surfactant is a measure of the degree to which it is hydrophilic or lipophilic and determined by calculating values for the different

regions of the molecule, as described by Griffin.[75] Detail calculations can be found in the literatures.[76] Other methods have been suggested by Davies.[77] It is a value between 0-60 defining the affinity of a surfactant for water or oil. HLB numbers are calculated for nonionic surfactants, and these surfactants have numbers ranging from 0-20. HLB numbers >10 have an affinity for water (hydrophilic) and number <10 have an affinity of oil (lipophilic). Ionic surfactants have recently been assigned relative HLB values, allowing the range of numbers to extend to 60. HLB is not the same as solubility, though there is an overall relationship. Thus, materials having low values tend to be oil soluble. On the other hand, materials having high values tend to be water soluble.

Critical packing parameter (CPP), a dimensionless shape factor that relates semi-empirical molecular parameters (head group area, chain length and hydrophobic tail volume) and intensive variables (temperature, ionic strength etc.) to surfactant microstructures mathematically can be expressed by-

$$\text{CPP} = v/a_o l_c$$

Where, v is the volume of the hydrophobic tail, a_o is the area of the hydrophobic head and l_c being the length of the hydrophobic tail. Changes in film curvature and microemulsion type can be addressed quantitatively in terms of CPP introduced by Israelachivili[78] and is widely used to relate surfactant molecular structure to interfacial topology. In terms of microemulsion type,

if $a_o > v/l_c$, then an o/w microemulsion forms,
if $a_o < v/l_c$, then a w/o microemulsion forms,
if $a_o \approx v/l_c$, then a middle-phase microemulsion is the preferred structure.[79]

Since the key component of the microemulsions is the surfactant, the nature of the surfactant governs the formation of microemulsions. Nature of the interfacial layers composed of surfactants and occasionally that of cosurfactants vary which can reversibly change from one kind to another. In addition, the composition of various components, HLB of the surfactant and the nature of the cosurfactant (short or medium chain alcohols) play an important role in determining the type of microemulsions to be formed. The shapes of the droplets of microemulsions also

depend on HLB[80] and CPP.[81] In general, low HLB (3–6) favors the formation of w/o microemulsions whereas high HLB (8–18) is better suited for the realization of o/w microemulsions. When CPP < 1/3, o/w globular structures are more probable, for CPP ≈1/2, o/w cylindrical structures form, for CPP ≈1, planar structures are favored, for CPP ≈2, w/o cylindrical structures are more probable and for CPP > 3, o/w droplets occur.[82]

Although there are no strict rules for choosing the appropriate components for microemulsion formation, still choosing surfactant is a crucial step. The surfactants such as cationic, anionic and nonionic that chosen must have[83]:

- Lower interfacial tension to a very small value to facilitates dispersion process.
- Provide a flexible film that can readily deform round small droplets.
- Be of appropriate HLB character to provide the correct curvature at the interfacial region for the desired micromulsion type.

Surfactant having HLB (>20) often require the presence of cosurfactants to reduce their effective HLB to value within the range required for microemulsion formation. The presence of cosurfactant in microemulsions helps by:

- Further reducing the interfacial tension by the dilution effect
- Increasing the mobility of the hydrocarbon tail and allowing greater penetration of the oil into this region.
- Influences the solubility properties of the aqueous and oily phases.
- Delaying the occurrence of liquid crystalline phases.

Depending on the polar phase, non-polar phase, surfactant HLB and nature of cosurfactant, different microstructures ranging from droplets of oil dispersed in a continuous water phase, o/w microemulsion over a bicontinuous ‘‘sponge’’ phase to water droplets dispersed in a continuous oil phase, w/o microemulsion can be formed where the latter can be used as nanoreactors for the synthesis of nanoparticles with a low polydispersity.[67,84]

1.7.2. W/o microemulsions as nanoreactors for the synthesis of nanoparticles

W/o microemulsion droplets/reverse micelles are thermodynamically stable supramolecular assemblies of nanometer-sized water droplets dispersed in a continuous oil phase and stabilized by a surfactant layer which lowers the interfacial

tension between the two immiscible liquids. Polar head-groups of surfactants (and cosurfactants) stabilize these nanostructures containing water inside their polar core while the aliphatic tails of surfactants penetrate into continuous oil phase (Figure 1.4). The size range of w/o microemulsion droplets normally is from 5 to 100 nm.[85] These surfactant-stabilized nanodroplets can be considered as true nanoreactors providing a cage-like effect that limits particle nucleation, growth, and agglomeration. In microemulsions Boutonnet et al. first synthesized metal nanoparticles, since then the microemulsion technique has been successfully used for the preparation of a variety metal nanoparticles.[86]

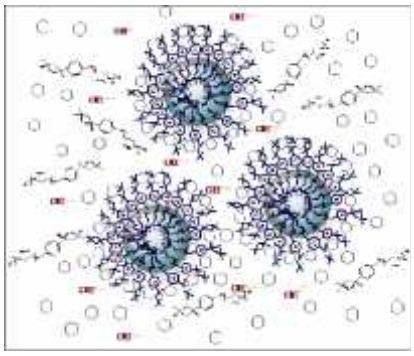

Figure 1.4. W/o microemulsion of TX-100/1-butanol/cyclohexane/water.

Water solublilized polar core of w/o microemulsion forming a so-called "water pool" is characterized by a parameter known as water to surfactant molar ratio, W_o.[87] It reflects the maximum amount of water that can be solubilized before phase transition. The water trapped inside the core is said to exhibit major changes from bulk behavior when $W_o < 20$.[88] This hydrophilic core water is said to have special properties, such as lower micropolarity, altered nucleophilicity and viscosity, which makes it a medium different from ordinary water. The aqueous interior of these w/o micrroemulsions allows the dissolution of polar moieties.[89] Thus reduction of metal salts can be carried out efficiently in the hydrophilic core which yields metal nanoparticles. Surfactant covered discrete aqueous droplets of microemulsions provide cage-like effect that limit the agglomeration of the particle thus attributing a controlled dimension to it. Excessive growth of particles is inhibited as surfactants adsorb on the particle surface when the particle size approaches to that of the water pool and act as steric stabilizers to inhibit aggregation. Henceforth the size and dispersity of the particles can be controlled.[90] Again because of the involvement of several variables such as surfactant, cosurfactant, solvent, amount of water, temperature, it is possible to fine-tune the

composition of the microemulsion. By manipulating these variables reverse micelles of different size and structure can be obtained. Thereby nanoparticles of varying size and shape can be prepared by microemulsion synthesis.[28]

1.7.3. Synthesis of nanoparticles in w/o microemulsion

Two reactant addition schemes[32,84] have been identified for the preparation of nanoparticles. These are single microemulsion or one microemulsion method and double microemulsion reactant addition scheme or two microemulsion method. One microemulsion method is further divided into two types including ‘‘energy triggering’’ and the ‘‘one microemulsion plus reactant’’ method. Energy triggering method needs a triggering agent to initiate the reaction within the single microemulsion containing the precursor that eventually leads to particle formation. For example, pulse radiolysis and laser photolysis are used to trigger the preparation of nanoparticles. One microemulsion plus reactant method involves the sequential addition of precursor to the same microemulsion (Figure 1.5 a). These processes are diffusion controlled since the second trigger/reactant has to diffuse through the interfacial wall of the microemulsion encapsulating the first reactant to accomplish the nanoparticle synthesis. The size of particles produced by the simple addition method can be much larger than the original droplet size. The most widely used method is two microemulsion method. In this method, two microemulsions carrying the separate reactants are mixed together in appropriate ratios (Figure 1.5 b). Brownian motion of the micelles helps them to come to closer approach resulting in intermicellar collisions and sufficiently energetic collisions leads to the formation of fused dimmer through which mixing of the micellar components takes place leading to chemical reaction.[84] Numerous intermicellar collisions are needed for the sufficient reactant exchange, their mixing and finally their reaction to take place. After reaction when free atoms (or ions) in solution come together to produce a thermodynamically stable cluster nucleation starts. When the cluster exceed a specific size (the critical size) determined by the competition between the aggregate curvature and the free energy favoring the growth of the new phase a supercritical nucleus is formed which is capable of further growth.[86] Growth commences instantly whenever a successful collision occurs between a water domain carrying a nucleus and another one carrying

the product monomers. This method produces nanoparticles of smaller sizes than the original droplet size.[84]

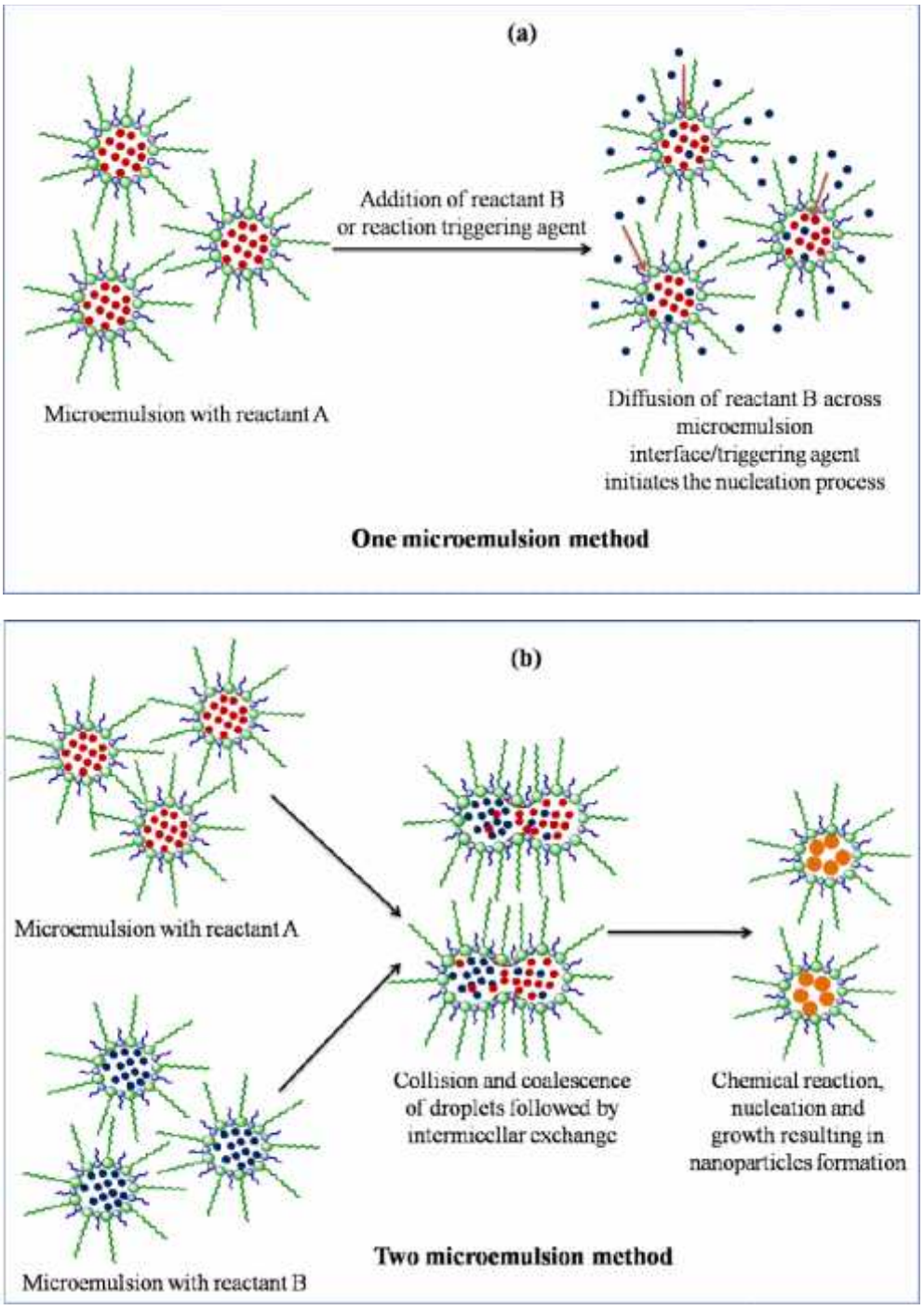

Figure 1.5. Various steps involved in one microemulsion process (a) and reaction sequence involved in the two microemulsion nanoparticles synthesis (b).

Microemulsion technique is used for the synthesis of the inorganic metal nanoparticles and functionalized nanoparticles. Metal nanoparticles can be prepared using microemulsion technique using the reduction strategy. Functionalized

nanoparticles can be prepared by reducing metal salts on the surface of other nanoparticles e.g. oxides using the w/o microemulsion method. Aqueous content, type of continuous phase, metal ion concentration, type and concentration of the reducing agent, structure and amount of the surfactant used are some of the key parameters that control the nanoparticles synthesis effectively.[32]

1.7.4. Challenges in nanoparticles preparation using microemulsion as template

Microemulsion as a liquid structure having a high surface area can be used as nanoreactor for the preparation of a wide range of nanoparticles of different chemical nature, size and shape. However, their separation and recovery from the microemulsion system as well as the recovery and recycling of the organic solvents remain a challenge.[91] Conventional separation techniques such as centrifugation, precipitation by antisolvent, flocculation by use of a photolyzable surfactant or temperature induced separation have been applied to recover nanoparticles from the w/o microemulsion system.[92] But after separation, aggregation probability cannot be ruled out resulting in larger particles with irregular shape[93] which reduces the antibacterial activity of different metal nanoparticles such as silver colloids.[94]

1.8. Metal nanoparticles embedded in polymer marix: polymer nanocomposites from w/o microemulsion

Stabilization of metal nanoparticles by high-molecular compounds presents a major branch of modern polymer colloidal science. Especially their tunable morphologies, chemical and structural nature and inherent long chains with relevant functional groups (which would act as targeted reactive sites allowing incorporation and the controllable immobilization of nanoparticles thereby formation of nanocomposite) are considered as the main reasons for choosing polymers as hosts and stabilizing agents.[94,95,96]. One procedure of this stabilization is the physical adsorption of macromolecules on the particle surface which presumes processes induced by van der Waals forces, dipolar interactions and weak and easily broken hydrogen bonds. Another process is the chemisorption of macromolecules in which polymer polar groups interact with surface atoms of the metal nanoparticles. The more electron-donor properties of polymer functional groups the stronger is their adhesion to dispersed phase particles. Covalent, ion or coordination links can be formed between

polymer chains and the atoms of the metal surface layer. When two metal nanoparticles covered by a layer of adsorbed soluble polymer chains approach to a distance less the total thickness of adsorption layers, the polymer layers start to interact bringing steric stabilization and leading to repulsion between the colloidal particles in the most of cases.[97] Particle stabilization against aggregation is due to the large decrease of their surface energy in comparison with bare particles.[96,98]

Thus the stabilization of metal nanoparticles in polymer matrices has recently gained great attention. For numerous practical applications especially in biomedical fields for antibacterial applications, metal nanoparticles are required to be well dispersed into or on the surface of polymer without the formation of large aggregates[94] and without high chances of their undesirable transfer into the environment keeping high efficiency with controlled release. Many methods have been developed to prepare metal nano/polymer composite where the nanoparticles release and their efficacy were found to be dependent on the nanoparticle content and on the method employed. There have been a variety of attempts to achieve metal nano/polymer composites. Overall, two different approaches are used to date, namely *in situ* and *ex situ* techniques. The first method consists of synthesis of metal nanoparticles inside the polymer matrix. This can be achieved by: i) reducing metal salt already present in the matrix by thermolysis, radiolysis or photolysis or by chemical reduction of metallic precursor salt dissolved in polymer by conventional reducing agent. In another way of *in situ* method, polymerization of monomer and formation of metal nanoparticles takes place simultaneously. The second approach, *ex situ* method comprise several steps: 1) formation of metal nanoparticles by soft-chemistry 2) their dispersion into polymeric matrixes or liquid monomer which is then polymerized. *In situ* approaches are currently getting much attention because of their obvious technological advantages over *ex situ* methods where a certain degree of aggregation still remains.[98,99,100]

Polymers can act as nanoreactors for the formation of nanoparticles.[98] In particular, within polymer diffusion of ions and growth of particles could be hindered, limited or directed. Confined medium of polymer can be further compartmentalized if polymeric matrix is incorporated in the core of the microemulsion. The template role of microemulsion together with the polymer host might ensure size-controlled selective

precipitation of nanoparticles in specific reaction sites of polymer chains to give uniform dispersity. In another approach if metal nano/polymer composites are prepared by the polymerization of monomer in preformed nanoparticles prepared by the reduction of metal salts in w/o microemulsion it would give polymeric nanoparticles with nanoparticles of metal for which the surface to volume ratio will increase thereby increasing efficiency. In both cases conservation of nanoparticle size can be attained even after separation from microemulsion because of stabilization by polymer. This has fuelled the investigation of the preparation of metal nano/polymer composites in w/o microemulsions. These metal nano/polymer composites will become more advantageous and advanced functional materials[94] as two different materials with different properties are combined and improved properties from synergism among the components can be obtained.[101]

1.9. Objectives of the work

The work was initiated to accomplish the following objectives.

- To synthesize antibacterial metallic nanoparticles with tunable dimension using w/o microemulsions.
- To synthesize functionalized nanoparticles in w/o microemulsions.
- To prepare metal nano/polymer composites with suitable polymers for antibacterial applications.

1.10. Present work

Surfactant, cosurfactant, amount of water are several variables of microemulsions which have tremendous effect on the their size and structure. Therefore this work aims at correlating the size of nanodroplets of microemulsions as a function of selected parameters: water content, different surfactant, surfactant/cosurfactant concentration and chain length of the cosurfactant. A systematic study has been performed to investigate the dependence of nanoreactor size of microemulsions on these variables and to gain a better understanding of their role in controlling droplet size. Microemulsions of anionic, cationic, and nonionic surfacans (SDS, CTAB and TX-100) with different composition have been prepared and the average

hydrodynamic diameters of the microemulsion droplets were ebvaluated from DLS measurements.

The water-containing reverse micelles of w/o microemulsions can accumulate hydrophilic precursors and thereby can act as true nanoreactors for the preparation of nanoparticles. Thus copper, zinc, silver and iron nanoparticles have been prepared using these w/o microemulsions by reducing metal salts with a reducing agent, $NaBH_4$. The elemental characterization of these metal nanoparticles was carried out by UV-visible spectroscopy, energy dispersive x-ray spectroscopic method and average size and morphology were examined by DLS measurements and scanning electron microscopy (SEM), respectively. Zeta potential measurements were also carried out to determine the stability of the synthesized nanoparticle in microemulsion of different surfactants.

The main focus of this study has been centered on the investigation of the effect of various dominant parameters of microemulsions on the size and size distribution of prepared nanoparticles. An attempt also has been made to correlate the droplet-sizes of microemulsions and the sizes of prepared nanoparticles in these systems. The antibacterial properties of the resultant nanoparticles were evaluated against two pathogenic bacteria, including Gram-positive, *Staphylococcus aureus* (*S. aureus*) and Gram-negative, *Escherichia coli* (*E. coli*) by means of zone of inhibition method. Fe_3O_4@Ag nanoparticles were also prepared using w/o microemulsion of TX-100. In microemulsions, Fe_3O_4 nanoparticles were formed via the chemical coprecipitation of ferric ion and ferrous ion using ammonia solution as the precipitating agent and a coating of Ag nanoparticles was performed by reducing silver salt. Fourier transform infrared (FTIR) spectroscopy, UV-visible spectra, SEM images and DLS measurements have been used to characterize the resultant functionalized nanoparticles. The antibacterial properties of Fe_3O_4@Ag nanoparticles against *S. aureus* and *E. coli* have also been studied.

Finally, two polymer nanocomposites, silver/polyaniline (Ag/PAni) and silver/poly(vinyl alcohol) (Ag/PVA) film have been also prepared using w/o microemulsions of TX-100. Ag/PAni nanocomposites were prepared using w/o microemulsions by chemical oxidation polymerization of aniline monomer in preformed Ag nanoparticles. For Ag/PVA nanocomposite film, reduction of metal salt

was carried out in the core of microemulsion droplet containing PVA polymeric matrix. The film was then prepared by solution casting method after separation from microemulsion. Nanocomposites were characterized by FTIR spectroscopy, specular reflectance spectroscopy, SEM images and thermogravimetric analysis. Zeta potential measurements were carried out in case of Ag/PAni to study the mechanism of formation of nanocomposite in the reverse micelles. The antibacterial properties of both nanocomposites against *S. aureus* and *E. coli* have also been explored.

References

(1) Lungu, M.; Neculae, A.; Bunoiu, M.; Biris, C. Nanoparticles' promises and risks. Springer International Publishing Switzerland, **2015**.

(2) Tavakoli, A.; Sohrabi, M.; Kargari, A. A review of methods for synthesis of nanostructured metals with emphasis on iron compounds. *Chem. Pap*. **2007**, *61*, 151-170.

(3) Liu, W.-T. Nanoparticles and their biological and environmental applications. *J. Biosci. Bioeng*. **2006**, *102*, 1-7.

(4) Santos, C. S. C.; Gabriel, B.; Blanchy, M.; Menes, O.; García, D.; Blanco, M.; Arconada, N.; Neto, V. Industrial applications of nanoparticles – a prospective overview. *Mater. Today:. Proc*. **2015**, *2*, 456 - 465.

(5) Stark, W. J.; Stoessel, P. R.; Wohlleben, W.; Hafner, A. Industrial applications of nanoparticles. *Chem. Soc. Rev.* **2015**, 1-13.

(6) Ju-Nam, Y.; Lead, J. R. Manufactured nanoparticles: An overview of their chemistry, interactions and potential environmental implications. *Sci. Total Environ*. **2008**, *400*, 396-414.

(7) Mody, V. V.; Siwale, R.; Singh, A.; Mody, H. R. Introduction to metallic nanoparticles. *J. Pharm. Bioall. Sci*. **2010**, *4*, 282-289.

(8) Capek, I. Nanocomposite structures and dispersions. Elsevier **2006.**

(9) Liu, W-T. Nanoparticles and their biological and environmental applications. *J. Biosci. Bioeng*. **2006**, *102*, 1-7.

(10) El-Sherbiny, S.; Morsy, F.; Samir, M.; Fouad, O. A. Synthesis, characterization and application of TiO_2 nanopowders as special paper coating pigment. *Appl. Nanosci.* **2014**, *4*, 305-313.

(11) Cao, Z.; Dobrynin, A. V. Nanoparticles as adhesives for soft polymeric materials. *Macromolecules* **2016**, *49*, 3586-3592.

(12) Blackman, J. A. Metallic nanoparticles. Elsevier **2009**.

(13) Sondi, I.; Salopek-Sondi, B. Silver nanoparticles as antimicrobial agent: a case study on E. coli as a model for Gram-negative bacteria. *J. Colloid Interf. Sci*. **2004**, *275*. 177-182.

(14) Gong, P.; Li, H.; He, X.; Wang, K.; Hu, J.; Tan, W.; Zhang, S.; Yang, X. Preparation and antibacterial activity of Fe_3O_4@Ag nanoparticles. *Nanotechnology* **2007**, *18*, 285604-285610.

(15) Furno, F., Morley, K, S., Wong, B., Sharp, B. L., Arnold, P. L., Howdle, S. M., Bayston, R., Brown, P. D.,Winship, P, D, Reid, H, J, Silver nanoparticles and polymeric medical devices: a new approach to prevention of infection. *J. Antimicrob. Chemother.* **2004**, *54***,** 1019-1024.

(16) Birringer, R. Nanocrystalline materials. *Mater. Sci. Eng.*, *A* **1989**, *117*, 33-43.

(17) Wright, J. B.; Lam, K.; Hansen, D.; Burrell, R. E. Efficacy of topical silver against fungal burn wound pathogens. *Am. J. Infect. Control* **1999**, *27*, 344-350.

(18) Cho, K. H.; Park, J. E.; Osaka, T.; Park, S. G. The study of antimicrobial activity and preservative effects of nanosilver ingredient. *Electrochimica Acta* **2005**, *51*, 956- 960.

(19) Shahverdi, A. R.; Fakhimi, A.; Shahverdi, H. R.; Minaian. S. Synthesis and effect of silver nanoparticles on the antibacterial activity of different antibiotics against Staphylococcus aureus and Escherichia coli. *Nonomedicine* **2007**, *3*, 168-171.

(20) Raffi, M.; Mehrwan, S.; Bhatti, T. M.; Akhter, J. I.; Hameed, A.; Yawar, W.; Hasan, M. M. Investigations into the antibacterial behavior of copper nanoparticles against Escherichia coli. *Ann Microbiol*. **2010**, *60*, 75-80.

(21) Rajamanickam, U.; Mylsamy, P.; Viswanathan, S.; Muthusamy, P. Biosynthesis of zinc nanoparticles using actinomycetes for antibacterial food packaging. International conference on nutrition and food sciences, Singapore, **2012**, *39*, 195-199.

(22) Naseem, T.; Farrukh, M. A. Antibacterial activity of green synthesis of iron nanoparticles using lawsonia inermis and gardenia jasminoides leaves extract. *Journal of Chemistry* **2015**, 1-7.

(23) Elechiguerra, J. L.; Burt, J. L; Morones, J. R.; Camacho-Bragado, A.; Gao, X.; Lara, H. H.; Yacaman, M. J. Interaction of silver nanoparticles with HIV-1. *J. Nanobiotechnol*.**2005**, 1-10.

(24) Anyaogu, K. C.; Fedorov, A. V.; Neckers, D. C. Synthesis, characterization, and antifouling potential of functionalized copper nanoparticles. *Langmuir* **2008**, *24*, 4340-4346.

(25) Hossain, S.; Fatema, U. K.; Mollah, M. Y. A.; Rahman, M. M.; Susan, M. A. B. H. Microemulsions as nanoreactors for preparation of nanoparticles with antibacterial activity. Journal of Bangladesh Chemical Society **2012**, *25*, 71-79.

(26) Morones, J. R.; Elechiguerra, J. L.; Camacho, A.; Holt, K.; Kouri, J.B.; Ramirez, J. T. The bactericidal effect of silver nanoparticles. *Nanotechnology* **2005**, *16*, 2346-2353.

(27) El-Nour, K. M. M. A.; Eftaiha, A.; Al-Warthan, A.; Ammar, R. A. A. Synthesis and applications of silver nanoparticles. *Arabian J. Chem*. **2010**, *3*, 135–140.

(28) Ranjan, R.; Vaidya, S.; Thaplyal, P.; Qamar, M.; Ahmed, J.; Ganguli, A. K. Controlling the size, morphology, and aspect ratio of nanostructures using reverse micelles: a case study of copper oxalate monohydrate. *Langmuir* **2009**, *25*, 6469-6475.

(29) López-Quintela, M. A.; Blancoa, C. T. M. C., Rio, L. G.; Leis, J.R. Microemulsion dynamics and reactions in microemulsions. *Curr. Opin. Colloid Interface Sci*. **2004**, *9*, 264-278.

(30) Milano-Brusco, J.; Prévost, S.; Lugo, D.; Gradzielski, M.; Schomäcker, R. Catalytic hydrogenation of dimethyl itaconate in non-ionic microemulsions: influence of the size of micelle. *New J. Chem*. **2009**, *33*, 1726-1735.

(31) Szcześ, A. Influence of the surfactant nature on the calcium carbonate synthesis in water-in-oil emulsion. *J. Cryst. Growth* **2009**, *311*,1129-1135.
(32) Solanki, J. N.; Murthy, Z. V. P. Controlled size silver nanoparticles synthesis with water-in-oil microemulsion method: a topical review. *Ind. Eng. Chem. Res*. **2011**, *50*, 12311-12323.
(33) Bagwe, R. P.; Khilar, K. C. Effects of the intermicellar exchange rate and cations on the size of silver chloride nanoparticles formed in reverse micelles of AOT. *Langmuir* **1997**, *13,* 6432-6438.
(34) Cason, J. P.; Miller, M. E.; Thompson, J. B.; Roberts, C. B. Solvent effects on copper nanoparticle growth behavior in AOT reverse micelle systems. *J. Phys. Chem. B* **2001,** *105,* 2297-2302.
(35) Marchand, K. E.; Tarret, M.; Lechaire, J. P.; Normand, L.; Kasztelan, S.; Cseri, T. Investigation of AOT-based microemulsions for the controlled synthesis of MoS_x nanoparticles : an electron microscopy study. *Colloids Surf., A* **2003**, *214*, 239-248.
(36) Charinpanitkul, T.; Chanagula, A.; Duttab, J.; Rungsardthongc, U.; Tanthapanichakoona, W. Effects of cosurfactant on ZnS nanoparticle synthesis in microemulsion. *Sci. Technol. Adv. Mater*. **2005**, 6, 266–271.
(37) Sengupta, A. K. Ion exchange and solvent extraction. CRC Press, Taylor & Francis Group, **2011**, *20*.
(38) Chaturvedi, S.; Dave, P. N.; Shah, N.K. Applications of nano-catalyst in new era. *J. Saudi Chem. Soc*. **2012**, *16*, 307-325.
(39) Blackman, J. A. Handbook of metal physics. Elsevier **2008**, *5*, 1-385.
(40) Nalwa, H. S.; (Ed.), Encyclopedia of nanoscience and nanotechnology, American scientific publishers, NewYork, **2004**.
(41) Mulvaney, P. Nanoscience vs nanotechnology-defining the field. *ACS NANO Editorial* **2015**, *9*, 2215-2217.
(42) Matijević, E. Fine particles in medicine and pharmacy. Springer US, **2012**.
(43) Lloyd, J.U. Elixirs and flavoring extracts: their history, formulae, and methods of preparation, New York: William Wood and Company, **1892**.
(44) Fulhame, Mrs. An Essay on Combustion with a View to a New Art of Dying and Painting. London, **1794**.
(45) Daniel M-C.; Astruc, D. Gold nanoparticles: assembly, supramolecular chemistry, quantum-size-related properties, and applications toward biology, catalysis, and nanotechnology. *Chem. Rev.* **2004,** *104,* 293-346
(46) Liz-Marzán, L. M. Nanometals: formation and color. *Mater. Today* **2004**, *7*, 26-31.
(47) Kreuter, J. Nanoparticles-a historical perspective. *Int. J. Pharm*. **2007**, *331*, 1-10.
(48) Taniguchi, N. On the Basic Concept of 'Nano-Technology'. In: Proceedings of the international conference on production engineering. Tokyo, Part II, Japan Society of Precision Engineering, **1974**, 18-23: Tokyo: JSPE
(49) Drexler, K. E. Engines of creation, the coming era of nanotechnology, **1986**.
(50) Dukes, M. J.; Jacobs, B. W.; Morgan, D. G.; Hegdec, H.; Kelly, D. F. Visualizing nanoparticle mobility in liquid at atomic resolution. *Chem. Commun*. **2013**, *49*, 3007-3009.
(51) Nagarajan, R. Nanoparticles: synthesis, stabilization, passivation, and functionalization. *ACS Symposium Series* **2008**, *996*.

(52) Caruso, F. Colloids and colloid assemblies: synthesis, modification, organization and utilization of colloidal particles. Wiley-VHC, **2004**.
(53) Allen, G. L.; Bayles, R. A.; Gile, W. W.; Jesser, W. A. Small particle melting of pure metals. *Thin Solid Films* **1986**, *144*, 297-308.
(54) Meyers, M. A.; Mishra, A.; Benson, D. J. Mechanical properties of nanocrystalline materials. *Prog. Mater Sci*. **2006**, *51*, 427-556.
(55) Murphy, C. J.; Sau, T. K.; Gole, A. M.; Orendorff, C. J.; Gao, J.; Gou, L.; Hunyadi, S. E.; Li, T. Anisotropic metal nanoparticles: synthesis, assembly, and optical applications. *J. Phys. Chem. B* **2005**, *109,* 13857-13870.
(56) Roduner, E. Size matters: why nanomaterials are different. *Chem. Soc. Rev*., **2006**, *35*, 583-592.
(57) Edmundson, M. C.; Capeness, M.; Horsfall, L. Exploring the potential of metallic nanoparticles within synthetic biology. *New Biotechnol*. **2014**, 1-7.
(58) Huang, X.; El-Sayed, M. A. Gold nanoparticles: Optical properties and implementations in cancer diagnosis and photothermal therapy. *J. Adv. Res.* **2010**, *1*, 13-28.
(59) Bhushan, B. Encyclopedia of nanotechnology. Springer **2012.**
(60) Schröfel, A.; Kratošová, Q. G.; Šafařík, I.; Šafaříková, M.; Raška, I.; Shor, L. M. Applications of biosynthesized metallic nanoparticles – A review. *Acta Biomater*. **2014**, *10*, 4023-4042.
(61) Rosarin, F. S.; Mirunalini, S. Nobel metallic nanoparticles with novel biomedical properties. *J. Bioanal. Biomed.* **2011**, *3*, 85-91.
(62) Wu, W.; He, Q.; Jiang, C. Magnetic iron oxide nanoparticles: synthesis and surface functionalization strategies. *Nanoscale Res. Lett*. **2008**, *3*, 3397-3415.
(63) Moscoso-Londoño, O.; Muraca, D.; Tancredi, P.; Cosio-Castañeda, C.; Pirota, K. R.; Socolovsky, L. M. Physicochemical studies of complex silver−magnetite nanoheterodimers with controlled morphology. *J. Phys. Chem. C* **2014**, *118*, 13168-13176.
(64) Liu, C. H.; Zhou, Z. D.; Yu, X.; Lv, B. Q.; Mao, J. F.; Xiao, D. Preparation and characterization of Fe_3O_4/Ag composite magnetic nanoparticles. *Inorg. Mater*., **2008**, *44*, 291-295.
(65) Niemeyer, C. M. Nanoparticles, proteins, and nucleic acids: biotechnology meets materials science. *Angew. Chem. Int. Ed*. **2001**;*40*, 4128-58.
(66) Keat, C. L.; Aziz, A.; Eid, A. M.; Elmarzugi, N. A. Biosynthesis of nanoparticles and silver nanoparticles. *Bioresour. Bioprocess.* **2015**, *2*, 1-11.
(67) Dhand, C.; Dwivedi, N.; Loh, X. J.; Ying, A. N. J.; Verma, N. K.; Beuerman, R. W.; Lakshminarayanan, R.; Ramakrishna, S. Methods and strategies for the synthesis of diverse nanoparticles and their applications: a comprehensive overview. *RSC Adv.* **2015**, 1-76.
(68) Starov, V. M. Nanoscience colloidal and inefacial aspects. CRC Press, Taylor & Francis Group, **2010.**
(69) Hoar, T. P.; Schulman, J. H. Transparent water-in-oil dispersions: the oleopathic hydro-micelle, *Nature*, **1943**, *152*, 102-103.
(70) Eccleston, G. M. Emulsions and microemulsions: Encyclopedia of pharmaceutical Technology*,* Marcel Dekker, NewYork, **1994**, *9*, 375-421.

(71) Lawrence, M. J.; Rees, G. D. Microemulsions-based media as novel drug delivery systems, *Adv. Drug Delivery Rev*., **2000**, *45*, 89-121.
(72) Schulman, J. H.; Stoekenius, D.; Prince, L. M. Mechanism of formation and structure of microemulsions by electron microscopy, J. Phys. Chem. **1959**, *63*, 1677-1680.
(73) Zhang, Y.; Zhao, H. Surfactant behaviors of amphiphilic polymer-tethered nanoparticles. *Langmuir*, 2016, *32*, 3567-3579.
(74) Schramm, L. L.; Stasiuk, E. N.; Marangoni, D. G. Surfactants and their applications, Annual Reports Section "C" (Physical Chemistry), **2003**, *99*, 3-48.
(75) Griffin W. C. Classification of surface-active agents by "HLB". *J. Soc. Cosm. Chem.* **1949**, *1*, 311-326.
(76) Griffin W. C. Calculation of HLB values of non-ionic urfactants. *J. Soc. Cosm. Chem.*, **1954**, *5*, 249-256.
(77) Davies J. T. *2nd Int. Cong. Sur. Act.*, **1957**, *1*, 426.
(78) Israelachvili J. N., Mitchell D. J., Ninham B. W. J., Theory of self-assembly of hydrocarbon amphiphiles into micelles and bilayers *Chem. Soc. Faraday Trans. 2*, **1976**, *72*, 1525.
(79) Cosgrove, T. Colloid science principles, methods and applications. Wiley, **2010**.
(80) Carlfors, J.; Blute, I.; Schmidt, V. Lidocaine in microemulsions-a dermal delivery system, *J. Dispersion Sci. Technol*. **1991**, *12*, 467-482.
(81) Hartley, G. S. Aqueous solutions of paraffin chain salts, Hermann, Paris, **1936**.
(82) Lawrence, M. J.; Rees, G. D. Microemulsions-based media as novel drug delivery systems, *Adv. Drug Delivery Rev*., **2000**, *45*, 89-121.
(83) Talegaonkar, S.; Azeem, A.; Ahmad, F. J.; Khar, R. K.; Pathan, S. A.; Khan, Z. I. Microemulsions: A novel approach to enhanced drug delivery, Recent Patents on Drug Delivery and Formulation, **2008**, *2*, 238-257.
(84) Malik, M. A.; Wani, M. Y.; Hashim, M. A. Microemulsion method: A novel route to synthesize organic and inorganic nanomaterials. Arabian J. Chem. **2012**, *5*, 397-417.
(85) Qi, L. Synthesis of inorganic nanostructures in reverse micelles. *Encyclopedia of Surface and Colloid Science*. **2006**, 6183-6207.
(86) Fanun, M. Microemulsions Properties and Applications, CRC Press, **2009**, *144*.
(87) Pilenia, M.P.; Lisieck, I. Nanometer metallic copper particle synthesis in reverse micelles. *Colloids Surf., A* **1993**, *80*, 63-68.
(88) Piletic, I. R.; Moilanen, D. E.; Spry, D. B.; Levinger, N. E.; Fayer, M. D. Testing the core/shell model of nanoconfined water in reverse micelles using linear and nonlinear IR spectroscopy. *J. Phys. Chem. A* **2006,** *110,* 4985-4999.
(89) Ganguli, A. K.; Ganguly, A.; Vaidya, S. Microemulsion-based synthesis of nanocrystalline materials. *Chem. Soc. Rev*. **2010**, *39*, 474-485.
(90) Zhang, W.; Qiao, X.; Chena, J. Synthesis of silver nanoparticles—Effects of concerned parameters in water/oil microemulsion. *Mater. Sci. Eng. B* **2007**, *142*, 1-15.
(91) Bajpai, S. K.; Yallapu, M. M. Recent Advances in Nanoscience and Technology. Bentham e Books. **2009**.

(92) Hollamby, M. J.; Eastoe, J.; Chemelli, A.; Rogers O. G. S.; Heenan, R. K.; Grillo, I. Separation and purification of nanoparticles in a single step. *Langmuir* **2010**, *26*, 6989-6994.

(93) Li, T.; Li, S.; Wang, S.; An, Y.; Jin, Z. Preparation of nanoiron by water-in-oil (w/o) microemulsion for reduction of nitrate in groundwater. *J. Water Resour. Prot*. **2009**, *1*, 1-57.

(94) Dallas, P.; Sharma, V. K.; Zboril, R. Silver polymeric nanocomposites as advanced antimicrobial agents: Classification, synthetic paths, applications, and perspectives. *Adv. Colloid Interface Sci*. **2011**, *166*, 119-135.

(95) Sharma, V. K.; Yngard, R. A.; Lin, Y. Silver nanoparticles: Green synthesis and their antimicrobial activities. *Adv. Colloid Interface Sci*. **2009**, *145*, 83-96.

(96) Virkutyte, J.; Varma, R. S. Green synthesis of metal nanoparticles: Biodegradable polymers and enzymes in stabilization and surface functionalization. *Chem. Sci*., **2011**, *2*, 837-846.

(97) Pomogailo, A. D.; Kestelman, V. N. Metallopolymer Nanocomposites. Springer Berlin Heidelberg. **2005**, *81*.

(98) Rozenberg, B.A.; Tenne, R. Polymer-assisted fabrication of nanoparticles and nanocomposites. *Prog. Polym. Sci*. **2008**, *33*, 40-112.

(99) Ananth, A. N.; Umapathy, S.; Sophia, J.; Mathavan, T.; Mangalaraj, D. On the optical and thermal properties of in situ/ex situ reduced Ag NP's/PVA composites and its role as a simple SPR-based protein sensor. *Appl. Nanosci*. **2011**, *1*,87-96.

(100) Abargues, R.; Abderrafi, K.; Pedrueza, E.; Gradess, R.; Marqués-Hueso, J.; Valdésa, J. L.; Martínez-Pastora, J. Optical properties of different polymer thin films containing in situ synthesized Ag and Au nanoparticles. *New J. Chem*. **2009**, *33*, 1720-1725.

(101) Schmidt, G.; Malwitz, M. M. Properties of polymer–nanoparticle composites. *Curr. Opin. Colloid Interface Sci*. **2003**, *8*, 103-108.

Abstract

Series of water in oil microemulsions have been prepared and the size and size distribution of microemulsion droplets have been studied by conducting dynamic light scattering measurements. The roles of different key parameters of microemulsions such as surfactant, water content and cosurfactant on the formation of microemulsions and their influences on the size of microemulsion droplets have been discussed. Different surfactants gave microemulsions of varying size. The average size was affected by water to surfactant ratio and surfactant concentration. Addition of cosurfactant also modulated the dimensions of microemulsion droplets. Increasing the amount and chain length of cosurfactant resulted in microemulsions with relatively smaller droplets. Thus it is possible to fine-tune the composition of microemulsions to obtain microemulsion droplets of desirable dimension.

2.1. Introduction

Microemulsions as discussed in chapter 1 are thermodynamically stable homogeneous mixtures composed of two mutually immiscible liquid phases, one spontaneously dispersed in the other with the assistance of one or more surfactants and cosurfactants.[1] Large amount of two immiscible liquids (e.g. water and oil) are brought into a single phase (macroscopically homogeneous but microscopically heterogeneous) by addition of an appropriate surfactant or a surfactant mixture. The surfactant and cosurfactant bring down the water/oil interfacial tension to a very low value originally, to a negative interfacial tension which imparts stability to microemulsions.[2] Microemulsions can be water-continuous (oil in water), oil-continuous (water in oil) or bicontinuous (middle phase). Among these in water in oil (w/o) microemulsions thermodynamically stable nanometer-sized water droplets are dispersed in continuous oil phase. These droplets embed water inside their polar core. Polar head-groups of surfactants and cosurfactants stabilize these core water while their hydrocarbon tails insert themselves into continuous oil phase.[3-5] The size and shape of these water domains as well as their concentration can be controlled by manipulating different variables of microemulsions.[6] Surfactant molar concentration, molar ratio between water and surfactant (W_o), the molar ratio between cosurfactant and surfactant (P_o), nature and length of the alkyl chain of the oil, nature of surfactant, chain length of cosurfactant, temperature are several variables of microemulsions which can fine-tune the composition of the microemulsions[7] and thereby can change

the size of water droplets. The morphology of reverse micelles also changes with the surfactant concentration. At a low surfactant concentration only spherical micelles are formed. When the concentration of surfactant attains to 40–50%, the spherical micelles change to rod-shaped or column-shaped micelles.[8]

This unique class of optically clear thermodynamically stable w/o microemulsions has been the subject of extensive research over the last two decades primarily because of their scientific and technological importance. They have been extensively used as nanoreactors to prepare monodisperse nanosized particles, such as metal, metal borides and metal oxides.[9] Surfactant covered water droplets act as nanoreactors in which reaction, nucleation and growth take place. Determination of the size and size distribution of the microemulsion droplets is thus an important feature to know whether they can act as the nanoreactors to prepare nanoparticles of desirable dimension. Numerous attempts have been made to investigate the average diameter of microemulsion droplets by varying different parameters of microemulsion. The size of droplets in w/o microemulsions has been reported to increase with increase either in temperature, oil chain length[10] and W_o[11,12] or with decreasing surfacant/cosurfactant chain length[10] and salt concentration.[13] A linear relationship of W_o [11,14] with the radii of the water cores is also well-established. Hydrodynamic radii of micellar aggregates and radius of the water pool determined by quasi-elastic light scattering and time-resolved fluorescence quenching techniques showed that an increase in cosurfactant to surfactant molar ratio brings about a decrease in core water size.[15] Dynamic light scattering (DLS) experiments are described as an appropriate[16] and popular[17] method for measuring droplet size and size distributions in microemulsions because of its ease of use. This reports a systematic study to understand the influence of different variables of microemulsions on the size and size distribution of droplets by DLS measurements.

2.2. Experimental

2.2.1. Materials

Sodium dodecyl sulfate (SDS, Sigma Aldrich), cetyltrimethyl ammonium bromide (CTAB, Qualichems), triton X-100 (TX-100, Sigma Aldrich), cyclohexane (Merck), 1-butanol (LAB-SCAN), 1-pentanol (Merck), 1-hexanol (Sigma Aldrich), 1-heptanol (Merck) and 1-octanol (Merck) were used as received without any further

purification. De-ionized water (conductivity: 0.055 μScm^{-1} at 25.0 °C) from HPLC grade water purification systems (BOECO, Germany) was used in the experiments.

2.2.2. Methods

2.2.2.1. Preparation of w/o microemulsions

Microemulsions were prepared with variation in the surfactant, water content and cosurfactant to understand their effect on the size of microemulsion droplets.

2.2.2.1.1. Preparation of microemulsions with variation in the type of surfactant

To investigate the effect of types of surfactant on the size of microemulsion droplets three different surfactants were used for the preparation of microemulsions where the number of moles of each component were kept constant. The surfactant (SDS, CTAB or TX-100), cosurfactant (1-butanol, 1-BuOH), and oil phase (cyclohexane) with the molar ratio 1.0:7.8:19.8 were first mixed and then water was added, with W_o value fixed at 7.7 (Table 2.1).

Table 2.1. Composition of microemulsions with variation in the type of surfactant

Microemulsions (ME)	% wt of				
	Surfactant	Cyclohexane	1-BuOH	Water	W_o
SDS ME	10.80	62.30	21.70	5.20	7.7
CTAB ME	13.65	62.30	21.70	5.20	7.7
TX-100 ME	23.41	62.30	21.70	5.20	7.7

2.2.2.1.2 Preparation of microemulsions with variation in water content

To investigate the effect of aqueous content on the size of microemulsion droplets microemulsions were prepared with increasing W_o and concentration of surfactant. W_o was varied using microemulsions of SDS, TX-100 and CTAB. The specific systems studied are SDS/1-penanol/cyclohexane/water, TX-100/1-butanol/cyclohexane/water and CTAB/1-butanol/cyclohexane/water. For SDS microemulsions W_o was changed from 7.7 to 28.7 where P_o was fixed at 6.6 (Table 2.2).

Table 2.2. Composition of SDS microemulsions with variation in W_o

% wt of				
SDS	Cyclohexane	1-pentanol	Water	W_o
10.8	62.3	21.7	5.2	7.7
10.2	59.3	20.5	10.0	15.7
10.0	56.8	20.2	13.0	20.8
9.6	53.9	19.3	17.2	28.7

For TX-100 microemulsions W_o increased from 3.5 to 10. The composition is shown Table 2.3. Above W_o = 10, microemulsions could not be prepared.

Table 2.3. Composition of TX-100 microemulsions with variation in W_o

% wt of				
TX-100	Cyclohexane	1-butanol	Water	W_o
10.00	83.00	6.00	1.00	3.5
10.00	83.00	4.75	2.25	7.8
10.00	83.00	4.10	2.88	10.0

For CTAB microemulsions W_o increased from 9.7 to 30 as shown in Table 2.4.

Table 2.4. Composition of CTAB microemulsions with variation in W_o

% wt of				
CTAB	Cyclohexane	1-butanol	Water	W_o
20.0	3.4	67.0	9.6	9.7
20.0	3.4	56.8	19.8	20.0
20.0	3.4	46.9	29.7	30.0

The effect of surfactant concentration on the size of microemulsion droplets were studied using TX-100 microemulsions with varying W_o values (Table 2.5).

Table 2.5. Composition of TX-100 microemulsions with variation in [TX-100]

% wt of					[TX-100]
TX-100	Cyclohexane	1-pentanol	Water	W_o	(M)
55.00	5.00	30.00	10.00	6.3	0.88
45.00	15.00	30.00	10.00	7.7	0.72
35.00	25.00	30.00	10.00	9.9	0.56

2.2.2.1.3. Preparation of microemulsions with variation in cosurfactant

To study the effect of cosurfactant on the size of microemulsion droplets, microemulsions were prepared with variation in concentration of cosurfactant and also with increasing chain length of cosurfactant. For TX-100/cyclohexane/1-pentanol/water at W_o = 6.3 the concentration of 1-pentanol was varied at both low (0.16 M) and high concentrations of surfactant (0.88 M). At low concentration of TX-100, microemulsion could not be prepared without 1-pentanol.

Table 2.6. Composition of TX-100 microemulsions with variation in [1-pentanol] at [TX-100] = 0.16 M

% wt of				W_o	P_o	Surfactant to oil molar ratio × 10^{-1}
TX-100	Cyclohexane	1-pentanol	Water			
10.000	86.351	1.834	1.815	6.3	1.3	0.156
10.000	84.515	3.670	1.815	6.3	2.6	0.159
10.000	83.000	5.501	1.815	6.3	3.9	0.162

At high concentrations of TX-100, microemulsion could be prepared without the assistance of a cosurfactant, 1-pentanol (Table 2.7).

Table 2.7. Composition of TX-100 microemulsions with variation in [1-pentanol] at [TX-100] = 0.88 M

% wt of				W_o	P_o	Surfactant to oil molar ratio × 10^{-2}
TX-100	Cyclohexane	1-pentanol	Water			
55.00	35.00	-	10.00	6.3	0	21.16
55.00	25.00	10.08	10.00	6.3	1.3	29.62

To study the effect of cosurfactant chain length, alcohols with increasing carbon chain length from 1-butanol to 1-octanol were used for TX-100 microemulsions where number of moles of cosurfactants were kept constant (Table 2.8).

Table 2.8. Composition of TX-100 microemulsions with variation in chain length of cosurfactant

Surfactant	Oil	Cosurfactants*					Water
TX-100	Cyclohexane	BuOH	PeOH	HexOH	HepOH	OctOH	
10.00	83.00	4.75	5.65	6.55	7.45	8.35	2.25

*BuOH = 1-butanol, PeOH = 1-pentanol, HexOH = 1-hexanol, HepOH = 1-heptanol, OctOH = 1-octanol

2.2.3. Measurement of droplet size

The hydrodynamic diameters of different microemulsion droplets were measured using a Zetasizer Nano ZS90 (ZEN3690, Malvern Instruments Ltd., UK) by DLS method. The particle size detection limit was about 0.3 nm–5 μm (diameter) and accuracy of the average diameter determined has been ±2%. A He-Ne laser beam of 632.8 nm wavelength was used and the measurements were made at a fixed scattering angle of 90°. Prior to the measurements the laser was illuminated for about 30 min to

stabilize the system. Samples were filtered using VALUPREP 0.45 μm polytetrafluoroethylene (PTFE) filter and for the scattering measurements of 1 mL of each of the samples a universal glass dip-cell of 10 mm diameter was used. The refractive indices and viscosities of the bulk continuous phase of microemulsions were used in the analysis.[18,19] The average diameters were determined from cumulants mean of the intensity average of 50 runs using Stokes–Einstein equation, $R_h = KT/6\pi\eta D_{eff}$, where R_h is hydrodynamic radius, K, the Boltzmann constant, T, the temperature, η, the solvent viscosity, and D_{eff}, the diffusion coefficient. The reproducibility was checked from at least 3 measurements. The temperature of the apparatus was controlled automatically within ±0.01K by a built-in Peltier device.

2.3. Results and discussion

2.3.1. Effect of type of surfactant on the droplets of microemulsions

In order to evaluate the effect of the nature of surfactant on the sizes of microemulsion droplets, three different surfactants having different charge, polar head group and hydrophobic chain (Table 2.9) were used. Other parameters of microemulsions (water content, oil phase and cosurfactant) were kept constant (Table 2.1).

Table 2.9. Surfactants used in this work and their basic features[20,21]

Surfactants	Formula	Formula weight (g mol^{-1})	HLB	Type
SDS	$C_{12}H_{25}SO_4Na$	288.38	40.0	Anionic
TX-100	$C_8H_{17}C_6H_4O(CH_2CH_2O)_{9.5}H$	625.00	13.4	Cationic
CTAB	$[CH_3(CH_2)_{15}N(CH_3)_3]Br$	364.46	10.0	Nonionic

DLS measurments gave the average size of the microemulsion droplets which is different for different surfactant microemulsions. Average size of the microemulsion droplets decreased in the order SDS > TX-100 > CTAB microemulsion in the order of decreasing surfactant HLB value. The surfactant with higher HLB value is more hydrophilic showing strong tendency to form micelles whereas that with the lower

number is more lipophilic in nature favoring preferential formation of reverse micelles.[20,22] In a w/o microemulsion system, the more lipophilic surfactant leads to smaller droplets while the more hydrophilic surfactant produces larger droplets[20] for their structures and packing parameters. SDS with higher HLB value produces microemulsion droplets with larger average diameter (Figure 2.1) among the same microemulsion system for CTAB and TX-100. Depending on the values of HLB, SDS is far more water loving than TX-100 and CTAB is highly oil loving. Therefore, CTAB can easily form w/o or reverse micoemulsion. Based on the HLB values the tendency of surfactants solubilization in microemulsion will vary meaning that to form a reverse micellar droplet low number of oil loving surfactant will be sufficient whereas in case of water loving surfactant high number of surfactant molecules will be needed. So for the formation of w/o microemulsion droplet, the aggregation number of surfactant will be higher for SDS than TX-100 and for CTAB it will be lower. Therefore, with increasing hydrophilicity/HLB of surfactant average size of w/o microemulsions increases.

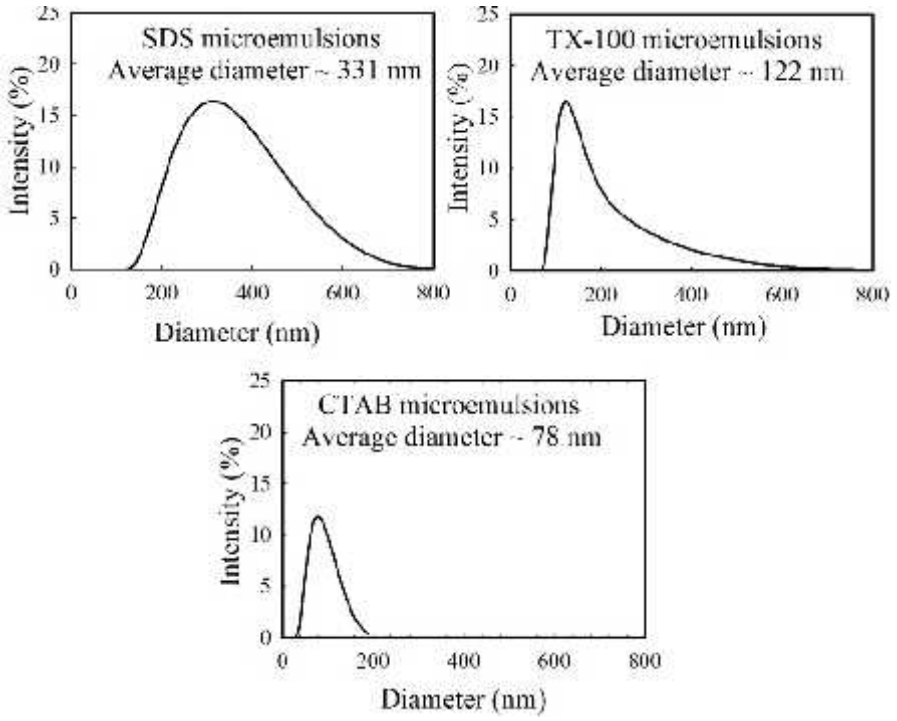

Figure 2.1. Average size of microemulsion droplets of SDS, TX-100 and CTAB microemulsions.

2.3.2. Effect of water content on the size of microemulsions

To understand the dependence of the size of microemulsion on the water content measurements were carried out at varying W_o (Tables 2.2, 2.3, 2.4). Measurements were also conducted at varying concentration of surfactant(Table 2.5). It may be worth mentioning that the total water content of w/o microemulsion depends on W_o and concentration of surfacatant.[23,24] Average size and size distribution of microemulsion droplets are shown in Figures 2.2 and 2.3.

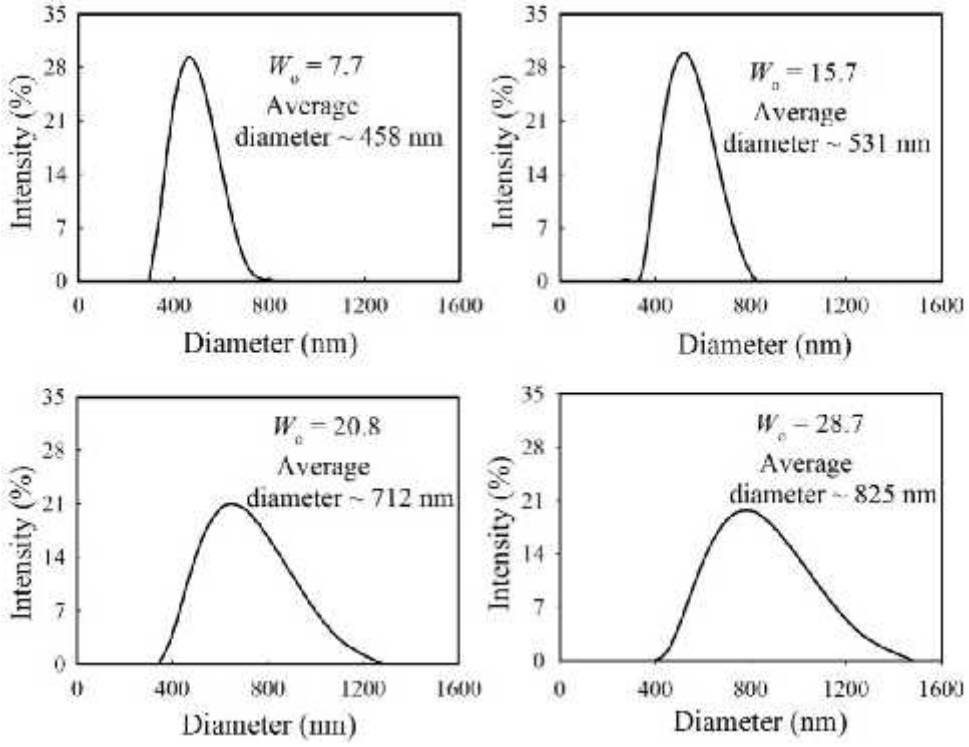

Figure 2.2. Average size and size distribution of microemulsion droplets of SDS microemulsions with W_o.

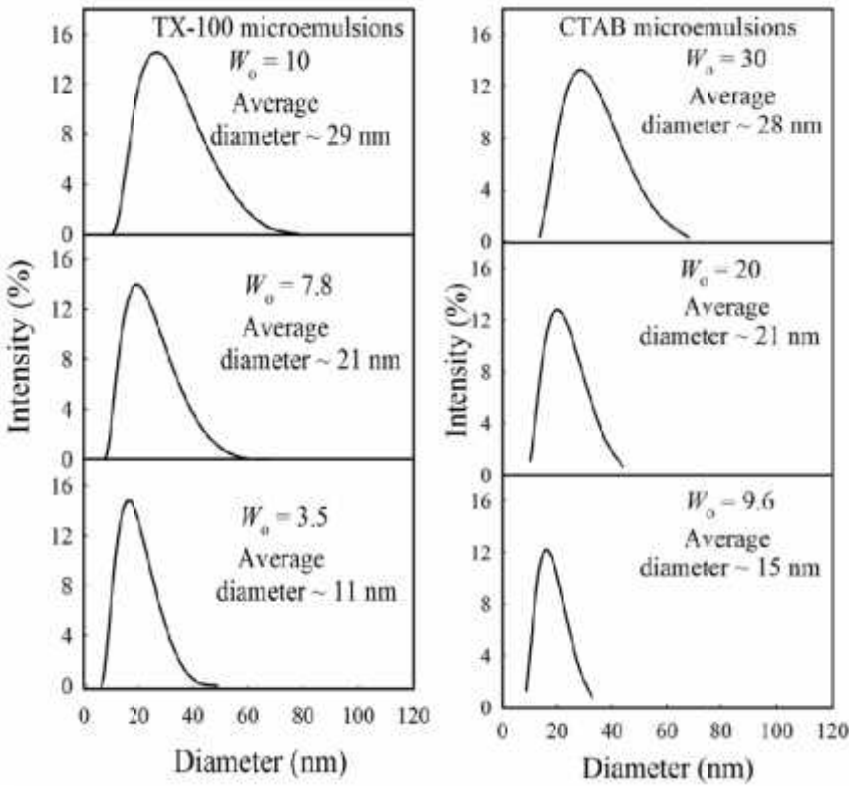

Figure 2.3. Average size and size distribution of microemulsion droplets of TX-100 and CTAB microemulsions with W_o.

A gradual increase in the size and size distribution of microemulsion droplets with W_o is observed for all the three microemulsion systems. At constant surfactant concentration with low water content, surfactants bind the solubilized water in the polar core of reverse micelles which ultimately strengthen the boundary. At high water content, the bound water would turn into bulk water as water swell in the core and droplet size increases (Figure 2.4). The increase in size can be attributed to the fact that an increase in water content increases the film fluidity of the reverse micelles. Coalescence of the reverse micelles, which are in continuous Brownian motion, results in collision and hence the droplets combine to form larger droplets.

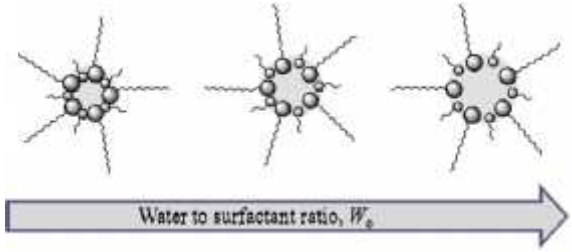

Figure 2.4. Increase in size of droplets of microemulsions with increasing W_o.

With increasing concentration of surfactant (Table 2.5) the hydrodynamic diameter of droplets of TX-100 microemulsion decreased from approximately 37 nm to about 15 nm (Figure 2.5). As the concentration of surfactant increases W_o decreases resulting in

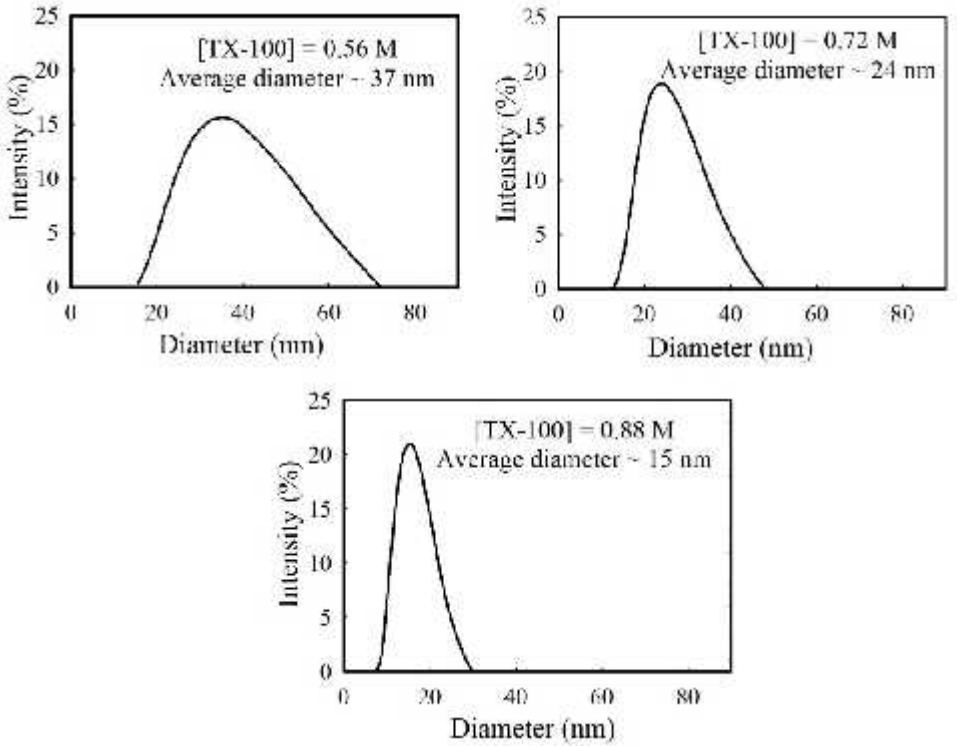

Figure 2.5. Average size and size disribution of microemulsion droplets of TX-100 microemulsions with [TX-100].

the formation of small aqueous cores in the droplets (Figure 2.6). More the concentration of surfactant, higher is the solubilization of all aqueous components in the head group layer of the surfactant to form reverse micelles with smaller aqueous pools.[25] Again higher surfactant concentration gives high stability against droplets coalescence and thus generates smaller droplet size.[26]

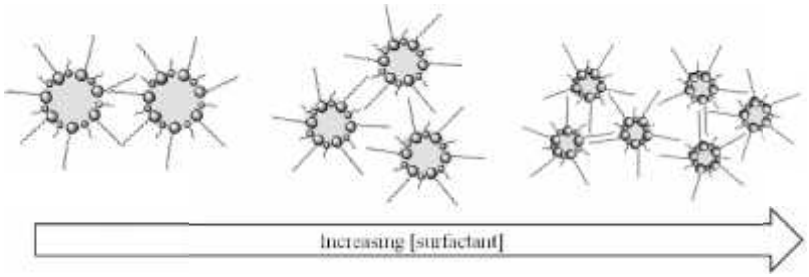

Figure 2.6. Decrease of size of microemulsion droplets with [surfactant].

2.3.3. Effect of cosurfactant on the size of microemulsions

To understand the effect of cosurfactant on the formation of microemulsions, microemulsions of TX-100 with and without assistance of cosurfactant, 1-pentanol have been prepared at both low (0.16 M) and high (0.88 M) concentrations of surfactant. At low surfactant concentrations (Table 2.6) TX-100 did not form microemulsions without the assistance of a cosurfactant. With increasing P_o the size of microemulsion droplets decreased and size distribution became narrower (Figure 2.7).

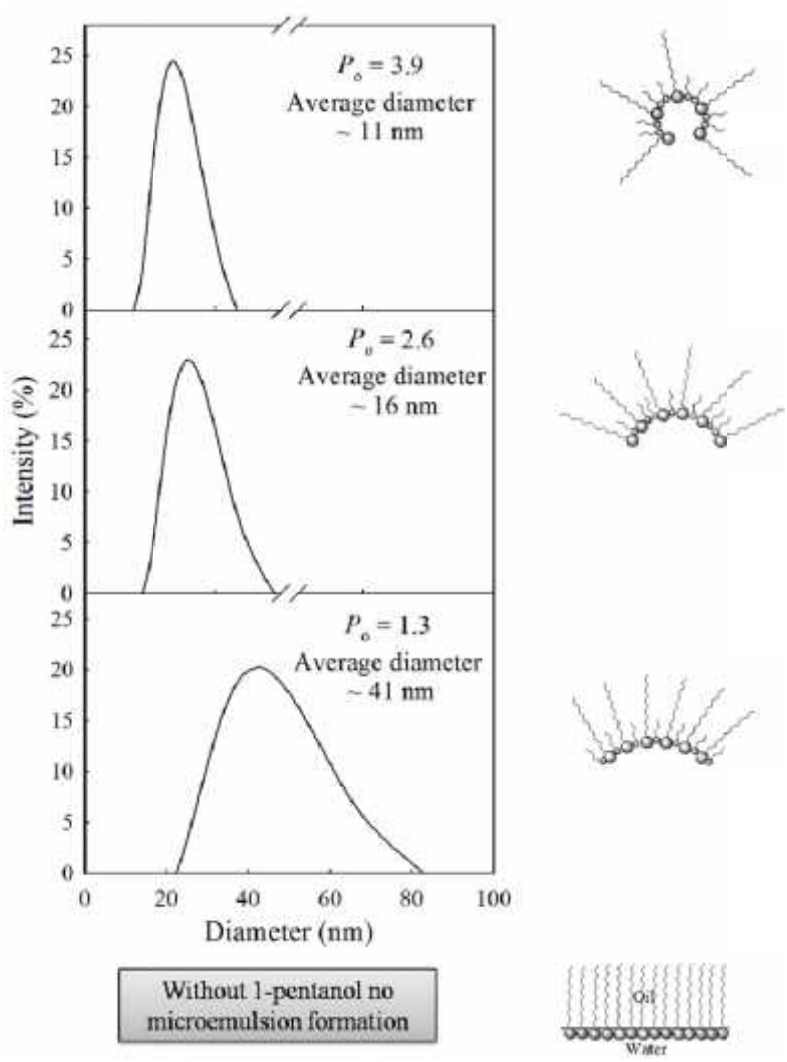

Figure 2.7. Average size and size distribution of microemulsion droplets of TX-100 microemulsions with increasing concentration of 1-pentanol at low surfactant concentration ([TX-100] = 0.16 M) and the corresponding bending of interfacial film of microemulsion droplets.

The size of the microemulsion droplets became a function of the cosurfactant concentration. The more the cosurfactant, the lower was the droplet size. At higher surfactant concentrations microemulsion was formed even without addition of 1-pentanol (Table 2.7). The addition of 1-pentanol caused lowering of the size and size distribution of microemulsion droplets (Figure 2.8).

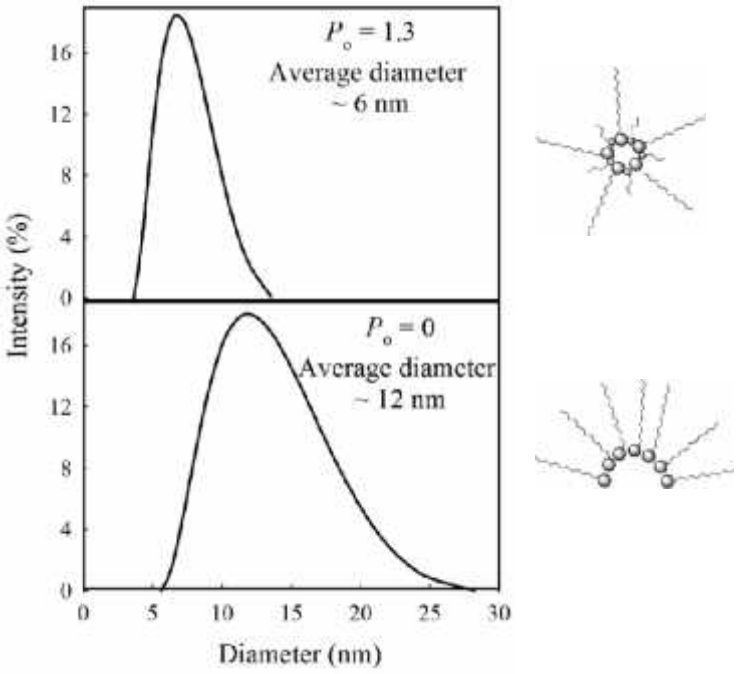

Figure 2.8. Average size of microemulsion droplets of TX-100 microemulsions with increasing 1-pentanol at high surfactant concentration ([TX-100] = 0.88] and the corresponding bending of interfacial film of microemulsion droplets.

There is always a bending stress associated with droplet formation in micoemulsion. When surfactant concentration was low, surfactant alone (without 1-pentanol) could not bend oil-water interface and phase separation occurred. But addition of cosurfactant gave stable microemulsion. This is because, surface active cosurfactant molecules easily snuggled themselves among the surfactant molecules at the droplet/liquid interface whereby releasing the bending stress[2] assisting surfactant to lower the oil-water interfacial tension[27] to bend the interface and microemulsion was thus formed. With increasing cosurfactant, adsorption of alcohols at the surfactant interfacial film modifies the surfactant packing parameters[28] and bend the film to a greater degree which ultimately decreased the curvature radius of microemulsion droplets. At higher surfactant concentrations, surfactant itself was enough to reduce oil-water interfacial tension and microemulsion of smaller dimension was formed compared to the droplets obtained with lower surfactant concentration at the same W_o

and P_o. In both cases (lower and higher surfactant concentration) higher alcohol concentration makes surfactant molecules pack more closely which reduces the water uptake and thereby reduces the size of reverse micelles.[29]

To study the effect of chain length of cosurfactant, alcohols with increasing carbon chain length, from 1-butanol to 1-octanol were used for TX-100 microemulsions keeping all other parameters constant at a fixed W_o for all the systems (Table 2.8). DLS measurments show the size distribution of microemulsion droplets with increasing chain length of the cosurfactants for TX-100 microemulsions (Figure 2.9).

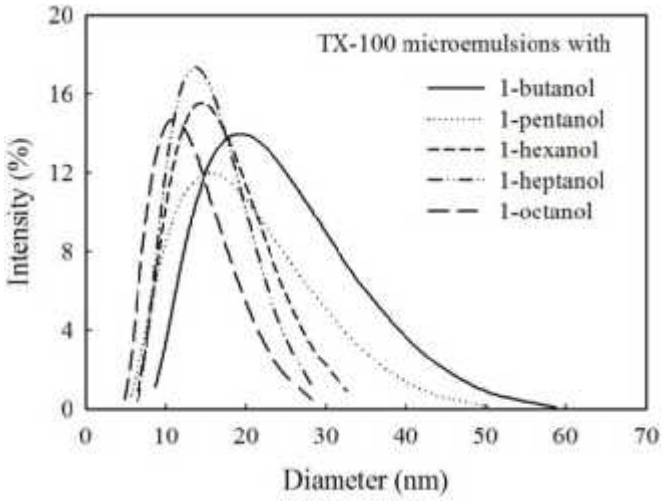

Figure 2.9. Size distribution of microemulsion droplets with increasing chain length of the cosurfactants for TX-100 microemulsions.

DLS results show the decrease in the droplet-size and size distribution in the microemulsions with an increase in the carbon chain length of the cosurfactant (Figure 2.9 and Table 2.10).

Table 2.10. Average diameter of microemulsion droplets of TX-100 microemulsions with increasing carbon chain length of cosurfactant

Cosurfactants	Average diameter of microemulsion droplet (nm) from DLS measurements
1-butanol	21
1-pentanol	17
1-hexanol	15
1-heptanol	14
1- octanol	12

The cosurfactant influences the geometric packing of surfactant and consequently alters the curvature of the interfacial films. Addition of shorter chain cosurfactant gives positive curvature effect as alcohol swells the head region more than the tail region. So, it becomes more hydrophilic and o/w type microemulsion is favored. While longer chain cosurfactant favors w/o type by alcohol swelling more in chain region than head region.[30] For the formation of stable w/o microemulsion the role of the cosurfactant is to reduce the stress at both sides of the droplet interfacial layer. All cosurfactants used in this experiment have a single OH group in contact with water and have the same effect on the stress at the headgroup side but this stress at the tail-group side of the layer reduces more as the carbon chain length increases[10] because interaction energies of alcohol with oil increase with the number of carbon atoms of the alcohol.[29] This results in a decrease in the spontaneous radius of curvature as the carbon chain length of cosurfactant increases (Figure 2.10).[10] Thus for a fixed alcohol concentration, with increasing carbon chain length interfacial film become flexible enough to deform readily around droplets and bend to a greater extent. So longer the hydrocarbon chain of alcohol, the smaller is the water uptake of reverse micelles.[29] For these reasons longer the cosurfactant chain length smaller is the size of microemulsion droplets.

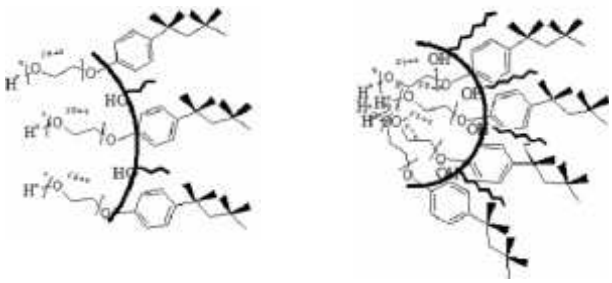

Figure 2.10. Increase of mean curvature of microemulsion droplets as the chain length of cosurfactant increases.

2.4. Conclusions

Microemulsion droplet diameter could be tuned by the proper choice of microemulsion variables. The dependence of diameter of microemulsion droplets on surfactant (type and concentration), water content, cosurfactant (concentration and chain length) was measured. An increase in the size of microemulsion with increasing hydrophilicity of the surfactant was observed. Higher surfactant concentration generated smaller droplet size. The W_o also influenced the average size of the microemulsion droplets. As the W_o increased, the droplet-size in the microemulsions

increased. At low surfactant concentration cosurfactant was required for stability of w/o microemulsions and with increasing the amount of cosurfactant the droplet-size in the microemulsions decreased. But at higher surfactant concentrations, micoemulsion was formed without the assistance of cosurfactant and in this case also addition of cosurfactant caused lowering of the droplet-size in the microemulsions. Cosurfactant with longer chain length reduced the size of the droplets. All these results suggest that, it is possible to fine-tune the droplet-size in w/o microemulsions.

References

(1) Meyers, D. Surfaces, interfaces and colloids, VCH Publishers, Inc., New York, 1991.
(2) Fanun, M. Microemulsions: Properties and application, CRC press, **2009**, *144*.
(3) Luisi, P. L.; Straube, B. E, Reverse Micelles, Plenum Press, New York, 1984.
(4) Moulik S.P.; Paul B.K. Structure, dynamics and transport properties of microemulsions. *Adv. Coll. Int. Sci*. **1998**, *78*, 99-195.
(5) Langevin, D. Microemulsions. *Acc. Chem. Res*. **1988**, *21*, 255-260.
(6) Magno, L. M.; Angelescu, D. G.; Siglec, W.; Stubenrauchad, C. Microemulsions as reaction media for the synthesis of Pt nanoparticles. *Phys. Chem. Chem. Phys*. **2011**, *13*, 3048-3058.
(7) Ranjan, R.; Vaidya, S.; Thaplyal, P.; Qamar, M.; Ahmed, J.; Ganguli, A. K. Controlling the size, morphology, and aspect ratio of nanostructures using reverse micelles: a case study of copper oxalate monohydrate. *Langmuir* **2009**, *25*, 6469-6475.
(8) Zhang, W.; Qiao, X.; Chen, J. Synthesis of silver nanoparticles—Effects of concerned parameters in water/oil microemulsion. *Mater. Sci. Eng. B* **2007**, *142*, 1-15.
(9) Kumar, P.; Mittal, K. L. Handbook of microemulsion science and technology, CRC Press, **1999**, 849.
(10) Lang, J.; Lalem, N.; Zana, R. Droplet size and dynamics in water-in-oil microemulsions. *Colloids and surfaces* **1992**, *68*, 199-206.
(11) Petit, C.; Bommarius, A. S.; Pileni, M-P.; Hatton, T. A. Characterization of a four-component cationic reversed micellar system: dodecyltrilmethylammonium chloride/hexanol/n-heptane and 0.1 M KCl solution. *J. Phys. Chem.* **1992**, *96*, 4653-4658.
(12) Lang, J.; Mascolo, G.; Zana, R.; Luisi, P. L. Structure and dynamics of cetyltrimethylammonium bromide water-in-oil microemulsions. *J. Phys. Chem*. **1990**, *94*, 3069-3074.
(13) Lang, J.; Jada, A.; Malliaris, A. Structure and dynamics of water-in-oil droplets stabilized by sodium bis(2-ethylhexyl) sulfosuccinate. *J. Phys. Chem*. **1988**, *92*, 1946-1953.
(14) Zhang, W.; Qiao, X.; Chen, J. Synthesis of silver nanoparticles—effects of concerned parameters in water/oil microemulsion. *Mater. Sci. Eng., B* **2007**, *142*, 1-15.

(15) Lang, J.; Lalem, N.; Zana, R. Quaternary water in oil microemulsions. 1. effect of alcohol chain length and concentration on droplet size and exchange of material between droplets. *J. Phys. Chem*. **1991**, *95*, 9533-9541.
(16) Goddeeris, C.; Cuppo, F.; Reynaers, H.; Bouwman, W. G.; Mooter, G. V. d. Light scattering measurements on microemulsions: Estimation of droplet sizes. *Int. J. Pharm*. **2006**, *312*, 187-195.
(17) Schatzel, K. Light-scattering - Diagnostic methods for colloidal dispersions. *Adv. Colloid Interface Sci*. **1993**, *46*, 309-332.
(18) Gutiérrez-Becerra, A.; Barcena-Soto, M.; Soto, V.; Arellano-Ceja, J.; Casillas, N.; Prévost, S.; Noirez, L.; Gradzielski. M.; Escalante, J. I. Structure of reverse microemulsion-templated metal hexacyanoferrate nanoparticles. *Nanoscale Res. Lett*. **2012**, *7*, 1-12.
(19) Khan, M. F.; Singh, M. K.; Sen, S. Measuring size, size-distribution and polydispersity of water-in-oil microemulsion droplets using fluorescence correlation spectroscopy: comparison to dynamic light scattering. *J. Phys. Chem. B* **2016**, 1-14.
(20) Housaindokht, M. R.; Pour, A. N. Study the effect of HLB of surfactant on particle size distribution of hematite nanoparticles prepared via the reverse microemulsion. *Solid State Sci*. **2012**, *14*, 622-625.
(21) Emmanuel, E.; Hanna, K.; Bazin, C.; Keck, G.; Clément, B.; Perrodin, Y. Fate of glutaraldehyde in hospital wastewater and combined effects of glutaraldehyde and surfactants on aquatic organisms. *Environ. Int.* **2005**, *31*, 399- 406.
(22) Liveri, V. T. Controlled synthesis of nanoparticles in microheterogeneous systems. Springer, **2006**, New York, USA.
(23) Eastoe, J.; Hollamby, M. J.; Hudson, L. Recent advances in nanoparticle synthesis with reversed micelles. *Adv. Colloid Interface Sci*. **2006**, *128-130*, 5-15
(24) Kimijima, K.; Sugimoto, T. Effects of the water content on the growth rate of AgCl nanoparticles in a reversed micelle system. *J. Colloid Interf. Sci*. **2005**, *286*, 520-525.
(25) Chang, C.-L.; Fogler, H. S. Controlled formation of silica particles from tetraethyl orthosilicate in nonionic water-in-oil microemulsions. *Langmuir* **1997**, *13*, 3295-3307.
(26) Chin, S. F.; Azman, A.; Pang, S. C. Size controlled synthesis of starch nanoparticles by a microemulsion method. *J. Nanomater*. **2014**, 1-7.
(27) Marchand, K.E.; Tarret, M.; Lechaire, J.P.; Normand, L.; Kasztelan, S.; Cseri, T. Investigation of AOT-based microemulsions for the controlled synthesis of MoS_x nanoparticles : an electron microscopy study. *Colloids Surf., A* **2003**, *214*, 239-248.
(28) Curri, M. L.; Agostiano, A.; Manna, L.; Monica, M. D.; Catalano, M.; Chiavarone, L.; Spagnolo, V.; Lugarà, M. Synthesis and characterization of CdS nanoclusters in a quaternary microemulsion: the role of the cosurfactant. *J. Phys. Chem. B* **2000**, *104*, 8391-8397.
(29) D. S.; Mathew, Juang, R-S. Role of alcohols in the formation of inverse microemulsions and back extraction of proteins/enzymes in a reverse micellar system. *Sep. Purif. Technol*. **2007**, *53*, 199-215.
(30) Fanun, M. Colloids in Biotechnology. CRC Press, *152*, **2011**.

Abstract

In this study, metal nanoparticles (copper (Cu), zinc (Zn), silver (Ag) and iron (Fe)) have been prepared by reduction of corresponding metal salts in microemuslions. The effects of various size controlling parameters of microemulsions on the size of metal nanoparticles prepared in these systems have been correlated with the size of microemulsion droplets; in other words, the correlation between the size controlling parameters and the tunability of the size of metal nanoparticles has been discussed. DLS results showed that microemulsions prepared from different surfactants result in the formation of nanoparticles of varying size. The average size of nanoparticles was affected by water to surfactant ratio, W_o and surfactant concentration. The cosurfactant also played a major role in regulating the dimensions of nanoparticles. Increasing the concentration and chain length of the cosurfactant resulted in relatively smaller nanoparticles. In most of these cases there was a concomitant relation between the size of nanoparticles and microemulsion droplets and this study focuses on understanding the template role of microemulsion droplets to control over the size of nanoparticles. Then antibacterial sensitivities of the nanoparticles against Gram-negative *Escherichia coli* (*E. coli*) and Gram-positive *Staphylococcus aureus* (*S. aureus*) were tested by zone of inhibition method. All the nanoparticles showed antibacterial activity against *E. coli* and *S. aureus* at very low concentrations. Ag nanoparticles showed higher antibacterial activities compared to other nanoparticles. At high concentrations, Ag and Cu nanoparticles showed sensitivity comparable to conventional antibiotics against *E. coli*. The concentration dependence of antibacterial activity, however, has been less pronounced.

3.1. Introduction

In recent years, resistance traits in bacteria and other pathogens because of the continuous selection of antibiotics. Therefore the development of new and effective antimicrobial agents has become an important topic of current research.[1-8] Metallic nanoparticles having dimensions in the order of 100th of nm or less as discussed in section 1.5, have been embraced by biomedical sectors with their huge potential in antimicrobial functionality.[9] Different metallic nanoparticles, including copper (Cu), zinc (Zn), silver (Ag) and iron (Fe) are known for their antibacterial capability.[10-15] Although metallic Ag has been used for their antimicrobial activity from the age of ancient Egyptians with little hazardous side effects to mammalian cells its widespread

uses become limited because of high cost. Preparation of nanoparticles solves this by reducing the cost. Furthermore, high specific surface area and high fraction of surface atoms of nanoparticles make them more effective as antimicrobial agent compared to bulk metal.[16] Thus Ag nanoparticles exhibit excellent biocidal activity against 650 types of bacteria, viruses and fungi[17] limiting the development of resistant microbial strains[7,18,19] at exceptionally low concentrations[20] with low toxicity toward mammalians.[21] Among other antibacterial metallic nanoparticles Cu,[22.23] Zn and Fe are also of great interest nowadays because of their low cost and easy availability. But the practical applications of metallic nanoparticles are mainly size and morphology dependent and they show dimension dependent antibacterial activity.[24-27] Precise control of the size of nanoparticles is therefore very important in recent years and nanoparticles with controlled size are highly desirable. Different synthetic methods for the preparation of nanoparticles have been developed amongst which w/o microemulsions allows the flexibility to control the size of nanoparticles with monodispersity.[28] As discussed in section 1.7, w/o microemulsion is a thermodynamically stable dispersion of water droplets in continuous oil medium which are stabilized by a surface monolayer (called the interphase) comprising closely arranged surfactant and cosurfactant molecules. In w/o microemulsions, these droplets are assumed spherical and mono disperse[29] which can solubilize metal salts and precipitating agent and thus provide a compartmentalized medium to carry out chemical reactions in restricted geometries where nucleation, growth and agglomeration of particles become limited.[30] The cage lake effect of these nanodroplets allow to obtain regular and monodispersed particles.[31] In other words, the diameter and morphology of nanoparticles obtained in such a medium can be controlled by the nanodroplets of microemulsion.[32] This control is due to the change in size of the dispersed phases with change in some control parameters of microemulsions such as surfactant, cosurfactant, amount of water. Earlier studies realized that these factors affect the size and shape of nanoparticles obtained from microemulsion synthesis.[33] Nature of surfactants- their type, size, charge, rigidity and HLB affect the microenvironment tremendously and hence play a crucial role in guiding the size, shape and stability of nanomaterials.[34,35] Many researchers showed that final particle size was dependent on the initial water to surfactant ratio, W_o and surfactant concentration of microemulsions.[36] Cosurfactant has effect on the flexibility of the interfacial film[37] and thereby influence dynamic exchange process in

w/o microemulsion.[38] Addition of cosurfactants can make the interfacial film more fluidic and thus increase coalescence rate of droplets to give larger particles.[39] Chain length of cosurfactant along with W_o can also alter morphology; spherical, ellipsoidal particles, nanotubes and nanorods in case of ZnS nanoparticles.[40] The role of surfactant, cosurfactant, and the aqueous content on the size and morphology of the copper oxalate have been discussed elaborately.[28] However, the effect of these parameters on the size of microemulsion droplets and the finally formed nanoparticles is not still clear. In chapter 2 it has been shown that the size of the microemulsion droplets could be modified by varying the relation of the components of the microemulsion and surfactant, cosurfactant, and the aqueous content could modulate the droplet size. In this chapter the aforementioned four metallic nanoparticles were prepared in the microemulsion systems. A systematic study was accomplished to understand the role of different parameters of micoemulsions on the size of nanoparticles and to know whether any correlation exist between the sizes of droplets and finally formed nanoparticles. The antibacterial properties of nanoparticles were then investigated against Gram-negative Escherichia coli (*E. coli*) and Gram-positive, Staphylococcus aureus (*S. areus*) by zone of inhibition method. The objective of this was to compare the bactericidal effect of the four nanoparticles. Such a comparative study would reveal strain specificities and would eventually lead to better utilization of nanoparticles for specific applications.

3.2. Experimental

3.2.1. Materials and methods

Materials used and methods followed for the preparation and characterization (size of droplets) of microemulsions have been described in detail in section 2.2.1, 2.2.2 and 2.2.3.

For the preparation of nanoparticles in microemulsions copper chloride (Merck), zinc chloride (Merck), ferric chloride (Merck), silver nitrate (BDH), and $NaBH_4$ (ACROS ORGANICS) were used as received without any further purification. Solutions were prepared with double distilled de-ionized water (conductivity: 0.055 μScm^{-1} at 25.0 °C) from HPLC grade water purification system (BOECO, Germany). Microemulsions were prepared with variation in the surfactant, cosurfactant and water content (described in section 2.2.2).

Nanoparticles were then synthesized using double microemulsions reactant addition scheme (outlined schematically in Figure 1.5 (b)). Breifly, 2 mL of two microemulsions, one solubilized with metal ions and the other with $NaBH_4$ as reducing agent were mixed after bubbling with high-purity N_2 gas and sonicated for about 30 min. An immediate color change was observed for all the metal nanoparticles. For Cu it changed from blue to brown suggesting a change in the oxidation state of Cu and formation of metallic particles.[41] For Zn the color of microemulsion changed from colorless to dark gray, for Ag it was from colorless to golden yellow and for Fe, color change was from light orange to black. All these imply the formation of corresponding metal nanoparticles incorporated in microemulsion.[42-44]

3.2.2. Characterizations

The optical absorption spectra for nanoparticles in microemulsion were recorded using a double beam Shimadzu UV-Visible spectrophotometer, UV-1650 PC. Rectangular quartz cells of path length 1 cm were used throughout the investigation. Size and size distribution of the nanoparticles synthesized in the water pools of the reverse micelles of w/o microemulsion were measured by DLS measurements following same methodology as described in section 2.2.3 with the necessary correction for absorbance at 632.8 nm obtained from the UV-visible spectroscopy. The same equipment was used to determine zeta potential (ζ) for surface charge of Cu nanoparicles. For this purpose, nanoparticles were prepared without using microemulsion simply by mixing equal volumes of aqueous copper chloride and $NaBH_4$. The cuvette used in this experiment was universal dip cell. The electrophoretic mobilities of the particles using Huckel equation were used for the calculation. Morphological analyses of nanoparticles were carried out using JEOL analytical scanning electron microscope (SEM), model JSM-6490LA at an acceleration voltage of 20 kV just after the preparation of nanoparticles. A drop of nanoparticles in the microemulsion was dropped on the carbon coated aluminum stubs by a micropipette. The sample on the stub was allowed to evaporate the solvent at ambient temperature. Energy dispersive X-ray (EDX) spectral analyses were also carried out (JSM-6490LA) to confirm the presence of elemental metal. For this, nanoparticles were separated from microemulsoin by centrifugation for 1 h and

dispersed in ethanol by sonication to make a ethanol suspension. A drop of suspension was dropped on the sample stage and allowed to evaporate at room temperature.

3.2.3 Antibacterial activity

The antibacterial activities of Cu, Zn, Ag and Fe nanoparticles were evaluated using zone of inhibition method against *E. coli* and *S. aureus*. The Mueller-Hinton agar was autoclaved, cooled down to room temperature, poured on a 90 mm plate at a depth of 4 mm and left to solidify. The suspension of bacterial culture was freshly grown in liquid medium at pH 7.2 and diluted approximately to 1.3×10^8 cells mL^{-1}. Using ascetic technique and sterile cotton swab this broth culture was streak on the agar plate uniformly by rotating the plate 90^o. Freshly prepared nanoparticles in TX-100 microemulsion ($W_o = 10$) were separated by the addition of excess amount of acetone and centrifugation for about 1 h. The as separated nanoparticles were washed with acetone several times followed by dispersion in de-ionized water. 10 μL of 0.1μg mL^{-1} dispersion of each nanoparticles were dropped in different zones of the plate. Water was used as control. After 20 h incubation at 37 ^oC the zones of inhibition were measured and the results were expressed in diameter (mm). For Ag and Cu nanoparticles antibacterial activities against *E. coli* were also tested at higher concentration. For this 30μL of 1μg mL^{-1} ethanol suspension of each nanoparticles and their diluted solutions (10 and 100 times dilution) were dropped in different zones of the plate. After incubation for 24 h at 37 ^oC the zone size for inhibition around each drop was measured and antibacterial activities were compared with conventional antibiotics.

3.3. Results and discussion

3.3.1. Effect of type of surfactant on the size of Cu nanoparticles

Cu nanoparticles were prepared in microemulsions of three different surfactants namely SDS, TX-100 and CTAB at W_o = 7.7. All other components of microemulsions (1-butanol, cyclohexane and water) were kept at fixed concentration in order to investigate the effect of surfactant on the size of Cu nanoparticles. For all of the systems, the final concentration of Cu^{2+} and $NaBH_4$ were 0.4 mmol and 0.8 mmol respectively for the reduction of $CuCl_2$.

UV–visible absorption spectra for Cu nanoparticles in three different microemulsions were recorded (Figure 3.1). UV–visible spectroscopy has been a frequently used technique to characterize the synthesized metal and metal oxide nanoparticles. It is used as a general experimental test of metallic free-electron behavior in metal clusters. The absorption spectra of the reduction products of $CuCl_2$ in SDS and TX-100 microemulsions, show an absorption peak at 300 nm. In CTAB microemulsions absorbance peak shifts to shorter wavelength at 280 nm. Colloidal metallic nanoparticles exhibit absorption bands or broad regions of absorption in the UV-visible range. This accounts for the effects of both the free-electron and electronic interband transition. The interaction of light with free electrons in metallic nanostructures can give rise to collective excitations known as plasmon resonances (discussed in section 1.5). The excitation of plasma resonances or interband transitions, are thus a very characteristic property of the metallic nature of the particles. But in all the three microemulsions, no characteristic absorption peak for surface plasmon resonance of Cu nanoparticles can be seen, which is generally found between 500-600 nm.[45] Nanoparticles show strong peak for surface plasmon resonance when plasmon resonant energies are well below the interband transitions. These nanoparticles can be treated as free-electron systems whose optical properties are determined by the conduction electrons leading to minimal damping of the plasmon. But for Cu, a less free-electron metal the effects of strong interband transitions near the same energies as the plasmon response of the solid metallic nanoparticles are responsible for a strong damping of the Cu nanosphere plasmon and thereby a weak plasmon resonance peak is visible on top of the strong background absorption.[46,47] But here no such peak is noticeable and absorption peak of Cu

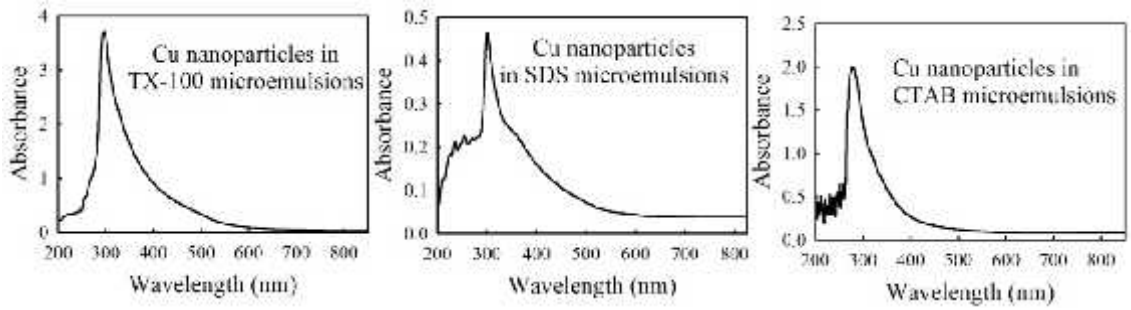

Figure 3.1. Absorption spectra of Cu particles obtained in three different microemulsions (W_o = 7.7).

colloids (prepared in microemulsions from low concentration Cu salt) observed in the UV region might be assigned to the metal interband transitions.[48] Also, no characteristic absorption band for Cu oxide around 800 nm was observed suggesting that the synthesized Cu nanoparticles is purely metallic and free of oxides.[49] It is known that the absorption in the UV region due to the interband transition is insensitive to the particle size but is sensitive to the particle quantity.[49] The increasing particle quantity results in the growth of the absorbance in the UV region. Therefore, the obtained spectra of Cu colloids suggest that the order of decreasing particle concentration in microemulsions is TX-100 > CTAB > SDS.

The average size and size distributions of Cu nanoparticles were measured by DLS. From the Figure 3.2 it can be seen that the size of Cu nanoparticles are different when prepared in different microemulsions. The decreasing order of size of Cu nanoparticles is SDS > CTAB > TX-100 microemulsions. DLS measurements gave different average size of droplets for microemulsions of different surfactants as discussed in section 2.3.1. As shown in the results average size of the microemulsion

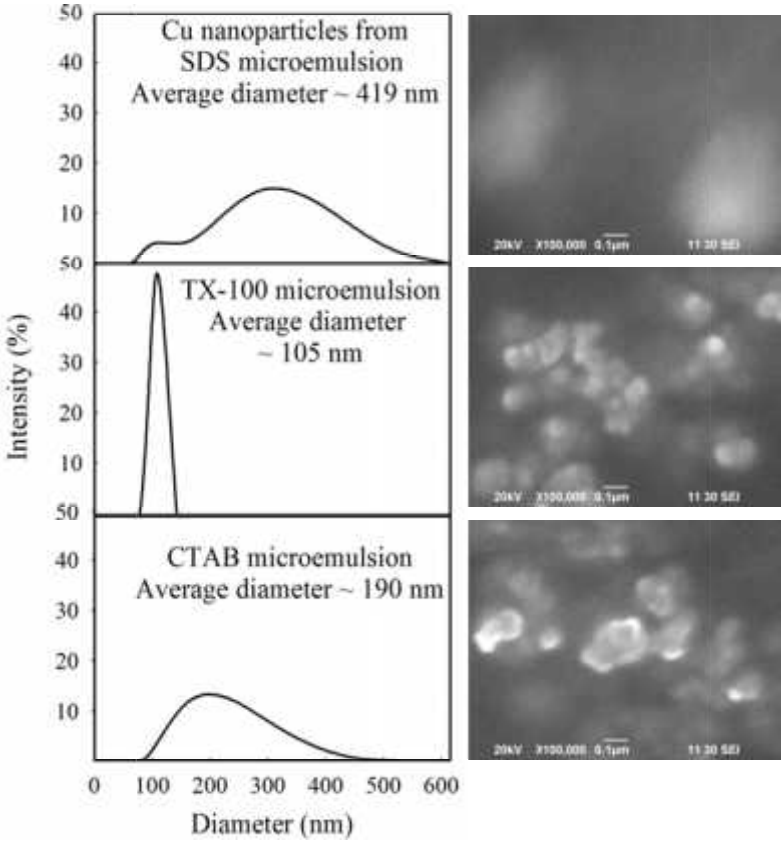

Figure 3.2. Average size of Cu nanoparticles from DLS measurement and their SEM images.

droplets decreased in the order SDS > TX-100 > CTAB microemulsion which decreased with HLB value of surfactants. But the size of Cu nanoparticles prepared in these systems did not follow the same trend as microemulsion droplets. In fact the size of nanoparticles depend on initial nucleation rate and also on the growth rate of nucleus. Among SDS and CTAB microemulsions for larger SDS micoemulsion droplets initial nucleation rate became slower for dilution effect. Again shorter hydrophobic chains (12 carbon chain) compared to those in CTAB (16 carbon chain) may lead to a less rigid interface[36] for SDS microemulsion thus potentially escalate intermicellar exchange and growth rate because the channel of fused dimmer through which growth occurs was larger than that of CTAB (Figure 3.3). In case of CTAB microemulsion a more favorable interaction of CTAB tails with solvent (cyclohexane) allowed the solvent to insert itself within the surfactant tails thus creating a more rigid micelle and for this reason viscosity of CTAB microemulion (2.4390 mPa s) is also higher than SDS microemulsion (1.9850 mPa s).[50] This low viscosity of SDS micoemulsion increased diffusion constant K ($K = 8000RT/3\eta$, R is the universal gas constant, T is the temperature and η is the dynamic viscosity of the medium)[51] which also facilitated higher exchange rate of intermiceller content. Particle growth through the dynamic intermicellar exchange of the micelle contents in case of SDS microemulsion thus became higher than CTAB microemulsion.

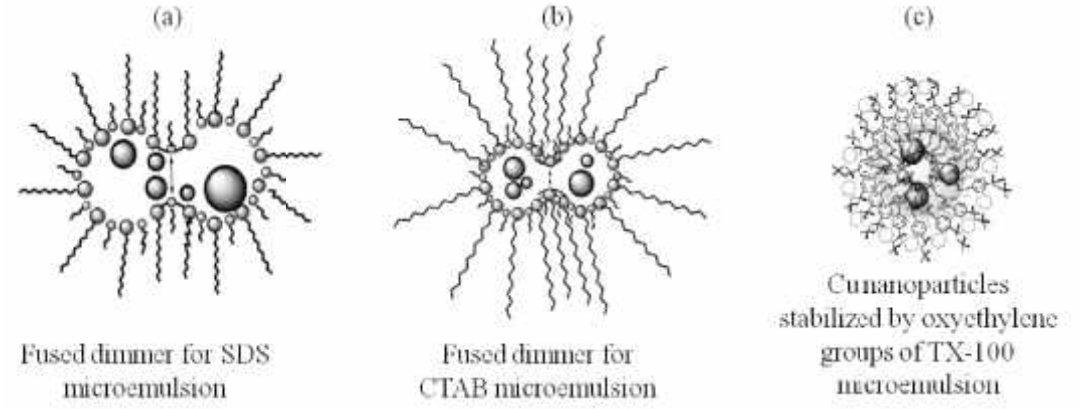

Figure 3.3. Growth process of Cu nanoparticles through the channel of fused dimmer in case of (a) SDS and (b) CTAB microemulsion and (c) stabilization of Cu nanoparticles in TX-100 microemulsions.

But the average size of Cu nanoparticles in TX-100 microemulsion is markedly smaller (from SEM image of Figure 3.2) though the average diameter of microemulsion droplets are larger than CTAB microemulsions. It might be due to the

fact that the rigidity of nonionic surfactant TX-100 is higher than CTAB[34] and viscosity of TX-100 microemulion [3.0662 mPa s] was highest among the three microemulsion systems for which further growth of nanoparticles was inhibited. In this case nanoparticles were stabilized by oxyethylene groups (Figure 3.3 (c)).[52] For this in TX-100 microemulsion Cu nanoparticles have been found to be stable for about several months without precipitation. But in CTAB, Cu nanoparticles were stable for about 15-20 days while in SDS within 2 h precipitation occurred. The stability of Cu nanoparticles might result from the surface charge of Cu nanoparticles and the type of surfactants. For surface charge of Cu nanoparticles zeta potential was measured in absence of microemulsion in aqueous system which gave a lower positive value (+4.31 mV). This implies that repulsion was not so strong and natural tendency of aggregation among the particles prevails in aqueous system.[53] In microemulsions surfactants self-align to form micelle by the interaction between hydrophilic head and hydrophobic tails. In CTAB microemulsions, Cu nanoparticles were captured in the center of micelle because of repulsion of surface charge on Cu nanoparticles with positively charged surfactants; hence these nanoparticles were protected by the surfactant. Repulsion cannot lead further growth by intermicellar exchange. For anionic surfactant (SDS), Cu nanoparticles were attracted by the negative charge of the surfactant. Intermicellar exchange can take place because of attraction between the opposite charges on Cu nanoparticles and surfactant. Hence agglomeration occurs near the inside of reverse micelles. Upon collision these aggregation increased for lower surfactant layer rigidity of SDS and agglomerated Cu nanoparticles then released out of the microemulsions and precipitated.

3.3.2. Effect of water content on the size of metal nanoparticles

To understand the effect of water content of microemulsions on the size of metal nanoparticles W_o for three different microemusions (SDS, CTAB and TX-100 microemulsions), the concentration of the surfactant at constant W_o for TX-100 microemulsions were varied (details are described in section 2.2.2.1.2).

3.3.2.1. Preparation of Cu, Ag and Fe nanoparticles in SDS microemulsions

Cu, Ag and Fe nanoparticles were prepared in SDS/1-pentanol/cyclohexane/water microemulsions at different W_o. The final concentration of Cu, Ag and Fe salts were 1

mmol, 0.3 mmol, 0.5 mmol, respectively with 13 mmol of the reducing agent, $NaBH_4$. After the reduction of metal salts UV-visible absorption spectra of nanoparticles in SDS microemulsion at W_o = 7.7 have been recorded. The UV-visible spectrum of Cu nanoparticles (Figure 3.4) does not exhibit the characteristic peaks for inerband transition and plasmon resonance. In this experiment the Cu concentration was high. Within the water droplets high amount of Cl^- anions were present that can form insoluble salt with Cu. CuCl may be strongly adsorbed on Cu particles to form a monolayer of CuCl, resulting in strong damping of characteristic bands for Cu nanoparticles. The results obtained from EDX spectrum (Figure 3.5) confirmed the presence of some CuCl (Cl^- K_α at 2.621 KeV) and Cu particles as the main products of reduction in microemulsions. High concentration of Cl^- anions can readily form insoluble CuCl with Cu^+ in w/o microemulsion media. Therefore, it is conceivable that the formation of a CuCl monolayer on the Cu particles is responsible for the disappearance of the plasmon peak in the absorption spectrum of Cu particles obtained in this work.[54,55] But UV-visible spectrum of Ag nanoparticles shows a band around 400 nm which is caused by surface plasmon resonance of Ag nanoparticles.[55] A band around 300 nm was observed in the spectrum for Fe nanoparticles, which was caused by surface plasmon resonance of unoxidized Fe particles.[56]

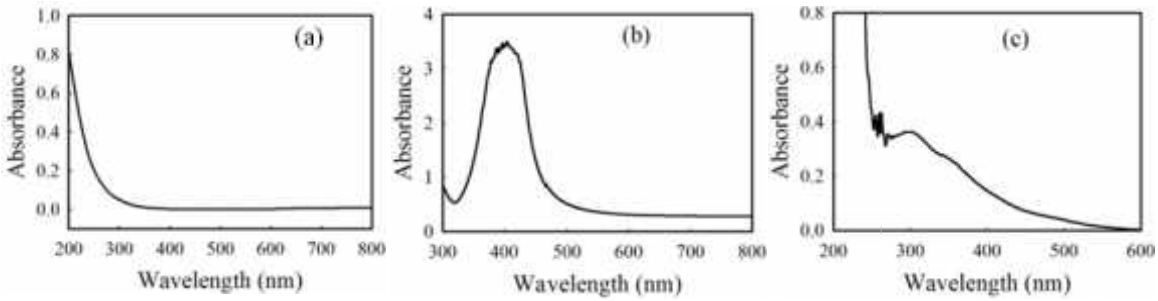

Figure 3.4. UV-visible spectrum of (a) Cu (b) Ag and (c) Fe nanoparticles in SDS microemulsions.

The EDX spectra confirm the presence of metallic Cu, Ag and Fe. The spectrum for Cu nanoparticles (Figure 3.5) shows K_α peak of Cu at 8.04 KeV which is almost equal to the calculated value from $E_{K\alpha}$ = (10.2 eV) $(Z-1)^2$ (where Z is the atomic number). There is also a peak of Al (K_α at 1.486 KeV) as it was the constituent of the sample stage. There are some other peaks for carbon and oxygen due to the ethanol suspension of Cu or probably from the hydrocarbon tail of surfactant.

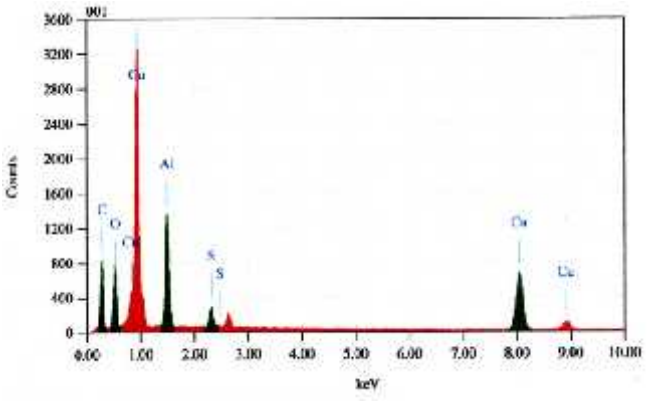

Figure 3.5. EDX spectrum of Cu nanoparticles.

The presence of Ag is observed from *L* peak of Ag at 2.983 KeV (Figure 3.6(a)). Presence of carbon and oxygen was also observed due to the ethanol suspension of Ag or probably from the surfactant where presence of sulfur and sodium was from the surfactant, SDS used in the experiment. Fe shows K_α peak of Fe at 6.398 KeV (Figure 3.6(b)) which is almost equal to theoretical calculations from the given equation. In this case also presence of other peaks were due to the above reasons.

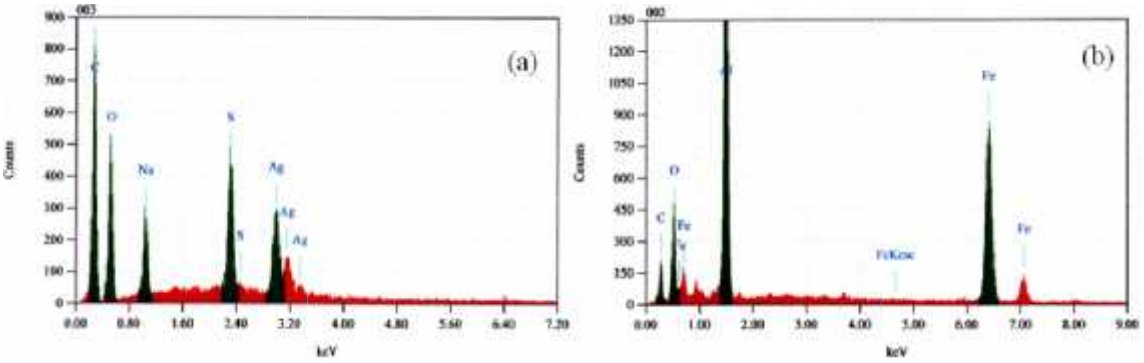

Figure 3.6. EDX spectra of (a) Ag and (b) Fe nanoparticles.

Figure 3.7. shows SEM images of three metal nanoparticles prepared in SDS microemulsions at different W_o. It is evident from the images, that Cu (a, b, c, d), Ag (e, f, g, h) and Fe (i, j, k, l) particles at different W_o are formed in nanodimensions. As W_o increased the average diameter of nanoparticles also increased. This trend is very similar to the variation in microemulsion droplet sizes shown in Figure 2.2.

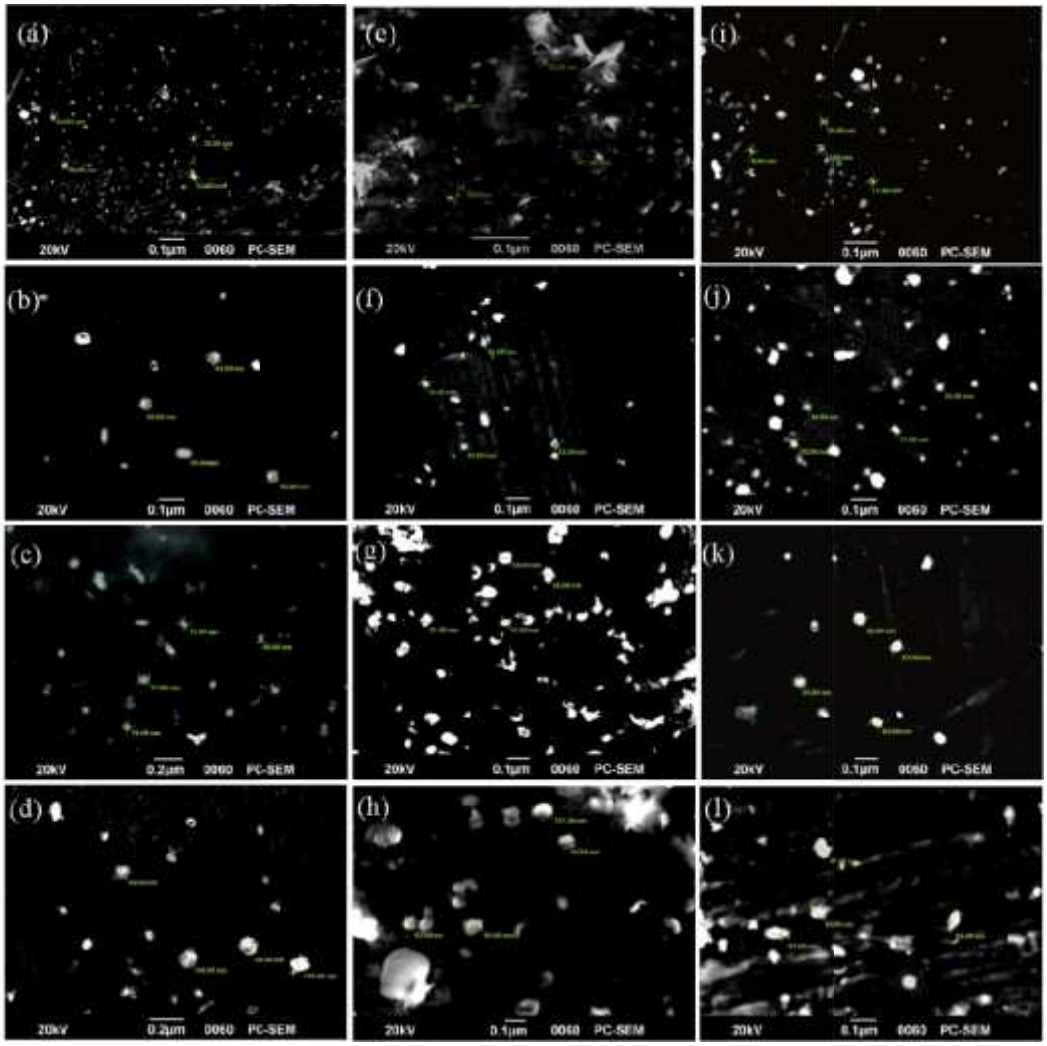

Figure 3.7. SEM images of Cu (a, b, c, d), Ag (e, f, g, h) and Fe (i, j, k, l) nanoparticles obtained in SDS microemulsions at different W_o: (a), (e), (i) 7.7; (b), (f), (j) 15.7; (c), (g), (k) 20.8; (d), (h), (l) 28.7.

From the average particle size of Cu, Ag and Fe estimated from SEM images, it is

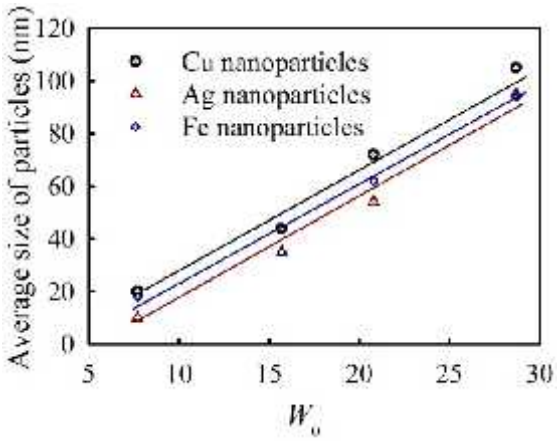

Figure 3.8. Average size of nanoparticles of Cu, Ag and Fe in SDS microemulsions as a function of W_o.

apparent that an increase in W_o causes a linear increase in the particle size in the microemulsions of SDS (Figure 3.8).

3.3.2.2. Preparation of Zn nanoparticles in CTAB and TX-100 microemulsions

Zn nanoparticles have been synthesized in cationic and nonionic w/o microemulsions of CTAB/1-butanol/cyclohexane/water and TX-100/1-butanol/cyclohexane/water. For the reduction of Zn salt in microemulsions the concentration of Zn^{2+} and reducing agent were 0.25 mmol and 0.5 mmol, respectively. The UV-visible absorption spectra of Zn nanoparticles (Figure 3.9. a, b) were then taken in microemulsion which revealed the formation of particles in nanodimension. The spectra show a band around at 265 nm in CTAB based microemulsions and 295 nm in TX-100 based microemulsions which were caused by surface plasmon resonance of Zn nanoparticles. The absorption band of Zn nanoparticles lies in the 242–285 nm range.[57,58] However, surface plasmon band location of Zn nanoparticles are dependent on medium polarity as reported in the literature. In aqueous solution of SDS, this absorption band lies at 242 nm[57] where in reverse micelles when the polarity of the medium decreases a bathochromic shift of this band occurs.[59] For Zn nanoparticles in solid matrices the strong and broad surface plasmon peaks lie at 260–285 nm.[58] At low W_o in case of TX-100 based microemulsions when micropolarity of the core water of microemulsion droplets is substantially lower than aqueous solution, the band can be expected to appear at longer wavelength.[59] The absence of characteristic absorption peak for Zn oxide at about 350 nm, suggest that the synthesized Zn particles are purely metallic and free of oxides.[57]

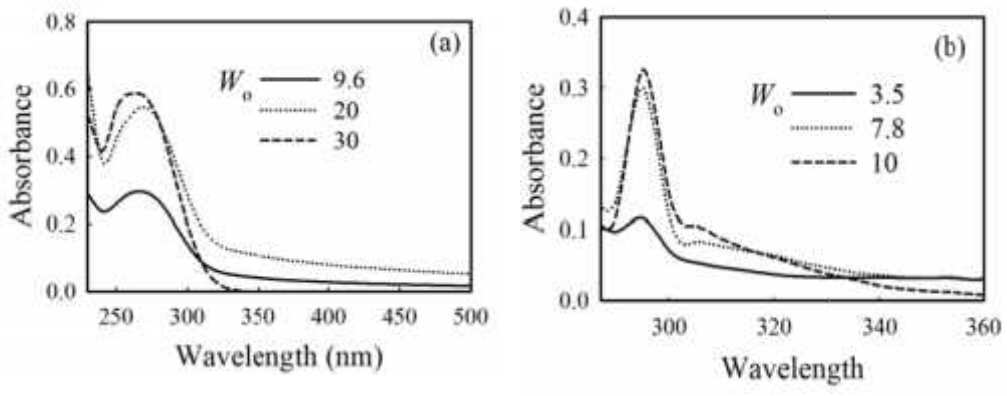

Figure 3.9. UV-visible absorption spectra of Zn nanoparticles obtained in w/o microemulsion of (a) CTAB and (b) TX-100 at different W_o.

Metallic Zn has the similar electron configuration as Au, Ag and Cu with closed *d*-bands. Therefore the shape and full width at half maximum (FWHM) of surface plasmon absorption peak of Zn nanoparticles are like noble metals, rather than transition metals where *d*-bands are partially filled.[58] FWHM of Zn nanoparticles in microemulsions were calculated. Figure 3.10 shows a representative plot to evaluate FWHM.The values of FWHM for different W_o have been tabulated in Table 3.1.

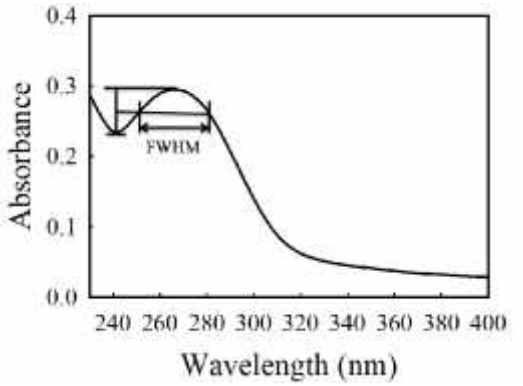

Figure 3.10. FWHM caculated from UV-visible absorbance spectrum of Zn nanoparticles in CTAB microemulsion at $W_o = 9.6$.

FWHM increased with increasing W_o for particles in both microemulsions. The FWHM is considered to be quite useful in understanding the particle size and their distribution within the medium and matrix[60] and in the present case, it is clear that narrow size distribution of the particles in microemulsions of lower W_o could be obtained.

Table 3.1. FWHM of Zn nanoparticles in two different microemulsions at different W_o

Microemulsions	W_o	FWHM (nm)
CTAB	9.6	30.0
CTAB	20.0	34.0
CTAB	30.0	37.0
TX-100	3.5	5.0
TX-100	7.8	7.0
TX-100	10.0	8.0

DLS measuements of Zn nanoparticles in both microemulsions further confirmed narrow size distributions at lower W_o (Figure 3.11).

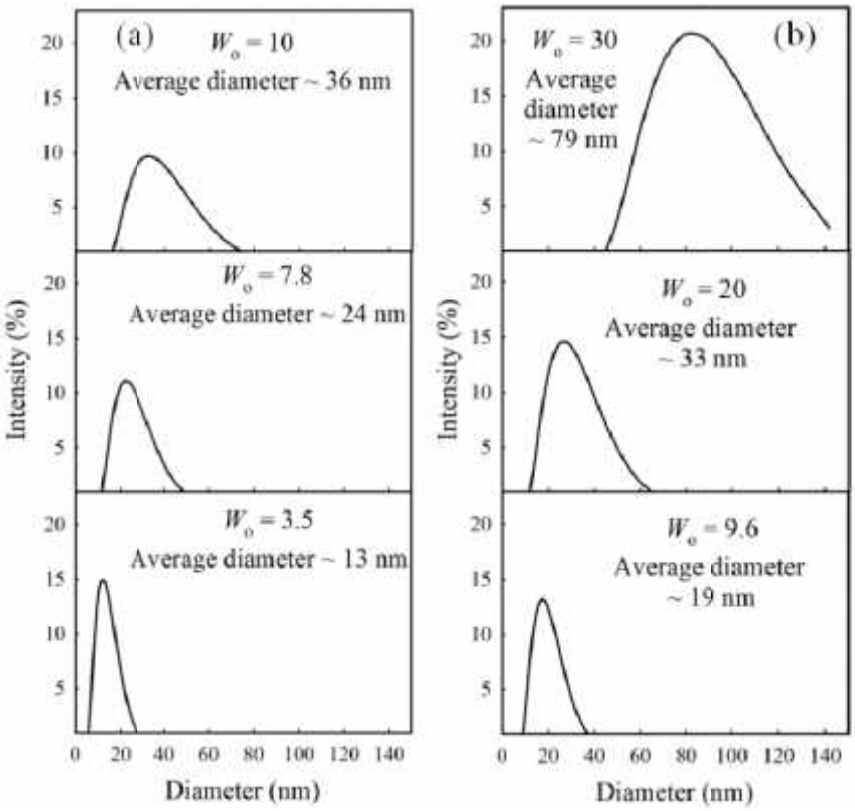

Figure 3.11. Average size and size distribution of Zn nanoparticles in (a) TX-100 microemulsions and in (b) CTAB microemulsions with increasing W_o.

From DLS measurements it is also observed that average size of nanoparticles increased with W_o in both microemulsions as the droplet size increased (shown in Figure 2.3).

3.3.2.3. Dependence of the size of nanoparticles on W_o of microemulsions

Syntheses of metallic nanoparticles were carried in three different microemulsions with increasing W_o values. A gradual increase in the size of microemulsion droplets as well as particles with W_o is observed. At constant surfactant concentration with low water content, surfactants bind the solubilized water in the polar core of reverse micelles which ultimately strengthens the boundary (Figure 3.12) and decreases the intermicellar exchange rate. This results in the formation of monodisperse nanoparticles with small particle size. At high water content, the size of microemulsion droplets increases because of swelling of water in the core and the bound water would turn into bulk water which introduces a dilution effect and reduces initial nucleation rate within individual reverse micelles. Less interaction between the surfactant head groups and the nanoparticles and less surface rigidity of the surfactant

protective layer (Figure 3.12) are likely to induce aggregation of the nanoparticles. The increase in the particle size with increasing W_o is therefore, attributed to slow nucleation accompanied by particle growth and aggregation.[36,55]

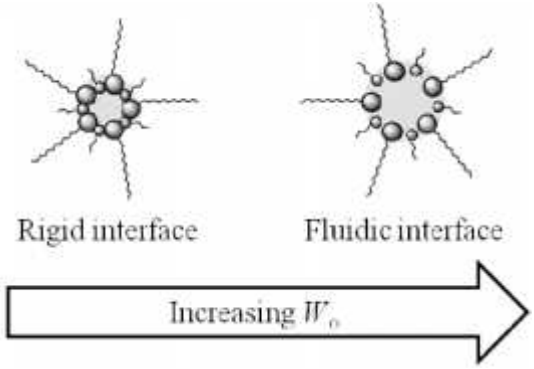

Figure 3.12. Increasing interfacial film fluidity with increasing W_o.

3.3.2.4. Dependence of the size of nanoparticles on the concentration of surfactant of microemulsions

Cu nanoparticles were prepared by reducing 0.4 mmol Cu^{2+} by 0.8 mmol $NaBH_4$ in TX-100/1-butanol/cyclohexane/water microemulsions at different concentration of TX-100. The hydrodynamic diameter of microemulsion droplets decreased with increasing concentration of the surfactant (Figure 2.5). The trend of variation of the average size of Cu nanoparticles in microemulsions with surfactant concentration is similar to the variation in the sizes of microemulsion droplets shown in Figure 3.13. The average size and size distribution of nanoparticles decreased as the concentration of surfactant of microemulsions increased. The size of particles formed in w/o microemulsions was directly influenced by the number of microemulsion droplets that host reacting species. In TX-100 microemulsions with constant water content, as the surfactant concentration increases the number of droplets increased significantly (Figure 3.13).[61] The greater the number of droplets there are, the greater will be the physical compartmentalization of reacting species to form more nuclei and fewer free atoms for further growth which ultimately results in smaller final particles. Besides, more monodispersed particles were obtained due to the strong surfactant film barrier which created the steric stabilization to prevent the aggregation of nanoparticles. At lower surfactant concentration, microemulsion droplets increased in size because of swelling of water but decrease in number; thus, reacting species were less

compartmentalized and diluted. For this, initial nucleation rate decreased leaving more free atoms for the growth process.

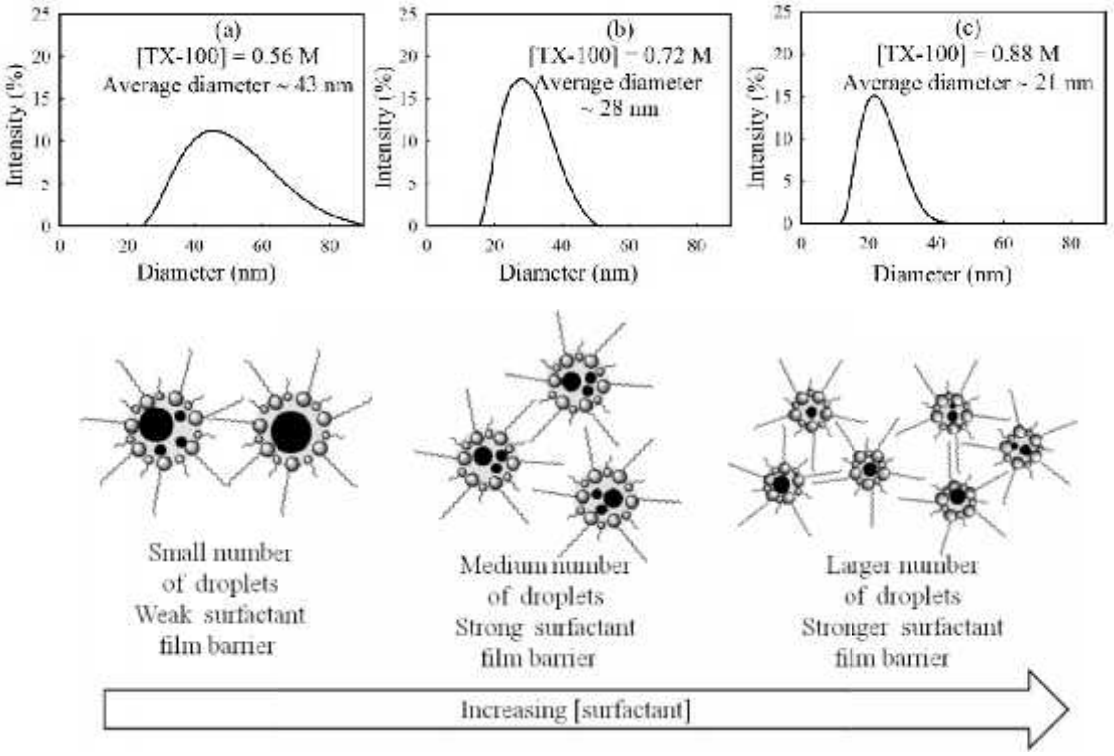

Figure 3.13. Size distribution of Cu nanoparticles in TX-100 microemulsion (a, b, c) with increasing concentration of surfactant with a schematic illustration of its effect on the formation of Cu particles.

3.3.3. Effect of cosurfactant on the size of nanoparticles

To understand the effect of cosurfactant on the size of Cu nanoparticles, microemulsions of TX-100 with and without assistance of cosurfactant, 1-pentanol at both low (0.16 M) and high (0.88 M) concentration of surfactant were prepared. For TX-100 microemulsions at low surfactant concentration no microemulsion was formed unless a cosurfactant was added as discussed in section 2.3.3. With the addition of cosurfactant microemulsion was formed and with increasing cosurfactant to surfactant molar ratio (P_o) size of microemulsion droplets decreased. In this case at lower P_o addition of reactants made microemulsions turbid and no reaction took place inside the droplets as reactant could not enter inside the droplets because of strong surfactant film barrier though the size of microemulsion droplets was larger to accommodate. But at higher P_o reduction of the metal salt inside the droplets gave highly monodisperse Cu nanoparticles (Figure 3.14). With increased cosurfactant

concentration, the interfacial film of microemulsion droplets became less compact and more fluidic.[39] So reactants could easily enter inside the droplets which facilitated initial nucleation. Again at higher P_o, the number of droplets increased with smaller size thereby increasing compartmentalization of reacting species. Thus there are more nuclei at the initial stage leaving small number of free atoms for the further growth. These resulted in smaller Cu particles with narrow size distribution.

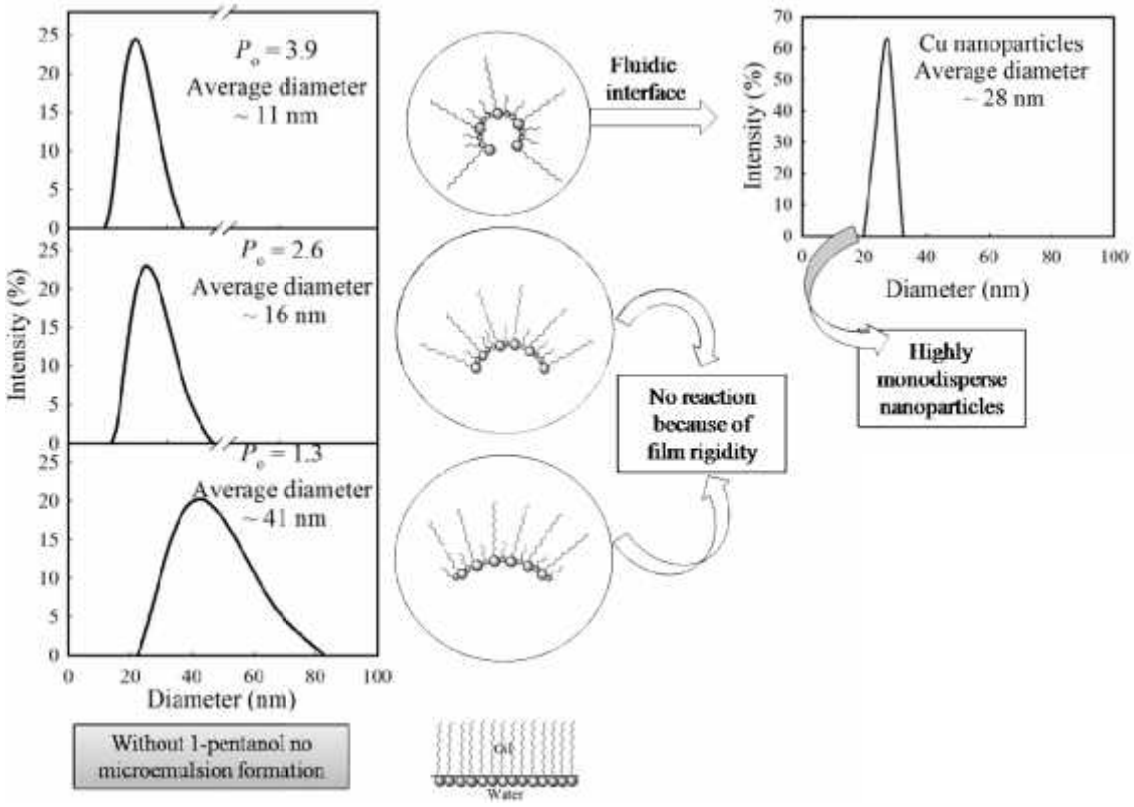

Figure 3.14. Size distribution of microemulsion droplets in TX-100/1-pentanol/cyclohexane/water microemulsions at [TX-100] = 0.16 M with increasing P_o and formation of Cu nanoparticles in these systems; $[Cu^{2+}]$ = 0.4 mmol and $[NaBH_4]$ = 0.8 mmol.

At higher TX-100 concentration (0.88 M), microemulsion was formed even without 1-pentanol. In this case also addition of 1-pentanol lowered the size of microemulsion droplets (Figure 2.8) and Cu nanoparticles as well (Figure 3.15). Here surfactant itself was enough to reduce oil water interfacial tension for the formation of microemulsion. With the addition of cosurfactant, microemulsion of smaller dimension was formed and the average diameter was also smaller compared to the droplets obtained with lower surfactant concentration at the same W_o and P_o because of increased surfactant concentration (Figure 2.7 and 2.8). For this high surfactant concentration, surfactant

film barrier should be stronger compared to those droplets obtained at lower surfactant concentration[61] allowing no reactants to enter into the microemulsion droplets. But here reactants entered inside the droplets and reaction took place. This can be ascribed to lower oil to surfactant ratio compared to those microemulsions with lower concentration of surfactant. The oil phase, cyclohexane is smaller, less bulky solvent molecules with lower molecular volumes which can easily penetrate between surfactant tails, increasing surfactant curvature and rigidity.[36] With higher concentration of surfactant the curvature of microemulsion droplets increased giving smaller microemulsion droplets in comparison with droplets obtained from lower concentration of surfactant (Figure 2.7 and 2.8). But lower amount of oil decreased

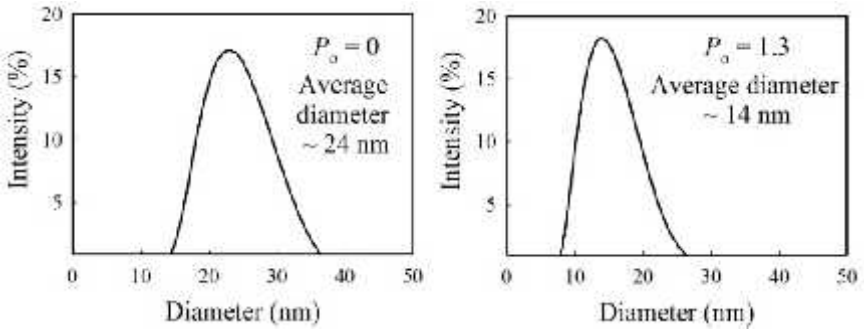

Figure 3.15. Cu nanoparticles prepared in TX-100 microemulsions without and with 1-pentanol at [TX-100] = 0.88 M; $[Cu^{2+}]$ = 0.4 mmol and $[NaBH_4]$ = 0.8 mmol.

the film rigidity for which reactants entered inside the droplets and reaction occurred even when no cosurfactant was present. The addition of cosurfactant further decreased the size of microemulsion droplets and nanoparticles also. Cosurfactant made interface flexible enough to increase nucleation whereas without cosurfactant compact interface with larger droplets diminishes nucleation rate which ultimately favors growth process (Figure 3.16).

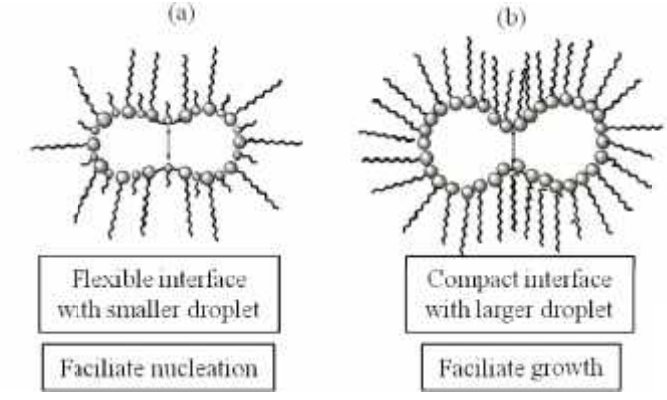

Figure 3.16. Transient fused dimmer of the droplets of microemulsions of TX-100 with (a) and without (b) cosurfactant.

To study the effect of chain length of cosurfactant on the size of Cu nanoparticles, alcohols with increasing carbon chain length, from 1-butanol to 1-octanol were used for TX-100 microemulsions keeping all other parameters constant with W_o fixed at 7.8 for all the systems. DLS measurments showed the decrease in the size of droplets of microemulsions with an increase in the carbon chain length of the cosurfactant (Figure 2.9). The size of nanoparticles also followed the same trend as microemulsion droplet size (Figure 3.17).

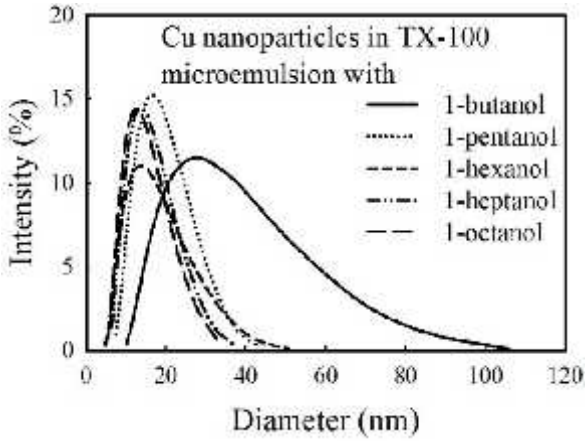

Figure 3.17. Cu nanoparticles in TX-100 microemulsions at W_o = 7.8 with increasing chain length of cosurfactant; $[Cu^{2+}]$ = 0.4 mmol and $[NaBH_4]$ = 0.8 mmol.

The average diameters of droplets of microemulsions and Cu nanoparticles from DLS measurements are shown in Table 3.2.

Table 3.2. Average diameter of microemulsion droplets and Cu nanoparticles prepared in TX-100 microemulsions with increasing carbon chain length of cosurfactant

Cosurfactant	Average diameter of microemulsion droplets (nm)	Average diameter of Cu nanoparticles in microemulsion (nm)
1-butanol	21	32
1-pentanol	17	18
1-hexanol	15	16
1-heptanol	14	15
1-octanol	12	14

For long chain cosurfactant, hydrophobic parts of surfactants and cosurfactants interact more strongly. This lowered the interfacial tension of oil and water reducing bending rigidity which increased the mean curvature of the microemulsion droplets.[39] This strong effective interaction also produced much more compact interfacial film which resulted in a reduced coalescence rate to inhibit growth process and Cu nanoparticles of smaller dimension were thus obtained.[28]

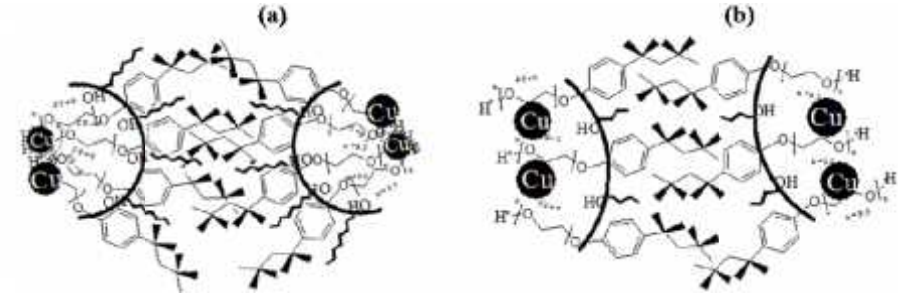

Figure 3.18. Interactions of hydrophobic parts of surfactants and cosurfactants for (a) long chain and (b) short chain cosurfactants.

3.3.4. Antibacterial activities of nanoparticles

Cu, Zn, Ag and Fe nanoparticles were prepared in TX-100/1-butanol/cyclohexane/water micoemulsions at W_o = 10. For the preparation of nanoparticles, equal volume of micremulsions (3 mL) one containing metal ions (0.15 mmol) and another reducing agent (0.6 mmol) were mixed. After preparation, DLS measurements of nanoparticles containing microemulsions were carried out to determine the size of nanoparticles (Figure 3.19).

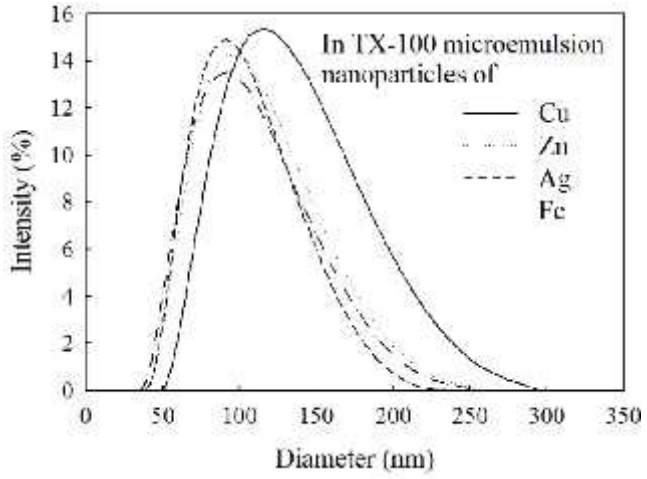

Figure 3.19. Size distribution of Cu, Zn, Ag and Fe nanoparticles in TX-100 microemulsions at W_o = 10.

From DLS measurements, the average diameters of microemulsion containing Cu, Zn, Ag and Fe nanoparticles were approximately 122 nm, 105 nm, 102 nm and 97 nm respectively. After separation from microemulsions nanoparticles were dispersed in 1 mL de-ionized water to obtain a concentration of 0.9 μM. The bacterial sensitivity of *E. coli* and *S. aureus* to these nanoparticles were then tested by zone of inhibition method. Antibacterial activity test results are shown in Figure 3.20 and Table 3.3. De-ionized water that was used as control does not show any zone of inhibition against all two pathogens studied.

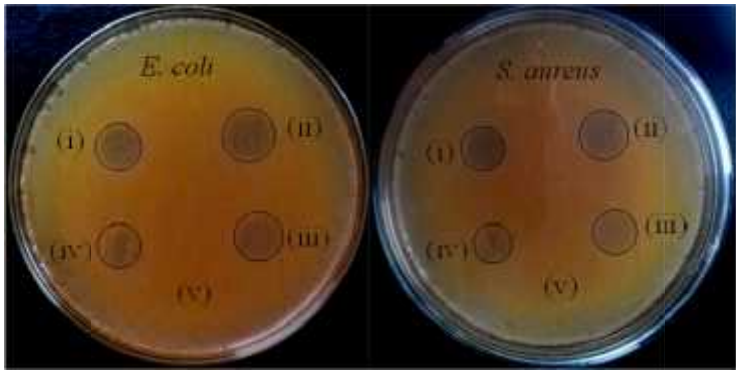

Figure 3.20. Antibacterial activity test against pathogens; *E. coli* and *S. aureus* [(i) Cu, (ii) Ag, (iii) Zn, (iv) Fe nanoparticles (v) de-ionized water as control].

The results reveal that all the four nanoparticles possess antibacterial activity that is identified by the zone of inhibition. The sensitivity of *E. coli* to these metal nanoparticles are somewhat stronger than that of *S. aureus*. Ag shows the strongest antibacterial activity against both bacteria among the four metal nanoparticles studied. But after dilution no effect was observed for all these nanoparticles.

Table 3.3. Zone of inhibition in agar diffusion test of Cu, Ag, Zn and Fe nanoparticles against *E. coli* and *S. aureus*

Bacterial strains	Zone of inhibition (mm)			
	Cu	Ag	Zn	Fe
E. coli	12	14	12	11
S. aureus	11	12	11	10

The antibacterial activities of Cu and Ag nanoparticles were then tested against *E. coli* at higher concentration (~ 9 μM). Ag shows a strong antibacterial activity against *E. coli* (zone inhibition ~ 20 mm) where Cu shows comparatively less antibacterial

activity (zone inhibition ~ 18 mm). As the concentration decreased, antibacterial activity decreased gradually indicating the concentration dependence of antibacterial activity (Figure 3.21).

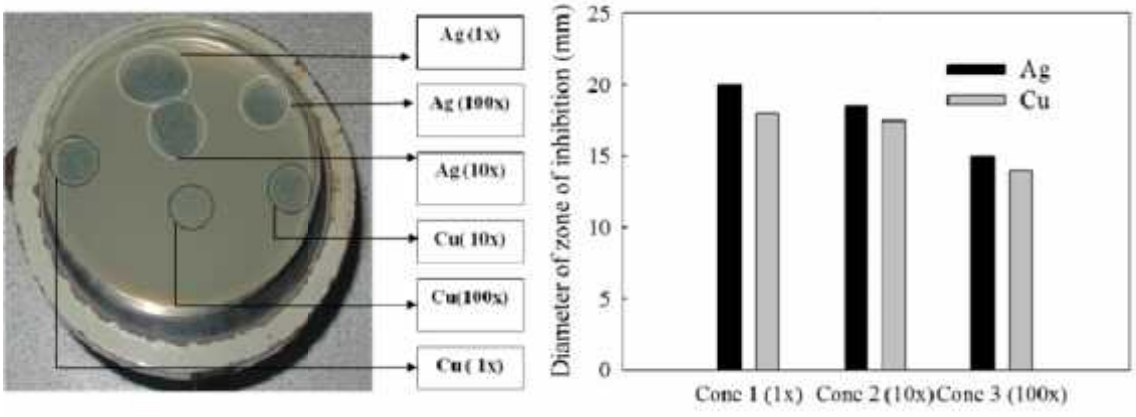

Figure 3.21. Diameter of zone of inhibition of Cu and Ag nanoparticles in ethanol suspension against *E. coli* at different concentration.

A comparison of sensitivity of Ag and Cu nanoparticles with sensitivity of conventional antibiotics is shown in the Figure 3.22. From the Figure it can be said that Ag and Cu nanoparticles show almost equivalent sensitivity as the conventional antibiotics.

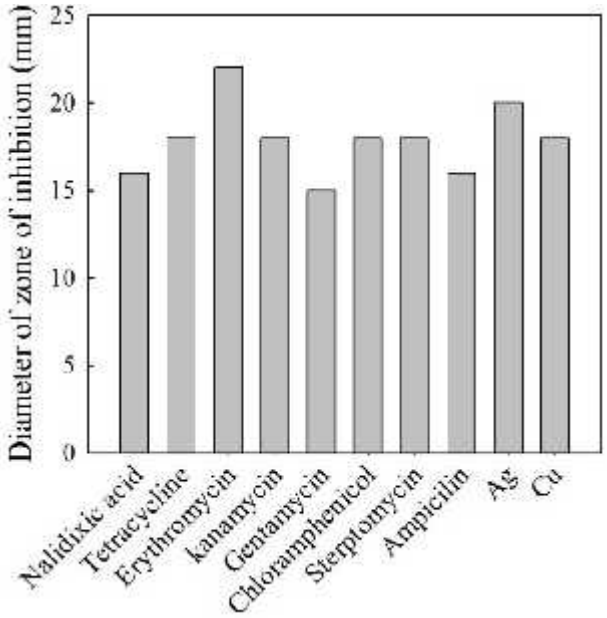

Figure 3.22. A comparison of bacterial sensitivity to Ag and Cu nanoparticles with sensitivity to conventional antibiotics.

The antibacterial activity of Cu, Ag, Zn and Fe can be explained by oligodynamic effect. The oligodynamic effect (Greek oligos = few, dynamis = power) was

discovered in 1893 by the Swiss Karl Wilhelm von Nägeli as a toxic effect of metal-ions[62] on living cells, algae, molds, spores, fungus, virus, prokaryotic and eukaryotic microorganisms, even in relatively low concentrations. This antimicrobial effect is shown by ions of mercury, silver, copper, iron, lead, zinc, bismuth, gold, aluminium and other metals.[63] Especially heavy metals show this effect. These metal ions denature proteins (enzymes) of the target cell or organism by binding to reactive groups resulting in their precipitation and inactivation.[63] Cationic Ag binds to negatively charged components of proteins and nucleic acids which causes structural changes and deformations in bacterial cell walls, membranes, and nucleic acids. Ag ions generally interact and react with a number of electron donor functional groups like thiols, phosphates, hydroxyls, imidazoles, indoles, and amines[64] and diminish their activities whereas Cu is susceptible to amines and carboxylic groups.[65] Bacteria (Gram-positive and Gram-negative) are in general affected by the oligodynamic effect.[63] The toxic effect is fully developed often only after a long time (many hours).
But the mechanism of bactericidal action of nanoparticles has not been fully understood yet and the elucidation is still underway. A variety of hypotheses have been proposed, including physical disruption of cell structures, disturbances of permeability and respiration, and damage of DNA or enzymatic proteins by metal ions released from the nanoparticles.[66] Several studies insist that the mode of antimicrobial action of Ag nanoparticles is similar to that of Ag ions although the nanoparticles were reported to be effective at significantly lower concentration than that of the ions.[67] The most common mechanisms proposed for the antibacterial activity of Ag nanoparticles are: (i) gradual release of free Ag ions from the nanoparticles that either bind DNA to block transcription or bind cell surface components that interrupt bacterial respiration and adenosinetriphosphate (ATP) synthesis, (ii) direct damage to cell membranes by Ag nanoparticles as they are able to penetrate inside the bacteria causing further damage by possibly interacting with sulfur- and phosphorus-containing compounds such as DNA, and (iii) Ag nanoparticles and Ag ion generation of reactive oxygen species.[64]

Actually it is difficult to distinguish between the bactericidal activity of nanoparticles from that of the ions released by the nanoparticles.[68] In the agar nutrient medium release of ions might be possible due to reaction with the nutrient media constituents. Suspension of nanoparticles would ensure continuous release of ions into the nutrient

media.[67] Again the overall charge of the cell surface of the bacteria at biological pH values is negative, because of dissociation of the excess number of carboxylic and other groups. So electrostatic interactions occur between positively charged ions released by the nanoparticles and the negatively charged bacterial cell wall. Thus nanoparticles tightly bind with the bacteria surface because of this electrostatic forces[69] and might rupture the cellular envelope leading to protein denaturation and cell death.[70] On the other hand, negatively charged Ag nanoparticles have been reported by Sondi *et al*. which interact with "building elements" of the bacterial membrane, causing structural changes and degradation and finally, cell death. The exact mechanism of interaction between these particles and the constituents of the outer membrane of *E. coli* unfortunately remains unresolved. They reported that the antimicrobial activity of Ag nanoparticles on Gram-negative was closely associated with the formation of pits in the cell wall of bacteria which probably interact with the internal components of the cell.[71] Morones *et al*. also found considerable numbers of Ag nanoparticles inside the bacteria. They suggested that nanoparticles found inside tend to react with sulfur-containing proteins in the interior of the cell, as well as with phosphorus-containing compounds, DNA.[72] But in this study the size of nanoparticles were larger compared to Ag nanoparticles studied by Sondi *et al* and Morones *et al*. Therefore, in this case it is speculated that Ag nanoparticles might adhere with the cell surface of *E. coli* and causes structural changes by reacting with functional groups present on the cell wall. The outer membrane of *E. coli* consists of lipopolysaccharide complexes composed of proteins and phospholipids organized in a complex way. So Ag ions from Ag nanoparticles can easily react with phosphate (present in lipid bilayer) and amine and sulfur groups (present in membrane protein). For the disruption of cell function by Cu nanoparticles several mechanisms might act simultaneously.[13] One action is the release of Cu ions due to direct oxidation of the Cu surface by the contact with cells[73] which then solidify protein structure possibly due to the reaction with amines and alter enzyme function. Here lower sensitivity of *E. coli* to the Cu nanoparticles compared to Ag nanoparticles is observed which might be attributed to lower abundance of amines and carboxyl groups on cell surface of *E. coli* and greater affinity of Cu towards these groups.[55] No report for the antibacterial activity of Zn nanoparticles was found in literature. It can be speculated that Zn react with amino acids of membrane protein and can form complexes while react with phosphates of lipid bilayer to form precipitates. Thereby inhibition of bacterial growth

is due to the disorganization of cell membranes that disrupt cellular function. For the antibacterial activity of Fe nanoparticles Lee *et al*. proposed that reductive decomposition of functional groups in the proteins and lipopolysaccharides of the outer membranes of *E. coli* with strong reductant Fe ($E_H°$ ($Fe^{2+/}Fe^0$) = -0.447 V), significantly disrupt the cell membranes and subsequently leakage of the intracellular contents occur.[66] During this process, Fe nanoparticles may have been oxidized by intracellular oxygen, leading to oxidative damages via the Fenton reaction. It was suggested that under deaerated conditions Fe(II) ion released from metallic Fe can contribute to the bactericidal activity of Fe nanoparticles. These resulted in enhancement of antibacterial activity of Fe nanoparticles compared to that of Ag nanoparticles. But in this study the experiments are not deaerobic and Fe(II) can easily convert into Fe(III) due to oxidation which cannot inactivate *E. coli* possibly because of the low solubility of the Fe(III) ion in neutral aqueous solution. In contrast Ag nanoparticles showed a higher activity here probably because of the oxygen-induced dissolution of Ag ion (Ag^+). From antibacterial activity at higher concentration, it can also be seen that for *E. coli* Ag nanoparticles demonstrates greater bactericidal efficiency compared to conventional antibiotics such as ampicilin, tetracycline, gentamycin, kanamycin, streptomycin etc (Figure 3.22). From this study it can also be observed that *S. aureus* is less sensitive to all the four metal nanoparticles. This might be due to the difference in the membrane structure of Gram-positive and Gram-negative bacteria. The outer membrane outside the peptidoglycan layer is lacking in Gram-positive organisms.[74] Gram-negative bacteria contain a thin layer (7-8 nm) of peptidoglycan present below the lipopolysaccharide layers whereas Gram-positive bacteria are composed of a thick layer (20-80 nm) of peptidoglycan, consisting of linear polysaccharide chains cross-linked by short peptides to form a three dimensional rigid structure.[75] So it can be suggested that the reduced amount (between 3- and 20- fold) of negatively charged peptidoglycans make Gram-negative bacteria more susceptible[76] to metal nanoparticles[77] whereas rigid and thicker peptidoglycan layer around its cell provides more protection to *S. aureus*.[78]

3.4. Conclusions

The diameter of microemulsion could be tuned by the proper choice of microemulsion variables and hence nanoparticles of varying size could be prepared in these templates. The surfactant (type and concentration), water content, cosurfactant

(concentration and chain length) have profound influences on the average size and size distribution of Cu, Zn, Ag and Fe nanoparticles. Microemulsions of different surfactants gave particles of varying size. The size of nanoparticles was governed by the HLB and rigidity of the surfactant. The average size of nanoparticles also has been found to be influenced by W_o and concentration of surfactant. Smaller particles were obtained at low W_o, while higher W_o yields larger particles as the droplet size increased with W_o. For the existence of stable w/o microemulsions of TX-100, cosurfactant was essential at low surfactant concentrations but was not necessary at higher concentrations. At low surfactant concentrations with high amount of cosurfactant monodisperse Cu particles with narrow size distribution was obtained; whereas at lower P_o reactants could not enter inside the droplets. But TX-100 microemulsions with high amount of surfactant the reaction occurred even in the absence of a cosurfactant and the addition of cosurfactant decreased the droplet-size in the microemulsions and hence the size of Cu nanoparticles. With increasing chain length of cosurfactant the size of Cu nanoparticles decreased with decreasing the size of droplets of microemulsions. Thus, it is possible to fine-tune the droplet-size in the microemulsions and hence this microemulsion method is advantageous to synthesize nanoparticles of precisely controlled size. All the four metal nanoparticles prepared in microemulsion showed bacterial sensitivity against both *E. coli* and *S. aureus* even at very low concentrations. At high concentrations, Cu and Ag showed good sensitivity as conventional antibiotics.

References

(1) Chen, C.; Pan, F.; Zhang, S.; Hu, J.; Cao, M.; Wang, J.; Xu, H.; Zhao, X.; Lu, J. R. Antibacterial activities of short designer peptides: a link between propensity for nanostructuring and capacity for membrane destabilization. *Biomacromolecules* **2010**, *11*, 402-411.

(2) Neoh, K. G.; Kang, E. T. Combating Bacterial Colonization on Metals via Polymer Coatings: Relevance to Marine and Medical Applications. *ACS Appl. Mater. Interfaces* **2011**, *3*, 2808-2819

(3) Dong, A.; Lan, S.; Huang, J.; Wang, T.; Zhao, T.; Xiao, L.; Wang, W.; Zheng, X.; Liu, F.; Gao, G.; Chen, Y. Modifying Fe_3O_4-functionalized nanoparticles with n-halamine and their magnetic/antibacterial properties. *ACS Appl. Mater. Interfaces* **2011**, *3*, 4228-4235.

(4) Han, H.; Wu, J.; Avery, C. W.; Mizutani, M.; Jiang, X.; Kamigaito, M.; Chen, Z.; Xi, C.; Kuroda, K. Immobilization of amphiphilic polycations by catechol functionality for antimicrobial coatings. *Langmuir* **2011***, 27*, 4010-4019.

(5) Bujdák, J.; Jurečeková, J.; Bujdáková, H.; Lang, K.; Šeršeň, F. Clay mineral particles as efficient carriers of methylene blue used for antimicrobial treatment. *Environ*. *Sci*. *Technol*. **2009**, *43*, 6202-6207.

(6) Kong, H.; Song, J.; Jang, J. Photocatalytic antibacterial capabilities of TiO_2−biocidal polymer nanocomposites synthesized by a surface-initiated photopolymerization. *Environ. Sci. Technol.* **2010**, *44*, 5672-5676.

(7) Waasbergen L. G. van; Fajdetic I.; Fianchini M.; Dias H.V. R. Antimicrobial properties of highly fluorinated tris(pyrazolyl)borates. *J. Inorg*. *Biochem*. **2007**, *101*,1180-1183.

(8) Chen, C.; Pan, F.; Zhang, S.; Hu, J.; Cao, M.; Wang,J.; Xu,H.; Zhao, X.; Jian R. Lu, J. R. Antibacterial activities of short designer peptides: a link between propensity for nanostructuring and capacity for membrane destabilization. *Biomacromolecules* **2010**, *11*, 402-411.

(9) Mody, V. V.; Siwale, R.; Singh, A.; Mody, H. R. Introduction to metallic nanoparticles. J. Pharm. Bioall. Sci. 2010, *4*, 282-289.

(10) Esteban-Cubillo, A.; Pecharromán, C.; Aguilar, E.; Santarén, J.; Moya, J. S. Antibacterial activity of copper monodispersed nanoparticles into sepiolite. *J. Mater. Sci*. **2006**, *41*, 5208-5212.

(11) Cho, K. H.; Park, J. E.; Osaka, T.;, Park, S. G. The study of antimicrobial activity and preservative effects of nanosilver ingredient. *Electrochimica Acta* **2005**, *51*, 956- 960.

(12) Shahverdi, A. R.; Fakhimi, A.; Shahverdi, H. R.; Minaian. S. Synthesis and effect of silver nanoparticles on the antibacterial activity of different antibiotics against Staphylococcus aureus and Escherichia coli. *Nonomedicine* **2007**, *3*, 168-171.

(13) Raffi, M.; Mehrwan, S.; Bhatti, T. M.; Akhter, J. I.; Hameed, A.; Yawar, W.; Hasan, M. M. Investigations into the antibacterial behavior of copper nanoparticles against Escherichia coli. *Ann Microbiol*. **2010**, *60*, 75-80.

(14) Rajamanickam, U.; Mylsamy, P.; Viswanathan, S.; Muthusamy, P. Biosynthesis of zinc nanoparticles using actinomycetes for antibacterial food packaging. International conference on nutrition and food sciences, Singapore, **2012**, *39*, 195-199.

(15) Naseem, T.; Farrukh, M. A. Antibacterial activity of green synthesis of iron nanoparticles using lawsonia inermis and gardenia jasminoides leaves extract. *Journal of Chemistry* **2015**, 1-7.

(16) Jia, Q.; Shan, S.; Jiang, L.; Wang, Y.; Li, D. Synergistic antimicrobial effects of polyaniline combined with silver nanoparticles. *J. Appl. Polym. Sci*. **2012**, 1-7.

(17) Ghaffari-Moghaddam, M.; Eslahi, H. Synthesis, characterization and antibacterial properties of a novel nanocomposite based on polyaniline/polyvinyl alcohol/Ag. *Arabian J. Chem.* **2014**, *7*, 846-855.

(18) Morones, J. R.; Elechiguerra, J. L.; Camacho, A.; Holt, K.; Kouri, J. B.; Ramírez, J. T. Yacaman, M. J. The bactericidal effect of silver nanoparticles. *Nanotechnology* **2005**, *16*, 2346-2353.

(19) Kumar, A.; Vemula, P. K.; Ajayan, P. M.; John, G. Silver-nanoparticle-embedded antimicrobial paints based on vegetable oil. *Nat. Mater.* **2008**, *7*, 236-241.

(20) Palza, H. Antimicrobial Polymers with Metal Nanoparticles. *Int. J. Mol. Sci.* **2015**, *16*, 2099-2116.

(21) Chaloupka, K.; Malam, Y.; Seifalian, A. M. Nanosilver as a new generation of nanoproduct in biomedical applications. *Trends Biotechnol.* **2010**, *28*, 580-588.
(22) Chakrapani, V.; Ahmed, K. B. A.; Kumar, V. V.; Ganapathy, V.; Anthony, S. P.; Anbazhagan, V. A facile route to synthesize casein capped copper nanoparticles: an effective antibacterial agent and selective colorimetric sensor for mercury and tryptophan. *RSC Adv*. **2014**, *4*, 33215-33221.
(23) Argueta-Figueroa, L.; Morales-Luckie, R. A.; Scougall-Vilchis, R. J.; Olea-Mejía, O. F. Synthesis, characterization and antibacterial activity of copper, nickel and bimetallic Cu–Ni nanoparticles for potential use in dental materials. *Prog. Nat. Sci*. **2014**, *24*, 321-328
(24) Raffi, M.; Mehrwan, S.; Bhatti, T. M.; Akhter, J. I.; Hameed, A.; Yawar, W.; Hasan, M. M. Investigations into the antibacterial behavior of copper nanoparticles against Escherichia coli. Ann Microbiol. 2010, *60*, 75-80.
(25) El-Nour, K. M. M. A.; Eftaiha, A.; Al-Warthan, A.; Ammar, R. A. A. Synthesis and applications of silver nanoparticles. Arabian J. Chem. 2010, *3*, 135-140.
(26) Zhang, Y.; Zhu, P.; Li, G.; Wang, W.; Chen, L.; Lu, D. D.; Sun, R.; Zhoub, F.; Wongd, C. Highly stable and re-dispersible nano Cu hydrosols with sensitively size-dependent catalytic and antibacterial activities. *Nanoscale* **2015**,*7*, 13775-13783.
(27) Raghupathi, K. R.; Koodali, R.T.; Manna, A. C. Size-dependent bacterial growth inhibition and mechanism of antibacterial activity of zinc oxide nanoparticles. *Langmuir* **2011**, *27*, 4020-4028.
(28) Ranjan, R.; Vaidya, S.; Thaplyal, P.; Qamar, M.; Ahmed, J.; Ganguli, A. K. Controlling the size, morphology, and aspect ratio of nanostructures using reverse micelles: a case study of copper oxalate monohydrate. *Langmuir* **2009**, *25*, 6469-6475.
(29) Fanun, M. Microemulsions Properties and Applications, CRC Press, **2009**, *144*.
(30) Capek, I. Preparation of metal nanoparticles in water-in-oil (w/o) microemulsions. Adv. *Colloid Interface Sci*. **2004**, *110*, 49-74.
(31) Szcześ, A. Influence of the surfactant nature on the calcium carbonate synthesis in water-in-oil emulsion. *J. Cryst. Growth* **2009**, *11*, 1129-1135.
(32) Zhang, W.; Qiao, X.; Chena, J. Synthesis of silver nanoparticles—Effects of concerned parameters in water/oil microemulsion. *Mater. Sci. Eng., B* **2007**, *142*, 1-15.
(33) Solanki, J. N.; Murthy, Z. V. P. Controlled size silver nanoparticles synthesis with water-in-oil microemulsion method: a topical review. *Ind. Eng. Chem. Res.* **2011***, 50,* 12311-12323.
(34) Ganguli, A. K.; Ganguly, A.; Vaidya, S. Microemulsion-based synthesis of nanocrystalline materials. *Chem. Soc. Rev*. **2010**, *39*, 474-485.
(35) Housaindokht, M. R.; Pour, A. N. Study the effect of HLB of surfactant on particle size distribution of hematite nanoparticles prepared via the reverse microemulsion. *Solid State Sci*. **2012**, *14*, 622-625.
(36) Eastoe, J.; Hollamby, M. J.; Hudson, L. Recent advances in nanoparticle synthesis with reversed micelles. *Adv. Colloid Interface Sci*. **2006**, *128130*, 5-15.

(37) Curri, M. L.; Agostiano, A.; Manna, L.; Monica, M. D.; Catalano, M.; Chiavarone, L.; Spagnolo, V.; Lugarà, M. Synthesis and characterization of cds nanoclusters in a quaternary microemulsion: the role of the cosurfactant. *J. Phys. Chem. B* **2000,** *104,* 8391-8397.

(38) Zhang, J.; Sun, L.; Liao, C.; Yan, C. Size control and photoluminescence enhancement of CdS nanoparticles prepared via reverse micelle method. *Solid State Commun*. **2002**, *124*, 45-48.

(39) Marchand, K. E.; Tarret, M.; Lechaire, J.P.; Normand, L.; Kasztelan, S.; Cseri, T. Investigation of AOT-based microemulsions for the controlled synthesis of MoS_x nanoparticles : an electron microscopy study. *Colloids Surf., A* **2003**, *214*, 239-248.

(40) Charinpanitkula, T.; Chanagula, A.; Duttab, J.; Rungsardthongc, U.; Tanthapanichakoona, W. Effects of cosurfactant on ZnS nanoparticle synthesis in microemulsion. *Sci. Technol. Adv. Mater*. **2005**, 6, 266-271.

(41) Qiu, S.; Dong, J.; Chen, G. Preparation of Cu nanoparticles from water-in-oil microemulsions. *J. Colloid Interf. Sci*. **1999**, *216*, 230-234.

(42) Egorova, E. M. Biochemical synthesis of gold and zinc nanoparticles in reverse micelles. *Russ. J. Phys. Chem. A* **2010**, *84*, 629-635.

(43) Solomon, S. D.; Bahadory, M. Jeyarajasingam, A. V.; Rutkowsky, S. A.; Boritz, C.; Mulfinger, L. *J. Chem. Educ*. **2007**, *84*, 322-325.

(44) Yunxia, Z.; Tielong, L.; Zhaohui, J.; Wei, W.; Shuaima, W. Synthesis of nanoiron by microemulsion with Span/Tween as mixed surfactants for reduction of nitrate in water. *Front. Environ. Sci. Engin. China* **2007**, *1*, 466-470.

(45) Athawale, A. A.; Katre, P. P.; Kumar, M.; Majumdar, M. B. Synthesis of CTAB–IPA reduced copper nanoparticles. *Mater. Chem. Phys*. **2005**, *91*, 507-512.

(46) Wang, H.; Tam, F.; Grady, N. K.; Halas, N. J. Cu nanoshells: effects of interband transitions on the nanoparticle plasmon resonance. *J. Phys. Chem. B*, **2005**, *109*, 18218-18222.

(47) Creighton, J. A.; Eadont, D.G. Ultraviolet-visible absorption spectra of the colloidal metallic elements. *J. Chem. Soc. Faraday Trans*. **1991**, *87*, 3881-3891.

(48) Yeh, M-S.; Yang, Y-S.; Lee, Y-P.; Lee, H-F.; Yeh, Y-H.; Yeh, C-S. Formation and characteristics of Cu colloids from CuO powder by laser irradiation in 2-propanol. *J. Phys. Chem. B* **1999,** *103,* 6851-6857.

(49) Lisiecki, I.; Billoudet, F.; Pileni, M. P. Control of the shape and the size of copper metallic particles. *J. Phys. Chem.* **1996,** *100,* 4160-4166.

(50) Sripriya , R.; Raja, K. M.; Santhosh, G.; Chandrasekaran, M.; Noel, M. The effect of structure of oil phase, surfactant and co-surfactant on the physicochemical and electrochemical properties of bicontinuous microemulsion. *J. Colloid Interf. Sci*. **2007**, *314*, 712-717.

(51) Spirin, M. G.; Bricklin, S. B.; Razumov, V. F. Growth kinetics for AgI nanoparticles in AOT reverse micelles: Effect of molecular length of hydrocarbon solvents. *J. Colloid interf. sci*. **2008**, *326*, 117-120.

(52) Spirin, M. G., Brichkin, S. B., and Razumov V. F. Synthesis and stabilization of gold nanoparticles in reverse micelles of aerosol OT and triton X-100. *Colloid J*. **2005**, *67*, 485-490.

(53) Miranda-M, M.; Gellini, C.; Giorgetti, E. Surface-enhanced raman scattering from copper nanoparticles obtained by laser ablation. *J. Phys. Chem. C* **2011**, *115*, 5021-5027.
(54) Qi, L.; Ma, J.; Shen, J. Synthesis of copper nanoparticles in nonionic water-in-oil microemulsions. *J. Colloid Interf. Sci*. **1997**, *186*, 498-500.
(55) Hossain, S.; Fatema, U. K.; Mollah, M. Y. A.; Rahman, M. M.; Susan, M. A. B. H.; Microemulsions as nanoreactors for preparation of nanoparticles with antibacterial activity. *J Bang Chem Soc*. **2012**, *25*, 71-79.
(56) Basu, S.; Chakravorty, D. Optical properties of nanocomposites with iron core–iron oxide shell structure. *J. Non-Cryst. Solids* **2006**, *352*, 380-385.
(57) Zeng, H.; Cai, W.; Li, Y.; Hu, J.; Liu, P. Composition/structural evolution and optical properties of Zno/Zn nanoparticles by laser ablation in liquid media. *J. Phys. Chem. B* **2005,** *109,* 18260-18266.
(58) Xiang, X.; Zu, X.T.; Zhu, S.; Zhang, C. F.; Wang, L. M. Optical absorption of metallic Zn nanoparticles in Zn ion implanted sapphire. *Nucl. Instr. and Meth. in Phys. Res. B* **2006**, *250*, 192-195.
(59) Egorova, E. M. Biochemical synthesis of gold and zinc nanoparticles in reverse micelles. *Russ. J. Phys. Chem. A* **2010**, *84*, 629-635.
(60) Khanna, P.K.; Singh, N.; Charan, S.; Subbarao, V.V.V.S.; Gokhale, R.; Mulik, U.P. Synthesis and characterization of Ag/PVA nanocomposite by chemical reduction method. *Mater. Chem. Phys*. **2005**, *93*, 117-121.
(61) Chang, C.-L.; Fogler, H. S. Controlled formation of silica particles from tetraethyl orthosilicate in nonionic water-in-oil microemulsions. *Langmuir* **1997**, *13*, 3295-3307.
(62) Massey, A. G.; Thompson, N. R.; Johnson, B. F. G. The Chemistry of Copper, Silver and Gold. Pergamon Press, **1973**.
(63) Shrestha, R.; Joshi, D. R.; Gopali, J.; Piya, S. Oligodynamic action of silver, copper and brass on enteric bacteria isolated from water of kathmandu valley. Nepal Journal of Science and Technology **2009**, *10*, 189-193.
(64) Dallas, P.; Tucek, J.; Jancik, D.; Kolar, M.; Panacek, A.; Zboril, R. Magnetically controllable silver nanocomposite with multifunctional phosphotriazine matrix and high antimicrobial activity. *Adv. Funct. Mater*. **2010**, *20*, 2347-2354.
(65) Montazer, M.; Dastjerdi, M.; Azdaloo, M.; Rad, M. M. Simultaneous synthesis and fabrication of nano Cu_2O on cellulosic fabric using copper sulfate and glucose in alkali media producing safe bio- and photoactive textiles without color change. *Cellulose* **2015**, *22*, 4049-4064.
(66) Lee, C.; Kim, J.; Lee, W. I.; Nelson, K. L.; Yoon, J.; Sedlak, D. L. Bactericidal effect of zero-valent iron nanoparticles on Escherichia coli. *Environ. Sci. Technol.* **2008,** *42,* 4927-4933.
(67) Ruparelia, J. P.; Chatterjee, A. K.; Duttagupta, S. P.; Mukherji, S. Strain specificity in antimicrobial activity of silver and copper nanoparticles. *Acta Biomaterialia* **2008**, *4*, 707-716.
(68) Yoon, K.; Byeon, J. H.; Park, J.; Hwang, J. Susceptibility constants of Escherichia coli and Bacillus subtilis to silver and copper nanoparticles. *Sci Total Environ* **2007**, *373*, 572-575.
(69) Stoimenov, P. K.; Klinger, R. L.; Marchin, G. L.; Klabunde, K. J. Metal Oxide Nanoparticles as Bactericidal Agents. *Langmuir* **2002,** *18,* 6679-6686.

(70) Lin, Y. E.; Vidic, R. D.; Stout, J. E.; Mccartney, C. A.; Yu, V. L. Inactivation of Mycobacterium avium by copper and silver ions. *Water Res* **1998**, *32*,1997-2000.
(71) Sondi, I.; Salopek-Sondi, B. Silver nanoparticles as antimicrobial agent: a case study on E. coli as a model for Gram-negative bacteria. *J. Colloid Interf. Sci*. **2004**, *275*,177-182.
(72) Morones, J. R.; Elechiguerra, J. L.; Camacho, A.; Holt, K.; Kouri, J. B; Ramírez, J. T.; Yacaman, M. J. The bactericidal effect of silver nanoparticles. *Nanotechnology* **2005**, *16*, 2346-2353.
(73) Santo, C. E.; Taudte, N.; Nies, D. H.; Grass, G. Contribution of copper ion resistance to survival of Escherichia coli on metallic copper surfaces. *Appl. Environ. Microbiol*. **2008**, *74*, 977-986.
(74) Amro, N. A.; Kotra, L. P.; Wadu-Mesthrige, K.; Bulychev, A.; Mobashery, S.; Liu, G-y. High-resolution atomic force microscopy studies of the Escherichia Coli outer membrane: structural basis for permeability. *Langmuir* **2000,** *16,* 2789-2796.
(75) Dhivya, C.; Vandarkuzhali, S. A. A.; Radha, N. Antimicrobial activities of nanostructured polyanilines doped with aromatic nitro compounds. *Arabian J. Chem.* **2015.**
(76) Argueta-Figueroa, L.; Morales-Luckie, R. A.; Scougall-Vilchis, R. J.; Olea-Mejía, O. F. Synthesis, characterization and antibacterial activity of copper, nickel and bimetallic Cu–Ni nanoparticles for potential use in dental materials. Progress in Natural Science: Materials International. **2014**, *24*.321-328.
(77) Abdullah, H.; Naim, N. M.; Azmy, N. A. N.; Hamid, A. A. PANI-Ag-Cu nanocomposite thin films based impedimetric microbial sensor for detection of E. coli bacteria. *J. Nanomater.* **2014**, 1-8.
(78) Poyraz, S.; Cerkez, I.; Huang, T-S.; Liu, Z.; Kang, L.; Luo, J.; Zhang, X. One-step Synthesis and characterization of polyaniline nanofiber/silver nanoparticle composite networks as anti-bacterial agents. *ACS Appl. Mater. Interfaces* **2014**,*6*, 20025-20034.

Abstract

Functionalized nanoparticles, Fe_3O_4@Ag with antibacterial properties were prepared by reducing silver nitrate on the surface of Fe_3O_4 nanoparticles using w/o microemulsion method. The nanoparticles were characterized by Fourier transform infrared (FTIR) spectroscopy, UV-visible spectroscopy, DLS and SEM. FTIR spectrum confirmed the presence of Fe-O in Fe_3O_4 nanoparticles. DLS showed that Fe_3O_4 particles in nanodimensions were formed. SEM images revealed spherical morphology of the functionalized nanoparticles and showed Ag formation of shell of aroundFe_3O_4. The antibacterial activity, evaluated by zone of inhibition method, showed antibacterial performance of Fe_3O_4@Ag nanoparticles against Gram-negative bacteria *E. coli* and Gram-positive bacteria *S. aureus*.

4.1. Introduction

In recent years, magnetic nanoparticles have gained great interest for researchers because of their applications in diverse fields, including magnetic fluids, data storage, catalysis and bioapplications. Their intrinsic magnetic properties make them applicable for biomedical uses. Important biomedical applications of magnetic nanoparticles include magnetic bioseparation and detection of biological entities (cell, protein, nucleic acids, enzyme, bacteria, virus, etc.), targeted drug delivery, biological labels, clinical diagnosis and therapy such as, magnetic resonance imaging (MRI) and magnetic fluid hyperthermia (MFH).[1-4] One reason for using magnetic materials in therapeutic treatment is that they provide the ability to be directed and concentrated by means of external magnetic field and to be removed once therapy is completed.[5] Certain transitional elements with unpaired electrons, such as Fe, Co, Ni, Mn, Cr or Gd containing materials are the common magnetic materials among which iron-based magnetic nanoparticles are most investigated. Iron, a basic element in human bodies is physiologically well tolerated.[4] Especially magnetic iron oxide nanoparticles are strong candidates for biomedical applications because of their strong magnetic properties. There have been several types of iron oxides- (i) Fe_3O_4 (magnetite, $Fe^{2+}Fe^{3+}{}_2O_4$), α-Fe_2O_3 (hematite), γ-Fe_2O_3 (maghemite), FeO (wüstite), ε-Fe_2O_3 and β-Fe_2O_3.[2] Among these Fe_3O_4 exhibits strong magnetism[6-8]. Thus among various magnetic nanoparticles, those of Fe_3O_4 deserve special attention due to their fast magnetic response and low cytotoxicity and biocompatibility.[5,9,10] But for the

applications of magnetic nanoparticles in biology and medical diagnosis and therapy they should be stable in water at neutral pH and physiological salinity.[11] For *in vivo* biomedical use they must be small enough to avoid detection by the immune system (as the major defence system of body known as reticuloendothelial system eliminates any foreign substance from bloodstream)[12] or to be circulated through the bloodstream and should be stable enough to remain in the body for a sufficient time.[7] So the challenge is to control size and stability.

Magnetic iron oxide nanoparticles have a large surface-to-volume ratio and therefore possess high surface energies. The high chemical activity of nanoparticles is usually the main reason for undesirable strong and often irreversible processes such as aggregation.[13] Consequently, aggregation by strong magnetic dipole-dipole attractions between particles[14] reduces the specific surface area and the interfacial free energy, thereby diminishing particle reactivity.[2] Moreover, the naked Fe_3O_4 are very much susceptible to air oxidation[15] (because of presence of Fe^{2+}) generally resulting in loss of magnetism and dispersibility.[2] Therefore, proper surface coating i.e., development of effective surface functionalized strategies are required to keep the stability of Fe_3O_4. There are several strategies of functionalization of Fe_3O_4 nanoparticles among which one way is coating with an inorganic layer of noble metal[16] such as Ag. Coating by Ag shells prevents oxidation of Fe_3O_4. Because of vacant *d*-orbitals of Ag, further functionalization is possible which might protect Ag from natural tendency of aggregation[17] and also prevent dissolution in acidic environment. More importantly Ag nanoparticles exhibit remarkable antimicrobial properties.[18] They effectively eliminate bacteria at relatively low concentrations of Ag nanoparticles[19] (as observed in chapter 3); concentrations that are not toxic for human cells.[20] Because Fe_3O_4 and Ag nanoparticles exhibit several distinct features, so functionalization of Fe_3O_4 with Ag nanoparticles might deliver more than one function simultaneously which could have unique advantages in biomedical applications.[21] For example, combination of magnetic property of Fe_3O_4 and antibacterial feature of Ag might predestinate to exploit them in medicine where they can be used for a targeted transport of antimicrobial agent and its subsequent removal by an external magnetic field.

There have been numerous synthetic routes for the preparation of magnetic nanoparticles.[22] The most widely used synthesis routes for iron oxide nanoparticles are based on precipitation from solution.[8,23] Magnetite nanoparticles can be easily

prepared by co-precipitation of Fe^{2+} and Fe^{3+} salts at the ratio of 1 to 2 in an alkaline solution.[24-26] However, coprecipitation protocol leads to reduced control of particle shape and results in polydisperse nanoparticle due to aggregation of particles.[8,27-30] The use of microemulsion is a promising preparation method for the formation of very small and uniform nanoparticles.[31] Better control over size, monodispersity and shape can be achieved using emulsions (water in oil) that provide a confined environment during nucleation and growth of the iron oxide nanoparticles. In chapter 3, also it was observed that w/o microemulsion serve as versatile synthetic templates for the preparation of nanomaterials with efficiently controllable size. Fe_3O_4 nanoparticles have therefore also been prepared using w/o microemulsion as synthetic template through a facile and convenient method, chemical coprecipitation. The use of w/o microemulsion might resolve the problem of broader size distribution. The Fe_3O_4 nanoparticles were functionalized with noble metal, Ag by sequential deposition of metallic components (reducing Ag salt) on the previously seeded Fe_3O_4 nanoparticles in w/o microemulsions. The antibacterial properties of the as prepared Fe_3O_4@Ag nanoparticles against Gram-negative, *E. coli* and Gram-positive, *S. aureus* were tested by zone of inhibition method.

4.2. Experimental

4.2.1. Materials

TX-100 (Sigma Aldrich), cyclohexane(Merck), 1-butanol (LAB-SCAN), ferric chloride (Merck), ferrous chloride (Merck), NH_3 solution (Merck), silver nitrate (BDH), and $NaBH_4$ (ACROS ORGANICS) were used as received without any further purification. De-ionized water (conductivity: 0.055 μScm^{-1} at 25.0 °C) from HPLC grade water purification systems (BOECO, Germany) was used in the experiments.

4.2.2. Methods

W/o microemulsion was prepared by mixing TX-100, cyclohexane, 1-butanol with mole ratio at 1.0:61.6:3.5 and then water was added so that water to surfactant mole ratio, W_o became 10 (Table 2.3). For the preparation of Fe_3O_4@Ag nanoparticles experiments were carried out at room temperature. First, Fe_3O_4 nanoparticles were prepared in a vial equipped with a gas inflow port for N_2 gas, an exit for gas which acts as the port for the addition of base solution also. The iron salts (0.0008 g of $FeCl_3 \cdot 6H_2O$ and 0.0004 g of $FeSO_4 \cdot 7H_2O$) were transferred to the vial containing 6

mL of TX-100 microemulsion after purging with N_2 gas for 30 min. Under constant flow of N_2 15 μL of 14.67 M NH_3 solution was then added to the iron salt containing TX-100 microemulsion so that the pH the mixture became above 10 [the molar ratio of ammonia to iron ions ($R = [NH_3]/[Fe^{2+} + Fe^{3+}]$) was much greater than 3. When $R > 3$, pure rounded magnetite nanoparticles can be obtained.[24] After addition of NH_3 the color of the microemulsion changed from light orange to dark brown indicating the formation of Fe_3O_4 nanoparticles.[32] The reaction was continued for 60 min. Fe_3O_4 thus prepared in microemulsion was then coated with Ag nanoparticles. For this, in another vial containing 6 mL TX-100 microemulsion, 7.4 μL of 0.1 M $AgNO_3$ was added (to obtain 1:1 molar ratio of prepared Fe_3O_4 and Ag) after purging N_2 for about 20 min and mixed with the Fe_3O_4 containing microemulsion. Then 7.4 μL of 0.2 M $NaBH_4$ was added to the mixture to reduce Ag salt. The mixture was sonicated at room temperature for 2 h.

4.2.3. Characterizations

The Fourier transform infrared (FTIR) spectrum was recorded with a Perkin Elmer FT-IR/NIR spectrometer (Frontier) in the spectral wavenumber range from 1800 to 400 cm^{-1}. FTIR spectrum of Fe_3O_4 nanoparticles were recorded after separation of nanoparticles from microemulsions. For this excess acetone was added to the mixture and the particles were recovered. The particles were washed several times with acetone and dispersed in it (due to the negligible presence of dissolved oxygen in acetone[33]). One drop of this dispersion was dropped on KBr pellet and was used for recording FTIR spectrum. The optical absorption spectra of nanoparticles in microemulsion were recorded using a double beam Shimadzu UV-Visible spectrophotometer, UV-1650 PC. Rectangular quartz cells of path length 1 cm were used throughout the investigation. The size and size distribution of the nanoparticles synthesized in w/o microemulsion were measured by DLS measurements with the same methodology as described in section 2.2.3 and 3.2.2. Morphological analyses of nanoparticles were carried out using JEOL analytical scanning electron microscope, model JSM-6490LA at an acceleration voltage of 20 kV just after the preparation of nanoparticles. A drop of nanoparticles in the microemulsion was dropped on the carbon coated aluminum stubs by a micropipette. The sample on the stub was allowed to evaporate the solvent at ambient temperature.

4.2.4 Antibacterial activity

The antibacterial activities of Ag, Fe_3O_4 and Fe_3O_4@Ag nanoparticles were evaluated using zone of inhibition method against *S. aureus* and *E. coli*. The agar medium was prepared following the method described in chapter 3 (section 3.2.3). Freshly prepared nanoparticles in microemulsions were separated by the addition of excess amount of acetone and centrifugation for about 20 min. The as separated nanoparticles were washed with acetone several times followed by dispersion in 1 mL de-ionized water. 10 μL of dispersions of each nanoparticles was dropped in different zones of the plate. Water was used as control. After 20 h incubation at 37 ^oC the zones of inhibition were measured and the results were expressed in diameter (mm).

4.3. Results and discussion

4.3.1. FTIR spectrum analysis

FTIR spectrum was recorded to confirm the synthesis of Fe_3O_4 nanoparticles. Figure 4.1 shows the FTIR spectrum of Fe_3O_4 nanoparticles. The bands in the spectrum around 1620 cm^{-1}, 578 cm^{-1} and 400 cm^{-1} are ascribed to the vibrations of Fe–O in Fe_3O_4.[34,35,36]

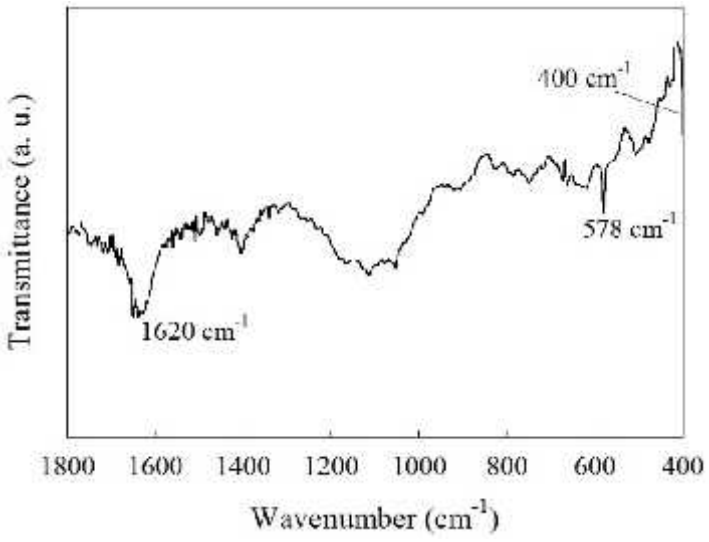

Figure 4.1. FTIR spectrum of Fe_3O_4 nanoparticles synthesized in TX-100 microemulsion.

4.3.2. UV–visible absorption spectra analysis

UV-visible spectra of Fe_3O_4 and Fe_3O_4@Ag nanoparticles are presented in Figure 4.2. Fe_3O_4 nanoparticles do not show any absorption band. The absorbance only increased from 600 to 300 nm.[37,38] When Ag nanoparticles were deposited onto the Fe_3O_4 nanoparticle surface, the absorption peak at 400 nm was remarkably observed indicating coating of Ag on the Fe_3O_4 by the deposition precipitation method. This peak is due to the Ag surface plasmon resonance band[39] and confirms the presence of Ag in the particles.[40,41,42]

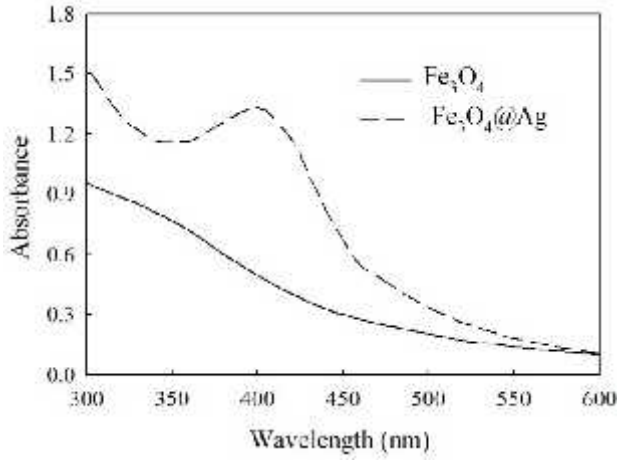

Figure 4.2. UV–visible absorption spectra of Fe_3O_4 nanoparticles and Fe_3O_4@Ag nanoparticles in TX-100 microemulsion.

4.3.3. Size, size distribution and morphological analysis

DLS measurements of Ag, Fe_3O_4 and Fe_3O_4@Ag nanoparticles in w/o microemulsions were carried out. Figure 4.3 shows the size distributions of these nanoparticles. The size of w/o micoemulsion droplets of the TX-100 microemulsion at W_o = 10 is 29 nm which infer them as nanoreactors (Figure 2.3). The sizes of Ag and Fe_3O_4 nanoparticles are 141 nm and 164 nm and those of the functionalized nanoparticles are 190 nm. The size and particle size distribution have been found to increase in the case of Fe_3O_4@Ag nanoparticles as compared to those of the Fe_3O_4 nanoparticles. This increase in the size of the synthesized Fe_3O_4@Ag nanoparticles indicates the formation of Ag shell on the Fe_3O_4 core.

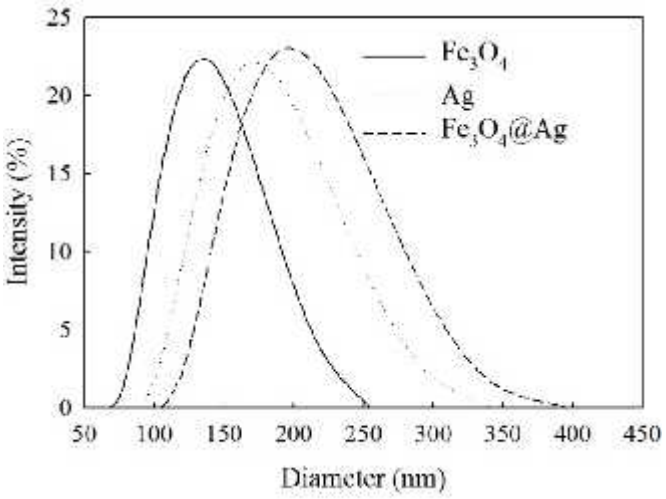

Figure 4.3. Size distribution of Fe_3O_4, Ag and Fe_3O_4@Ag nanoparticles in TX-100 microemulsions.

From the SEM images of Fe_3O_4@Ag nanoparticles formed in w/o microemulsion (Figure 4.4 (a)) it is clear that the functionalized nanoparticles formed are spherical in shape. It is precisely evident from the SEM images of Fe_3O_4 and Ag nanoparticles that the Ag nanoparticles exhibit brighter contrast whereas Fe_3O_4 show lighter contrast (Figure 4.4 (b) and 4.4 (c)). Due to its higher electron density Ag[43] showed brighter spots compared to magnetite in the SEM image.[44] For Fe_3O_4@Ag nanoparticles the shiny contrast reveals uniform coating of Ag around Fe_3O_4 core.

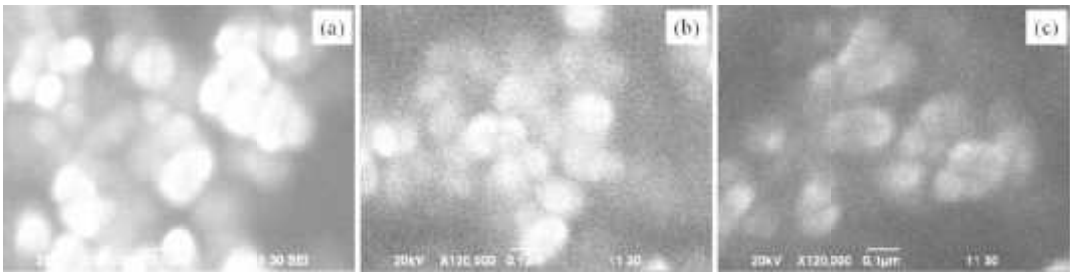

Figure 4.4. SEM images of Fe_3O_4@Ag, Ag and Fe_3O_4 nanoparticles in TX-100 microemulsion at $W_o = 10$.

The average sizes of synthesized Ag, Fe_3O_4 and Fe_3O_4@Ag nanoparticles were found to be 90 nm, 70 nm and 110 nm respectively measured from SEM images which are smaller than sizes obtained from DLS measurements. Image analysis on the SEM micrographs gives the 'true diameter' of the particles though determined on a statistically small sample, whereas DLS provides the 'hydrodynamic diameter' on an

ensemble average. That's why; the sizes of synthesized nanoparticles obtained through DLS are normally larger than those obtained from SEM results.

4.3.4. Antibacterial activities

The antibacterial activities of dispersions of Ag, Fe_3O_4 and Fe_3O_4@Ag nanoparticles in de-ionized water were tested using zone of inhibition method against both *E. coli* and *S. aureus*. The experiments showed no zones of inhibition for water which was used as a control.

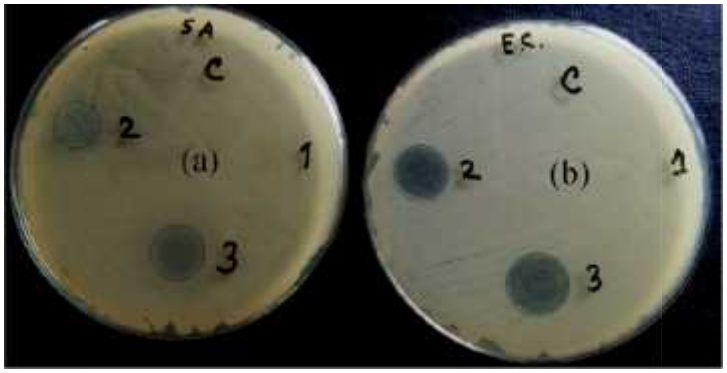

Figure 4.5. Antibacterial activity test against pathogens; (a) *S. aureus* (b) *E. coli*. De-ionized water was used as control (c). The samples are labeled as (1) Fe_3O_4, (2) Ag and (3) Fe_3O_4@Ag nanoparticles.

There was also no zones of inhibition for Fe_3O_4 nanoparticles against both bacteria. Ag and Fe_3O_4@Ag nanoparticles showed zones of inhibition where Fe_3O_4@Ag nanoparticles showed enhanced bacterial inhibitory properties. In literature it has been reported that Fe_3O_4 nanosystems exhibit antimicrobial activity[45] and strong antibacterial activity against bacterial species.[46] Several assumptions have been made to understand the mechanism of antibacterial action of nanoparticles: (i) attachment of nanoparticles to the cell membrane disturbing the cellular function. (ii) release of ions from nanoparticles, their reaction with different functional groups, their precipitation and inactivation (iii) penetration of small nanoparticles inside the cell producing physical damage to mitochondria and (iv) generation of hydrogen peroxide (H_2O_2) generated when Fe^{2+} responds with oxygen. The reduction of hydrogen peroxide with ferrous iron results in the formation of extremely reactive hydroxyl radical through Fenton reaction which damage the biological macro-molecules. But the bacterial inhibition of iron oxide depends on concentration[46] and at high concentration, Fe_3O_4 shows biocidal activity.[42] In this experiment the concentration of Fe_3O_4 nanoparticles

is low (0.34 μg mL^{-1}). So, there was no zone of inhibition. But Ag nanoparticles inhibited bacteria at low concentrations (similar result was also reported in chapter 3). The bacterial inhibitory activity of Fe_3O_4@Ag nanoparticles is higher which might be due to the synergistic antibacterial effect of Fe_3O_4 and Ag nanoparticles. In the present case, more sensitivity was observed against *E. coli* than *S. aureus*. As discussed in chapter 3, the difference in bacterial cell membrane structure might be responsible for this. The much more rigid thick layer of peptidoglycan of Gram-positive bacteria makes them less sensitive.

4. Conclusions

Fe_3O_4@Ag could be successfully prepared using w/o microemulsion method. FTIR spectrum confirmed the formation of Fe_3O_4 and UV–visible absorption spectra confirmed the presence of both Fe_3O_4 and Ag nanoparticles. The antibacterial effect determined by zone of inhibition method proves that the as prepared Fe_3O_4@Ag nanoparticles have bacterial inhibitory property against both *E. coli* and *S. aureus*.

References

(1) Tang, Y.; Liu, Y.; Li, W.; Xie, Y.; Li, Y.; Wu, J.; Wang, S.; Tian, Y.; Tian, W.; Teng, Z.; Lu, G. Synthesis of sub-100 nm biocompatible superparamagnetic Fe_3O_4 colloidal nanocrystal clusters as contrast agents for magnetic resonance imaging. *RSC Adv*. **2016**, *6*, 62550-62555.

(2) Wu, W.; He, Q.; Jiang, C. Magnetic iron oxide nanoparticles: synthesis and surface functionalization strategies. *Nanoscale Res Lett* **2008**, *3*, 397-415.

(3) Veiseh, O.; Gunn, J. W.; Zhang, M. Design and fabrication of magnetic nanoparticles for targeted drug delivery and imaging. *Adv. Drug Delivery Rev*. **2010**, *62*, 284-304.

(4) Fang, C.; Zhang, M. Multifunctional magnetic nanoparticles for medical imaging applications. *J. Mater. Chem*. **2009**, *19*, 6258-6266.

(5) Indira, T. K.; Lakshmi, P. K. Magnetic nanoparticles- a review. *Int. J. Pharm. Sci. Nanotechnol*. **2010**, *3*, 1035-1042.

(6) Dresco, P. A.; Zaitsev, V. S.; Gambino, R. J.; Chu, B. Preparation and properties of magnetite and polymer magnetite nanoparticles. *Langmuir* **1999**, *15*, 1945-1951.

(7) Mandal, M.; Kundu, S.; Ghosh, S. K.; Panigrahi, S.; Sau, T. K.; Yusuf, S. M.; Pal, T. Magnetite nanoparticles with tunable gold or silver shell. *J. Colloid Interf. Sci*. **2005**, *286*, 187-194.

(8) Majewski. P.; Thierry, B. Functionalized magnetite nanoparticles—synthesis, properties, and bio-applications. *Crit. Rev. Solid State Mater. Sci*. **2007**, *32*, 203-215.

(9) Petcharoena, K.; Sirivat, A. Synthesis and characterization of magnetite nanoparticles via the chemical co-precipitation method. *Mater. Sci. Eng., B* **2012**, *177*, 421-427.
(10) Wang, R.; Hu, Y.; Zhao, N.; Xu, F. Well Defined peapod-like magnetic nanoparticles and their controlled modification for effective imaging guided gene therapy. *ACS Appl. Mater. Interfaces* **2016**, *8*, 11298-11308.
(11) Tartaj, P.; Morales, M. d. P.; Veintemillas-Verdaguer, S.; González-Carreño, T.; Serna, C. J. The preparation of magnetic nanoparticles for applications in biomedicine. *J. Phys. D: Appl. Phys*. **2003**, *36*, 182-197.
(12) Kumar, C. Nanotechnologies for the Life Sciences Vol.1: Biofunctionalization of Nanomaterials, 2005, Wiley-VCH Pub.
(13) Virkutyte. J.; Varma, R. S. Green synthesis of metal nanoparticles: Biodegradable polymers and enzymes in stabilization and surface functionalization. *Chem. Sci*. **2011**, *2*, 837-846.
(14) Kim, D. K.; Zhang, Y.; Voit, W.; Rao, K. V.; Muhammed, M. Synthesis and characterization of surfactant-coated superparamagnetic monodispersed iron oxide nanoparticles. *J. Magn. Magn. Mater*. **2001**, *225*, 30-36.
(15) Fajaroh, F.; Setyawan, H.; Nur, A.; Lenggoro, I. W. Thermal stability of silica-coated magnetite nanoparticles prepared by an electrochemical method. *Adv. Powder Technol*.**2013**, *24*, 507-511.
(16) Campos, R. P.; Cuevas, A. C.; Muñoz, R. E. Materials Characterization, Springer, **2015.**
(17) Ye, D.; Zhong, Z.; Xu, H.; Chang, C.; Yang, Z.; Wang, Y.; Ye, Q.; Zhang, L. Construction of cellulose/nanosilver sponge materials and their antibacterial activities for infected wounds healing. *Cellulose* **2016**, *23*, 749-763.
(18) Ghaffari-Moghaddam, M.; Eslahi, H. Synthesis, characterization and antibacterial properties of a novel nanocomposite based on polyaniline/polyvinyl alcohol/Ag. *Arabian J. Chem.* **2014**, *7*, 846-855.
(19) Palza, H. Antimicrobial Polymers with Metal Nanoparticles. *Int. J. Mol. Sci.* **2015**, *16*, 2099-2116.
(20) Küünal, S.; Kutti, S.; Rauwel, P.; Guha, M.; Wragg, D.; Rauwel, E. Biocidal properties study of silver nanoparticles used for application in green housing. *Int. Nano Lett*. **2016**, *6*, 19-197.
(21) Gao, J.; Gu, H.; Xu, B. Multifunctional magnetic nanoparticles: design, synthesis, and biomedical applications. *Acc. Chem. Res*. **2009**, *42*, 1097-1107.
(22) Zheng, B.; Zhang, M.; Xiao, D.; Jin, Y.; Choi, M. M. F. Fast microwave synthesis of Fe_3O_4 and Fe_3O_4/Ag magnetic nanoparticles using Fe^{2+} as precursor. *Inorg. Mater*. **2010**, *46*, 1106-1111.
(23) Faraji, M.; Yamini, Y.; Rezaee, M. Magnetic nanoparticles: synthesis, stabilization, functionalization, characterization, and applications. *J. Iran. Chem. Soc.* **2010**, *7*, 1-37.
(24) Ahn, T.; Kim, J. H.; Yang, H-M.; Lee, J. W.; Kim, J-D.; Formation pathways of magnetite nanoparticles by coprecipitation method. *J. Phys. Chem. C* **2012**, *116*, 6069-6076.
(25) Hajdú, A.; Illés, E.; Tombácz, E.; Borbáth, I. Surface charging, polyanionic coating and colloid stability of magnetite nanoparticles. *Colloids Surf.*, *A* **2009**, *347*, 104-108.

(26) Iida, H.; Takayanagi, K.; Nakanishi, T.; Osaka, T.; Synthesis of Fe_3O_4 nanoparticles with various sizes and magnetic properties by controlled hydrolysis. *J. Colloid Interf. Sci*. **2007**, *314*, 274-280.

(27) Xu, J-K.; Zhang, F-F.; Sun, J-J.; Sheng, J.; Wang, F.; Sun, M. Bio and Nanomaterials Based on Fe_3O_4. *Molecules* **2014**, *19*, 21506-21528.

(28) Mohapatra, M.; Anand, S. Synthesis and applications of nano-structured iron oxides/hydroxides – a review. *Int. J. Eng. Sci.Technol*. **2010**, *2*, 127-146.

(29) Lu, A-H.; Salabas, E. L.; Schüth, F. Magnetic nanoparticles: synthesis, protection, functionalization, and application. *Angew. Chem. Int. Ed*. **2007**, *46*, 1222-1244.

(30) Vijayakumar, R.; Koltypin, Y.; Felner, I.; and Gedanken, A. Sonochemical synthesis and characterization of pure nanometer-sized Fe_3O_4 particles. *Mater. Sci. Eng.*, *A* **2000**, *286*, 101-105.

(31) Chin, A. B.; Yaacob, I. I. Synthesis and characterization of magnetic iron oxide nanoparticles via w/o microemulsion and Massart's procedure. *J. Mater. Process. Technol*. **2007**, *191*, 235-237.

(32) Basavegowda, N.; Mishra, K.; Lee, Y. R. Sonochemically synthesized ferromagnetic Fe_3O_4 nanoparticles as a recyclable catalyst for the preparation of pyrrolo[3,4 c]quinoline-1,3-dione derivatives. *RSC Adv*. **2014**, *4*, 61660-61666.

(33) Muniz-Miranda, M.; Gellini, C.; Giorgetti, E. Surface-enhanced raman scattering from copper nanoparticles obtained by laser ablation. *J. Phys. Chem. C* **2011**, *115*, 5021-5027.

(34) Liang, X.; Jia, X.; Cao, L.; Sun, J.; Yang, Y. Microemulsion synthesis and characterization of nano-Fe_3O_4 particles and Fe_3O_4 nanocrystalline. *J. Dispersion Sci. Technol*. **2010**, *31*,1043-1049.

(35) Togashi, T.; Naka, T.; Asahina, S.; Sato, K.; Takamid, S.; Adschiri, T. Surfactant-assisted one-pot synthesis of superparamagnetic magnetite nanoparticle clusters with tunable cluster size and magnetic field sensitivity. *Dalton Trans.* **2011**, *40*, 1073-1078.

(36) Cornell, R. M.; Schwertmann, U. Iron Oxides 2nd ed. **2003**, 146.

(37) Xu, Z.; Hou, Y.; Sun, S. Magnetic core/shell Fe_3O_4/Au and Fe_3O_4/Au/Ag nanoparticles with tunable plasmonic properties. *J. Am. Chem. Soc*. **2007**, *129*, 8698-8699.

(38) Yew, Y. P.; Shameli, K.; Miyake, M.; Kuwano, N.; Khairudin, N. B. B. A.; Mohamad, S. E. B.; Lee, K. X. Green Synthesis of magnetite (Fe_3O_4) nanoparticles using seaweed (kappaphycus alvarezii) extract. *Nanoscale Res. Lett*. **2016**, *11*, 276-282.

(39) Tang, D.; Yuan, R.; Chai, Y. Magnetic core-shell Fe_3O_4@Ag nanoparticles coated carbon paste interface for studies of carcinoembryonic antigen in clinical immunoassay. *J. Phys. Chem. B* **2006,** *110,* 11640-11646.

(40) Moosavi, R.; Afkhami, A.; Madrakiana, T. A simple cyanide sensing probe based on Ag/Fe_3O_4 nanoparticles. *RSC Adv.* **2015**, *5*, 15886-15891.

(41) Iglesias-Silva, E.; Rivas, J.; Isidro, L. M. L.; López-Quintela, M. A. Synthesis of silver-coated magnetite nanoparticles. *J. Non-Cryst. Solids* **2007**, *353*, 829-831.

(42) Gong, P.; Li, H.; He, X.; Wang, K.; Hu, J.; Tan, W.; Zhang, S.; Yang, X. Preparation and antibacterial activity of Fe_3O_4@Ag nanoparticles. *Nanotechnology* **2007**, *18*, 285604-285610.

(43) Huang, J.; Sun, Y.; Huang, S.; Yu, K.; Zhao, Q.; Peng, F.; Yu, H.; Wang, H.; Yang, J. Crystal engineering and SERS properties of Ag–Fe_3O_4 nanohybrids: from heterodimer to core–shell nanostructures. *J. Mater. Chem*. **2011**, *21*, 17930–17937.

(44) Nakhjavan, B.; Tahir, M. N.; Natalio, F.; Gao, H.; Schneider, K.; Schladt, T.; Ament, I.; Branscheid, R.; Weber, S.; Kolb, U.; Sönnichsen, C.; Schreiberc, L. M.; Tremel, W. Phase separated Cu@Fe_3O_4 heterodimer nanoparticles from organometallic reactants. *J. Mater. Chem*. **2011**, *21*, 8605- 8611.

(45) Anghel, I.; Grumezescu, A. M.; Andronescu, E.; Anghel, A. G.; Ficai, A.; Saviuc, C.; Grumezescu, V.; Vasile, B. S.; Chifiriuc, M. C. Magnetite nanoparticles for functionalized textile dressing to prevent fungal biofilms development. *Nanoscale Res. Lett*. **2012**, *7*, 501-506.

(46) Prabhu, Y. T.; Rao, K. V.; Kumari, B. S.; Kumar, V. S. S.; Pavani, T. Synthesis of Fe_3O_4 nanoparticles and its antibacterial application. *Int Nano Lett*, **2015**, *5*, 85–92.

Abstract

Polyaniline (PAni) was synthesized by chemical oxidative polymerization of aniline monomer by ammonium peroxydisulfate using w/o microemulsion and from aqueous solution. Ag/PAni nanocomposites were then prepared using w/o microemulsion by the same polymerization method in preformed Ag nanoparticles prepared by the reduction of metal salts in microemulsion. PAni and Ag/PAni nanocomposites were characterized by UV-visible and FTIR spectroscopy, DLS measurements, SEM images and thermogravimetric analysis (TGA). Both UV-visible and FTIR spectra revealed the formation of PAni and Ag/PAni composite. DLS results and SEM images showed that PAni synthesized in microemulsion was smaller in particle dimension than that obtained from bulk. TGA results showed that PAni from microemulsion has a lower thermal stability than PAni from bulk synthesis. But in comparison with PAni from microemulsion, Ag/PAni nanocomposites showed somewhat better thermal stability. The antibacterial properties against Gram-negative, *E. coli* and Gram-positive, *S. aureus* were tested by zone of inhibition method and the results demonstrated that Ag/PAni nanocomposites have enhanced antibacterial efficiency compared to PAni generated in microemulsion which is more efficient than PAni prepared from aqueous solution.

5.1. Introduction

Preparation of conducting polymeric materials in nanoscopic dimension has become an important branch of materials research as they are expected to exhibit unusual chemical and physical properties and find applications in diverse fields ranging from electronics to biomedical devices.[1] Among conducting polymers polyaniline (PAni) is of great interest in recent years[2] because of its excellent chemical, thermal and environmental stability,[3] low monomer cost, facile synthesis,[4,5] tunable physicochemical[2] and conducting properties,[6] good antibacterial as well as antifungal activities.[7,8] It has different oxidation states and depending on the oxidation state and protonation level, this polymer shows different conductivity and antibacterial activity.[9,10] PAni in the salt form shows better antibacterial property than PAni in the base form.[10] It shows size and morphology dependent properties which strongly depend on preparative method. Among different polymerization methods solution polymerization can hardly control the morphology of PAni.[11] But microemulsion

polymerization is very efficient in producing polymeric nanoparticles.[12,13] W/o microemulsion is microheterogeneous system in which monolayer surfactant and cosurfactant stabilize the dispersed water core in continuous oil phase. This system can be considered a nanoreactor that allows a polymerization reaction to be carried out in its caged inside.[14] The primary goal for the development of polymerization of organic monomers in microemulsion systems is to produce stable latexes with particle sizes close to those of the parent microemulsion droplets.[15] Thus nanoscopic PAni particles can be successfully synthesized in a stable w/o microemulsion.[1,16,17,] Morphology and crystallinity of PAni can also be controlled with water content of microemulsion.[11]

More recently, several reasons provoke to prepare and investigate PAni/metal nanocomposites[18] especially Ag/PAni nanocomposite. Among all the other metals Ag has high antibacterial property[19] (Ag nanoparticles exhibited the highest antibacterial activity among four metallic nanoparticles studied and reported in section 3.3.4) at exceptionally low concentrations[20] with low toxicity toward mammalian.[21] But it has two major problems. (1) uncontrolled release and (2) natural tendency of agglomeration which can reduce the antibacterial activity.[22] These problems can be resolved by the entrapment of Ag nanoparticles on various substrates and matrices which stabilize Ag nanoparticles from aggregation with a sustained release.[23-25] Considering these, polymers can be good host matrix because of their special morphological and chemical structures with the suitable functional groups on long polymeric chains allowing incorporation and immobilization of nanoparticles thereby formation of nanocomposites.[26,27] PAni has secondary amines and tertiary imines in the backbone structure which can bind metal ions[4] and metal and also Ag has strong affinity for nitrogen.[18] So binding of Ag nanoparticles in PAni matrix could effectively prevent Ag nanoparticles from aggregation which gives long-term reactivity. Furthermore, it would give new type highly efficient material having enhanced multifunctionalities.[28] Especially PAni containing Ag nanoparticles would give advanced antibacterial agent from synergism among the two components.[3]

Most of the studies reported so far on the preparation of PAni and Ag/PAni composite from w/o microemulsion focused on electrical properties.[1,11,16,29,30] However a systematic study on the preparation of PAni and Ag/PAni nanocomposite from microemulsion and exploitation of their antibacterial activity is yet to be explored. It

would also be interesting to compare antibacterial activity of PAni and Ag/PAni nanocomposite obtained from w/o microemulsion with PAni obtained from aqueous solution. This chapter reports the preparation of PAni and Ag/PAni composite nanospheres using a w/o microemulsion route and exploration of their antibacterial properties. Ag/PAni composites with low Ag content (~ 0.87 weight % with respect to aniline monomer) were prepared to understand the synergistic effect of Ag and PAni as bactericide. For a comparative study PAni was also prepared using solution polymerization and the size (obtained from these two different routes) and antibacterial activities were correlated.

5.2. Experimental

5.2.1. Materials

Aniline (99.5%, Merck) was distilled first before use. Ammonium peroxydisulfate (APS, 98%) was used as oxidative initiator for the polymerization. All the other chemicals $AgNO_3$ (BDH), $NaBH_4$ (ACROS ORGANICS), TX-100 (Sigma Aldrich), cyclohexane (Merck), 1-butanol (LAB-SCAN) were of analytical grade and used without further purification. De-ionized water (conductivity: 0.055 μScm^{-1} at 25.0 °C) from HPLC grade water purification systems (BOECO, Germany) was used throughout the experiments.

5.2.2. Methods

W/o microemulsion was prepared by mixing TX-100, cyclohexane, 1-butanol with mole ratio at 1.0:61.6:3.5 and then water was added so that water to surfactant mole ratio, W_o became 10 (Table 2.3). The mixture was sonicated until an optically clear solution was obtained. PAni was then synthesized by using double microemulsion reactant addition scheme. For this at first aniline monomer (0.016 g) and concentrated hydrochloric acid (17 μL, 10 M) was mixed in the ratio of 1:1 and 10 mL w/o microemulsion was poured into this. It was then sonicated so that aniline–HCl aqueous solution was obtained in the core of microemulsion. 0.039 g ammonium peroxydisulfate (APS) dissolved in another 10 mL microemulsion was then mixed rapidly with this ensuring aniline to oxidant mole ratio to be 1. The mixture was left in an ultrasonic bath at 25 °C for about 30 min. This was then left for 24 h without further agitation. During the process, the color of microemulsion changed from

colorless to dark brown and finally greenish black colloidal dispersion was obtained after 24 h. Excess acetone was then poured into the microemulsion to precipitate the PAni salt. It was centrifuged and washed with acetone and finally with de-ionized water more than four times to completely remove surfactants. The product was then dried at 60 °C for 6 h in an oven and greenish black PAni powder was obtained .

To make a comparison, aqueous polymerization of aniline was carried out without using TX-100 microemulsion with the same molar ratio of oxidant to aniline monomer at 25 ^{o}C.

Ag/PAni nanocomposite was prepared by *in situ* chemical oxidative polymerization of aniline monomer in the presence of preformed Ag nanoparticles in TX-100 microemulsion. In the synthesis process, Ag nanoparticles were prepared by chemical reduction of $AgNO_3$ with $NaBH_4$ with the molar ratio equal to 1:2 in TX-100 microemulsion. In $AgNO_3$ (6.5 μL 0.1 M) solubilized 10 mL microemulsion aqueous solution of $NaBH_4$ (6.5 μL 0.2 M) was added with constant stirring which gave instant color change from colorless to yellow indicating the formation of Ag nanoparticles. [31] The mixture was sonicated for 30 min at room temperature. Then PAni was synthesized using same chemical polymerization method as described above in the presence of Ag nanoparticles.

5.2.3. Characterizations

UV–visible spectroscopic analysis were carried for PAni and Ag/PAni nanocomposite dispersed in dimethyl sulfoxide (DMSO). The absorption spectra were recorded on a double beam Shimadzu UV-Visible spectrophotometer, model UV-1650 PC. Rectangular quartz cells of path length 1 cm were used throughout the investigation. Average sizes and size distributions of PAni and Ag/PAni nanocomposites dispersed in acetone were measured using Malvern Zetasizer Nano ZS90 with a scattering angle of 90^{o}. A He–Ne laser beam of 632.8 nm wavelength was used for the measurements. The morphological analysis of PAni and Ag/PAni was carried out with a JEOL analytical scanning electron microscope, model JSM-6490LA. PAni and Ag/PAni dispersions in acetone were dropped on the carbon coated aluminum stubs for the measurements at an acceleration voltage of 20 kV. FTIR spectra recorded with a Perkin Elmer FT-IR/NIR spectrometer (Frontier) in the spectral wavenumber range from 4000 to 400 cm^{-1}. KBr mixed PAni and Ag/PAni nanocomposite in the pellet

form were used for recording FTIR spectra. TGA were studied by a Hitachi instrument (TG/DTA 7200) in the temperature range of 35–550 ^{o}C at a heating rate of 10 ^{o}C per min under N_2 gas atmosphere.

5.2.4. Antibacterial activity

The antibacterial activities of PAni, Ag/PAni nanocomposites were evaluated using zone of inhibition method against Gram-negative bacteria, *E. coli* and Gram-positive bacteria, *S. aureus*. The agar medium was prepared following the procedure described in chapter 3 (section 3.2.3). 20 μL of 100 μg mL^{-1} DMSO dissolved solutions of PAni, Ag/PAni nanocomposite were dropped in different zones of the plate. DMSO was used as control. After 20 h incubation at 37 ^{o}C the zones of inhibition were measured and the results were expressed in diameter (mm).

5.3. Results and discussion

5.3.1. UV–visible absorption spectroscopy analysis

The UV-visible absorption spectra of PAni and Ag/PAni composite are shown in Figure 5.1. For PAni there are three characteristic absorption peaks at around 280, 340 and 580 nm attributed to π–π* transition of the benzenoid rings,[32] polaron/bipolaron transition,[33] and n-π* transition of the quinonoid, respectively[34] indicating the formation of PAni in the salt form. Actually PAni prepared by conventional method shows π-π* transition at 310 nm. But in this case peak shifted to shorter wavelength

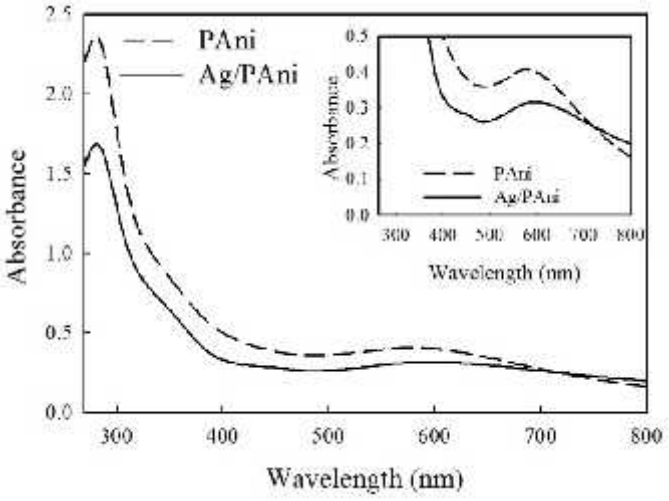

Figure 5.1. UV-visible spectra of DMSO dissolved PAni and Ag/PAni composite.

which can be attributed to PAni in the nanoscale.[32] For fully protonated PAni in salt form, the peak around 590–650 nm due to n–π* transition disappears and a new peak above 725 nm appears. This new peak corresponds to the π to localized polaron band. But in this case the peak above 725 nm was absent because of less conjugation.[34] For Ag/PAni similar absorption bands were observed with a red shifted peak for n-π* transition of the quinonoid which might be because of strong PAni and Ag interaction. Ag/PAni nanocomposites also exhibit a less intense peak at 450 nm (Figure 5.1) which is due to surface plasmon resonance nature of Ag nanoparticles.[35] The lower intensity is because of lower Ag content (only 0.87 wt% with respect to aniline monomer).

5.3.2. FTIR spectra analysis

FTIR spectra of PAni and Ag/PAni composites are shown Figure 5.2. The spectrum of PAni shows bands at 1570 cm^{-1} and 1490 cm^{-1} which are attributed to the C=N stretching of the quinoid[5] and the C=C stretching of the benzenoid,[18] respectively. The peaks at 1300 cm^{-1} and 1240 cm^{-1} correspond to the C-N vibration of -NH-(C_6H_4)-NH- and the C-N vibration of bipolaron.[29] The band at 600 cm^{-1} is because of C-N-C torsion.[36] The spectrum shows the bands that are similar and consistent with typical PAni, indicating the formation of PAni in TX-100 microemulsion. From Figure 5.2 it is observed that Ag/PAni composite have similar characteristic bands with those of PAni. But the band for C-N stretching at 1300 cm^{-1} slightly shifted to longer wavenumber (1307 cm^{-1}). This shift indicates an introduction of double bond

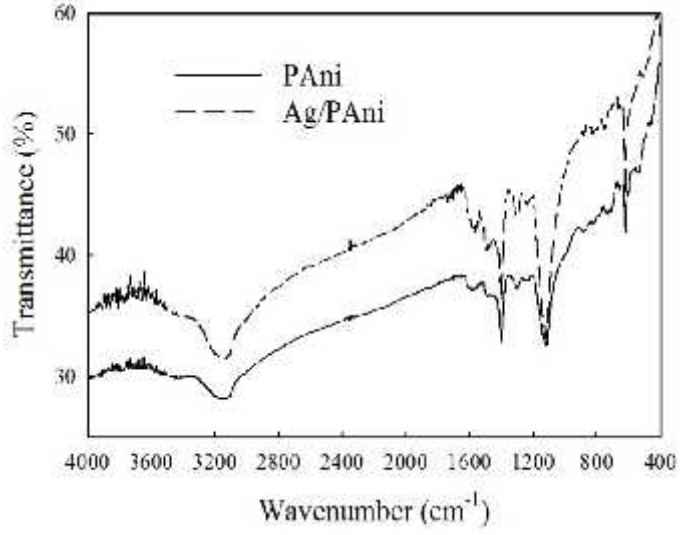

Figure 5.2. FTIR spectra of PAni and Ag/PAni composite.

character in C-N bond in benzenoid ring as a result of the formation of coordination bond between the lone pare of electrons of nitrogen and vacant *d*-orbitals of Ag nanoparticles which lowers bond length and increases the force constant.

5.3.3. Thermal analysis

Thermoravimetric (TG) and differential thermoravimetric (DTG) curves of PAni and Ag/PAni composite are shown in Figure 5.3. TG thermograms of PAni from bulk shows three main steps for weight loss. The first thermal step for weight loss below 100 °C is due to the evaporation of water in the PAni matrix and loss of HCl. The second weight loss process at around 200−300 °C is because of elimination of acid dopant (HCl) and oligoaniline from the PAni backbone.[37] At higher temperatures weight loss is due to the thermal degradation of PAni chains.[38]

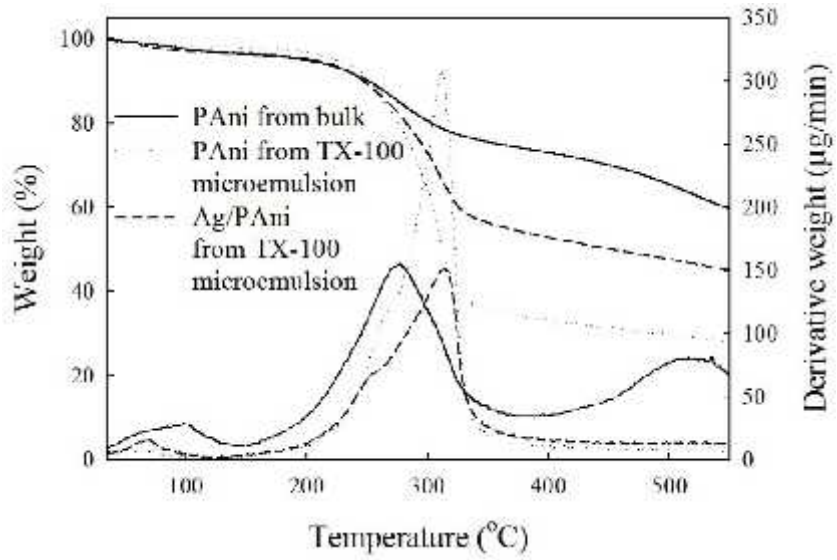

Figure 5.3. TGA for PAni from bulk and TX-100 microemulsion and Ag/PAni composite from X-100 microemulsion.

TG curves for PAni and Ag/PAni from microemulsion do not clearly show these weight loss steps. But from DTG thermogram, these three steps of weight loss behavior can be observed. In comparison with PAni from bulk, PAni from microemulsion have a lower thermal stability. As can be seen from Figure 5.3, second and third DTG peak maximum temperatures dropped from 275 ^{o}C to 252 ^{o}C and 514 ^{o}C to 300 ^{o}C. This significant lowering of third DTG peak maximum temperature might be due to the less conjugation in PAni chain prepared from microemulsion.[39] But in comparison with PAni from microemulsion, Ag/PAni composites from

microemulsions shows somewhat better thermal stability. As can be seen from Figure 5.3 second and third DTG peak maximum temperatures have been shifted from 252 ^{o}C to 263 ^{o}C and 310 ^{o}C to 315 ^{o}C. These changes reflect interactions of Ag nanoparticles and PAni in the composites.

5.3.4. Size, size distribution and morphological analysis

DLS measurements show the average diameter and size distribution of PAni and Ag/PAni composite (Figure 5.4). Average diameter and size distribution of PAni

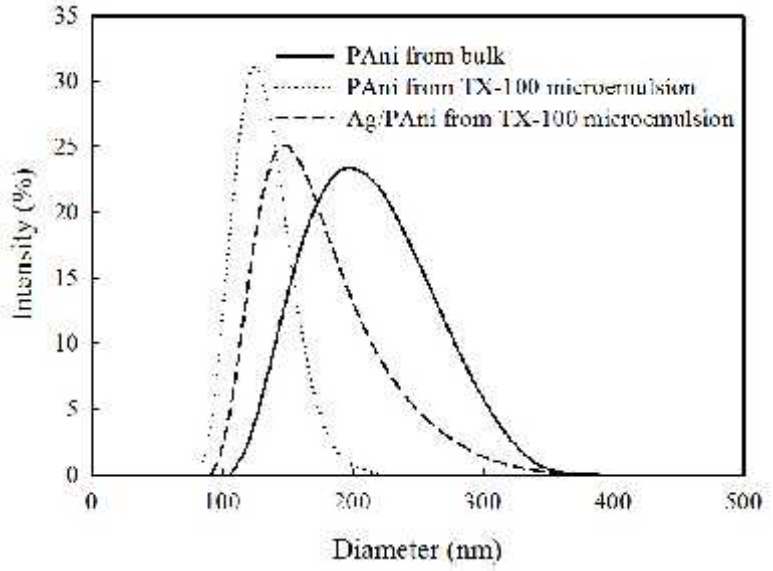

Figure 5.4. DLS of PAni from bulk and TX-100 microemulsion and Ag/PAni composite from TX-100 microemulsion.

from bulk is higher than that of PAni from microemulsion (Table 5.1).

Table 5.1. Average diameter of PAni from bulk, PAni and Ag/PAni from TX-100 microemulsion from DLS measurements

Materials	Average diameter (nm)
PAni from bulk	190
PAni from TX-100 microemulsion	122
Ag/PAni from TX-100 microemulsion	141

Figure 5.5 shows SEM images of the PAni and Ag/PAni composite. Sphere-like PAni and Ag/PAni composite nanoparticles of less than 100 nm could be prepared from

w/o microemulsion. In w/o microemulsion within a confined environment of microemulsion droplets polymerization occurred.[11] In this limited space PAni chains interact through various interchain/intrachain interactions such as H-bonding, π-π interaction, van der Waals bonding and other entanglements in much more compactly which make them aggregate giving thereby regular nanogranular structures as shown in SEM images.

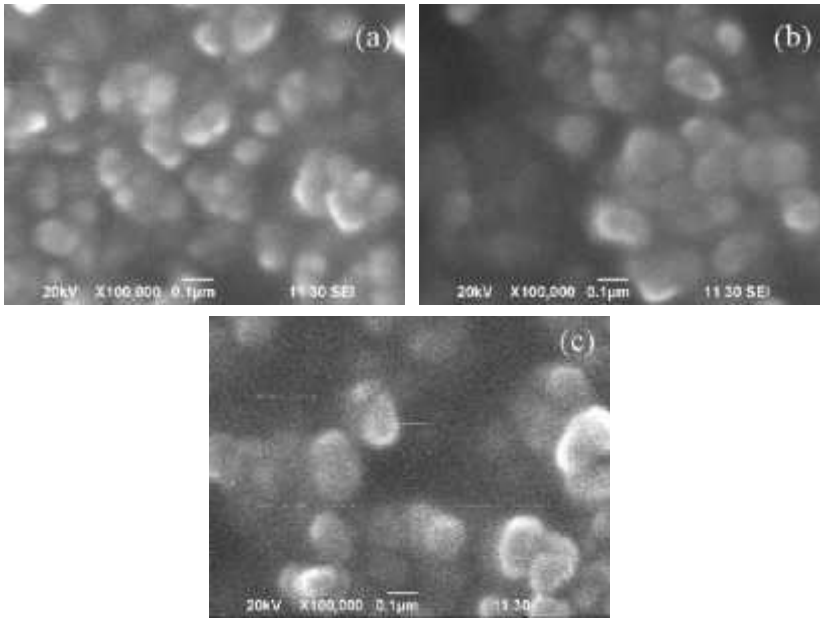

Figure 5.5. SEM images of (a) PAni and (b) Ag/PAni from TX-100 microemulsion and (c) PAni from bulk synthesis.

5.3.5. Formation of Ag/PAni nanocomposite in microemulsion

To understand the mechanism of formation of Ag/PAni nanocomposite in microemulsion zeta potentials of TX-100 microemulsion and Ag nanoparticles containing microemulsion were measured.

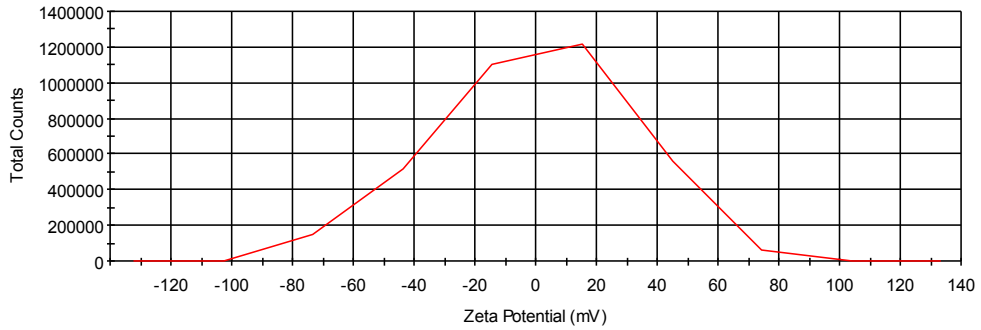

Figure 5.6. Zeta potential distribution of TX-100 microemulsion.

TX-100 microemulsion has zeta potential value of -0.0605 mV. After preparation of Ag nanoparticles it shows a negative value (-19.2 mV) for zeta potential which suggests negative surface charge on Ag particles. In the presence of Ag

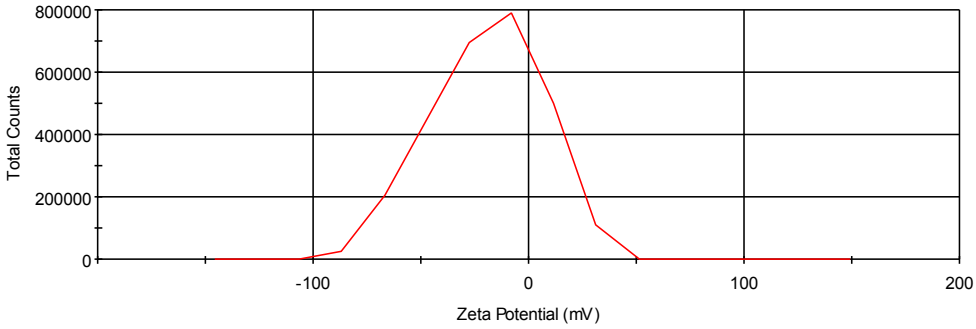

Figure 5.7. Zeta potential distribution of Ag nanoparicles in TX-100 microemulsion.

nanoparticles, when anilinum chloride is added they are easily attracted by negatively charged Ag nanoparticles (Figure 5.8). Thus, when an oxidant is added to induce the polymerization of aniline it occurs in the vicinity of Ag nanoparticles. Finally, polymer chains surround the surface of Ag nanoparticles. Strong affinity of Ag for nitrogen makes them well adhered on PAni and coordination bond is formed between vacant *d*-orbitals of Ag nanoparticles with lone pare of electrons on nitrogen of PAni. Within the confined environment of microemulsion the Ag coordinated PAni chains aggregate through various interchain/intrachain interactions (such as H-bonding, π-π interaction, vander Waals bonding and other entanglements), to form nanogranules as shown in SEM images.

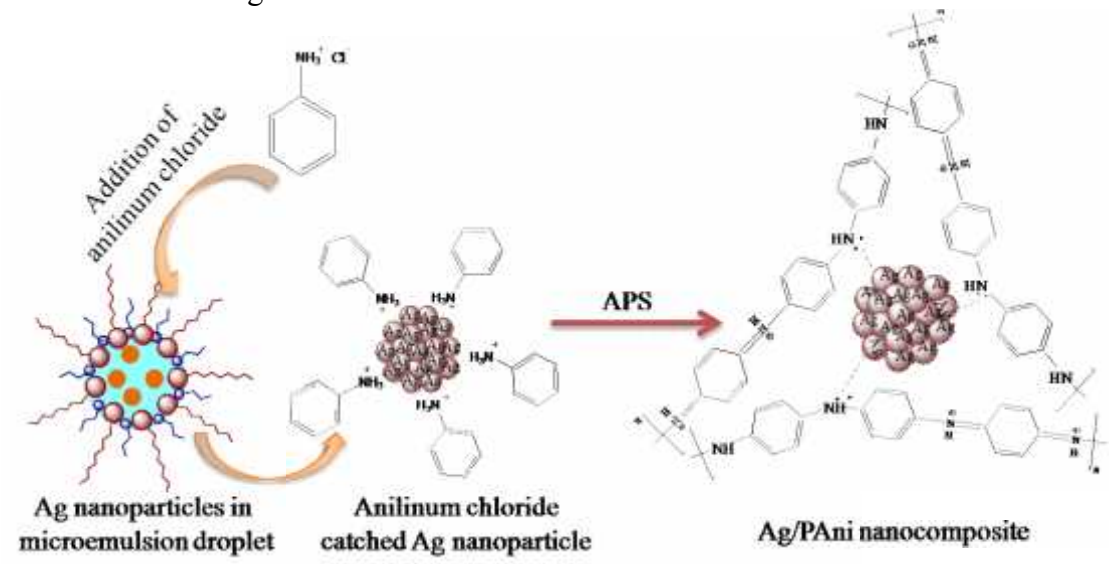

Figure 5.8. Mechanism of formation of Ag/PAni nanocomposite.

5.3.6. Antibacterial activity

The antibacterial activities of DMSO dissolved PAni and Ag/PAni nanocomposite were tested using zone of inhibition method against both *E. coli* and *S. aureus*. The experiments showed no zones of inhibition for DMSO which was used as a control.

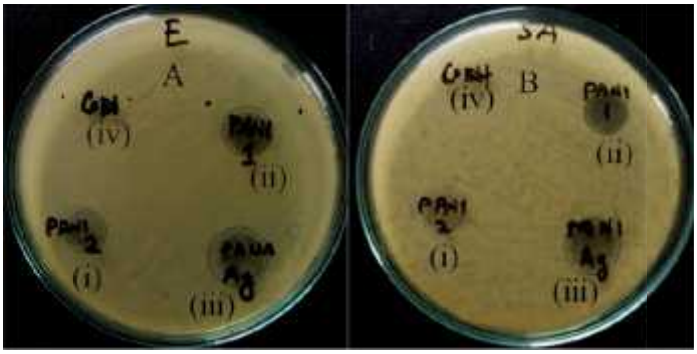

Figure 5.9. Antibacterial activity test against pathogens; (A) *E. coli* (B) *S. aureus*. The samples are labeled as: (i) PAni from aqueous synthesis (ii) PAni from w/o microemulsion (iii) Ag/PAni nanocomposite from w/o microemulsion and (iv) DMSO as control.

All PAni and Ag/PAni nanocomposite displayed antibacterial activity against *E. coli* and *S. aureus* (Figure 5.9). But there was an increase in the zones of inhibition for PAni prepared using w/o microemulsion. Ag/PAni nanocomposite showed highest antibacterial activity among these three materials. After dilution no zones of inhibition were formed against *S. aureus*. But *E. coli* showed sensitivity to PAni and Ag/PAni composite after 10 times dilution and Ag/PAni composite showed antibacterial activity even after 100 times dilution.

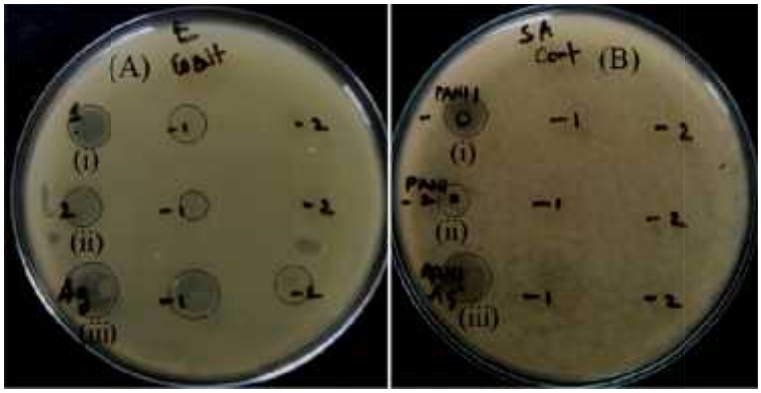

Figure 5.10. Diameter of zone of inhibition of (i) PAni from w/o microemulsion (ii) PAni from aqueous solution (iii) Ag/PAni nanocomposite from w/o microemulsion against (A) *E. coli* and (B) *S. aureus* at different dilution.

Antibacterial activities of PAni mainly come from acidic dopant molecules and inherent amino groups present.[3,7,8] As discussed in chapter 3 (section 3.3.4) the overall charge of the cell surface of the bacteria at biological pH values is negative which results from the dissociation of the excess number of carboxylic and other groups.[39] PAni chains with positive imino sites therefore can bind to the negatively charged outer walls of the cells. For this electrostatic attachment different polarity charge transfer process might take place providing antibacterial property for PAni. For all the three materials *E. coli* is somewhat more sensitive. This could be ascribed to the multi-layered Gram-negative cell walls with low osmotic pressure, which facilitated the physical interactions.[3] The PAni chains anchor to the cell walls at several sites cause damage to the membrane, by changing the potential gradients across the ion channels present on the cell membranes of *E. coli*. On the other hand, Gram-positive bacteria composed of a thick layer (20-80 nm) of peptidoglycan, consists of linear polysaccharide chains cross-linked by short peptides which form a three dimensional rigid structure. This rigid and extended crosslinking endows the cell wall with fewer anchoring sites for the PAni making it more difficult for the dopant ions (Cl^-) to penetrate inside.[40] Thus, the growth of Gram-negative bacteria is inhibited to a greater extent compared to Gram-positive bacteria. PAni prepared from microemulsion shows better bacterial inhibitory property. The reason for this is the formation of PAni nanoparticles which increased surface area and thereby enhance reactivity against bacteria. Their ease of attachment to the bacterial cell wall because of smaller size make them more active against bacteria. Ag/PAni nanocomposite possesses higher antibacterial activity than others. Ag shows antibacterial activity as discussed in chapter 3 (section 3.3.4). Therefore it can be said that synergistic antibacterial effect of PAni and Ag nanoparticles makes the nanocomposite more active against bacteria.

5.4. Conclusions

PAni nanoparticles and Ag/PAni nanocomposite could be successfully prepared using w/o microemulsion. Both PAni and Ag/PAni nanocomposite had smaller average size, narrower size distribution. The thermal stability decreased in the order PAni obtained from aqueous synthesis > Ag/PAni nanocomposite obtained from w/o microemulsion > PAni from w/o microemulsion. Ag/PAni nanocomposite prepared using w/o

microemulsion method had enhanced antibacterial activity against *E. coli* and *S. aurious* compared to pure PAni obtained from both microemulsion and aqueous synthesis. So Ag/PAni nanocomposite prepared using w/o microemulsion may be used as a potent antibacterial agent.

References

(1) Yan, F.; and Xue, G. Synthesis and characterization of electrically conducting polyaniline in water-oil microemulsion. *J. Mater. Chem*. **1999**, *9*, 3035-3039.

(2) Palaniappan, S.; John A. Polyaniline materials by emulsion polymerization pathway. *Prog. Polym. Sci.* **2008**, *33*, 732-758.

(3) Poyraz, S.; Cerkez, I.; Huang, T-S.; Liu, Z.; Kang, L.; Luo, J.; Zhang, X. One-step Synthesis and characterization of polyaniline nanofiber/silver nanoparticle composite networks as anti-bacterial agents. *ACS Appl. Mater. Interfaces* **2014**, 1-20.

(4) Jia, Q.; Shan, S.; Jiang, L.; Wang, Y.; Li, D. Synergistic antimicrobial effects of polyaniline combined with silver nanoparticles. *J. Appl. Polym. Sci*. **2012**, 1-7.

(5) Mostafaei, A.; Zolriasatein, A. Synthesis and characterization of conducting polyaniline nanocomposites containing ZnO nanorods. *Prog. Nat. Sci*. **2012**, *22*, 273-280.

(6) Vincent, B.; Waterson, J. Colloidal dispersions of electrically-conducting, spherical polyaniline particles. *J. Chem. Soc., Chem. Commun*. **1990**, 683-684.

(7) Shi, N.; Guo, X.; Jing, H.; Gong, J.; Sun, C.; Yang, K. Anibacterial effect of the conducting polyaniline. *J. Mater. Sci. Technol*. **2006**, *22*, 289-290.

(8) Seshadri, D. T.; Bhat, N. V. Use of polyaniline as an antimicrobial agent in textiles. *Indian J. Fibre Text. Res*. **2005**, *30*, 204-206.

(9) Marie, E.; Rothe, R.; Antonietti, M.; Landfester, K. Synthesis of polyaniline particles via inverse and direct miniemulsion. *Macromolecules* **2003**, *36*, 3967-3973.

(10) Kucekova, Z.; Kasparkova, V.; Humpolicek, P.; Sevcikova, P.; Stejskal, J. Antibacterial properties of polyaniline–silver films. *Chemical Papers* **2013**, *67*, 1103-1108.

(11) Zhou, Q.; Wang, J.; Ma, Y.; Cong, C.; Wang, F. The relationship of conductivity to the morphology and crystallinity of polyaniline controlled by water content via reverse microemulsion. *Colloid. Polym. Sci*. **2007**, *285*, 405-411.

(12) Li, L.; Yan, G.; Wu, J.; Yu, X.; Guo, Q. Preparation of polyaniline–metal composite nanospheres by in situ microemulsion polymerization. *J. Colloid Interf. Sci*. **2008**, *326*, 72-75.

(13) Kim, B-J.; Oh, S-G.; Han, M-G.; Im, S-S. Synthesis and characterization of polyaniline nanoparticles in SDS micellar solutions. *Synth. Met*. **2001**, *122*, 297-304.

(14) Huang, K.; Meng, Xiao-Hong.; Wan, M. Polyaniline hollow microspheres constructed with their own self-assembled nanofibers. *J. Appl. Polym. Sci*., **2006**, *100*, 3050-3054.

(15) Barton, J. Free-radical polymerization in inverse microemulsions. *Prog. Polym Sci*. **1996**, *21*, 399-438.
(16) Chan, H. S. O.; Gan, L. M.; Chew, C. H.; Ma, L.; Seow, S. H. Characterization of chemically and electrochemically prepared polyanilines in inverse microemulsions. *J. Mater. Chem*. **1993***,3*, 1109-1115.
(17) Gan, L. M.; Chew, C. H.; Chan, H. S. O.; Ma, L. Preparation of polyaniline particles in an inverse microemulsion. *Polym. Bull*. **1993**, *31*, 347-350.
(18) Choudhury, A. Polyaniline/silver nanocomposites: Dielectric properties and ethanol vapour sensitivity. *Sens. Actuators, B* **2009**, *138*, 318-325.
(19) Kolmas, J.; Groszyk, E.; Kwiatkowska-Róhycka, D. Substituted hydroxyapatites with antibacterial properties. *Biomed Res. Int.* **2014**, 1-15.
(20) Palza, H. Antimicrobial Polymers with Metal Nanoparticles. *Int. J. Mol. Sci.* **2015**, *16*, 2099-2116.
(21) Chaloupka, K.; Malam, Y.; Seifalian, A. M. Nanosilver as a new generation of nanoproduct in biomedical applications. *Trends Biotechnol.* **2010**, *28*, 580-588.
(22) Lv, M.; Su, S.; He, Y.; Huang, Q.; Hu, W.; Li, D.; Fan, C.; Lee, S.-T. Long-term antimicrobial effect of silicon nanowires decorated with silver nanoparticles. *Adv. Mater*. **2010**, *22*, 5463-5467.
(23) Silver, S. Bacterial silver resistance: molecular biology and uses and misuses of silver compounds. *FEMS Microbiol. Rev*. **2003**, *27*, 341-353.
(24) Voccia, S.; Ignatova, M.; Jérôme, R.; Jérôme, C. Design of antibacterial surfaces by a combination of electrochemistry and controlled radical polymerization. *Langmuir* **2006**, *22*, 8607-8613.
(25) Li, Z.; Lee, D.; Sheng, X.; Cohen, R. E.; Rubner, M. F. Two-level antibacterial coating with both release-killing and contact-killing capabilities. *Langmuir* **2006**, *22*, 9820-9823.
(26) Ghaffari-Moghaddam, M.; Eslahi, H. Synthesis, characterization and antibacterial properties of a novel nanocomposite based on polyaniline/polyvinyl alcohol/Ag. *Arabian J. Chem.* **2014**, *7*, 846-855.
(27) Dallas, P.; Sharma, V. K.; Zboril, R. Silver polymeric nanocomposites as advanced antimicrobial agents: Classification, synthetic paths, applications, and perspectives. *Adv. Colloid Interface Sci*. **2011**, *166*, 119-135.
(28) Tambolia, M. S.; Kulkarni, M. V.; Patil, R. H.; Gade, W. N.; Navale, S. C.; Kale, B. B. Nanowires of silver–polyaniline nanocomposite synthesized via in situ polymerization and its novel functionality as an antibacterial agent. *Colloids Surf., B* **2012**, *92*, 35-41.
(29) Li, Z.; Li, Y.; Lin, W.; Zheng, F.; Laven, J. Polyaniline/silver nanocomposites synthesized via Uv–vis-assisted aniline polymerization with a reversed micellar microemulsion system. *Polym. Compos*. **2014**, 1-8.
(30) Ichinohe, D.; Arai, T.; Rise H. Synthesis of soluble polyaniline in reversed micellar systems. *Synth. Met*. **1997**, *84*, 75-76.
(31) Hossain, S.; Fatema, U. K.; Mollah, M. Y. A.; Rahman, M. M.; Susan, M. A. B. H. Preparation of metal nanoparticles with antibacterial activity using microemulsions as nanoreactors. *J. Bangladesh Chem. Soc.* **2012**, *25*, 71-79.
(32) Silva, C. W. d. Mechatronic Systems devices, design, control, operation and monitoring. CRC press, **2008**.
(33) Boomi, P.; Prabu, H. G.; Manisankar, P.; Ravikumar, S. Study on antibacterial activity of chemically synthesized PANI-Ag-Au nanocomposite. *Appl. Surf. Sci*. **2014**, *300*, 66-72.

(34) Gottam, R.; Srinivasan, P. A novel process of alcohol promoted polymerization of aniline to form nano fibrous, fluorescent and highly crystalline polyaniline salt. *New J. Chem*. **2015**, 1-10.
(35) Khanna, P. K.; Singh, N.; Charan, S.; Viswanath, A. K. Synthesis of Ag/polyaniline nanocomposite via an in situ photo-redox mechanism. *Mater. Chem. Phys*. **2005**, *92*, 214-219.
(36) Islam, M. S.; Miran, M. S.; Rahman, M. M.; Mollah, M. Y. A.; Susan, M. A. B. H. Polyaniline-silica composite materials: influence of silica content on the thermal and thermodynamic properties. J. NANOSTRUCTURED POLYMERS AND NANOCOMPOSITES. **2013**, *9/3*, 84-90.
(37) Sarkar, N.; Sahoo, G.; Das, R.; Prusty, G.; Sahu, D.; Swain, S. K. Anticorrosion performance of three-dimensional hierarchical PANI@BN nanohybrids. *Ind. Eng. Chem. Res*. **2016**, *55*, 2921-2931
(38) Khan, J. A.; Qasim, M.; Singh, B. R.; Singh, S.; Shoeb, M.; Khan, W.; Das, D.; Naqvi, A. H. Synthesis and characterization of structural, optical, thermal and dielectric properties of polyaniline/$CoFe_2O_4$ nanocomposites with special reference to photocatalytic activity. *Spectrochim. Acta, Part A* **2013** *109*, 313-321.
(39) Stoimenov, P. K.; Klinger, R. L.; Marchin, G. L.; Klabunde, K. J. Metal Oxide Nanoparticles as Bactericidal Agents. *Langmuir* **2002,** *18,* 6679-6686.
(40) Dhivya, C.; Vandarkuzhali, S. A. A.; Radha, N. Antimicrobial activities of nanostructured polyanilines doped with aromatic nitro compounds. *Arabian J. Chem.* **2015**.

Abstract

Silver/poly(vinyl alcohol) (Ag/PVA) nanocomposite film was successfully prepared using TX-100/1-butanol/cyclohexane/water microemulsion. Reduction of metal salt was carried in the core of w/o microemulsion droplet containing PVA polymeric matrix. Ag/PVA nanocomposite film was then prepared by solution casting method after separation from the microemulsion. The nanocomposite film was characterized by FTIR spectroscopy, specular reflectance spectroscopy, SEM images and thermogravimetric analyses. The size and size distribution of Ag nanoparticles were measured by DLS measurements. Ag nanoparticles with average diameter of 105 nm could be synthesized using PVA, whereas in the absence of PVA the nanoparticles agglomerated once separated from the microemulsion. PVA effectively prevents the aggregation of nanoparticles. SEM images of the film prepared using microemulsion revealed the homogeneity and uniformity of Ag nanoparticles on PVA surface, whereas the film prepared through *in situ* generation of Ag nanoparticles by chemical reduction process on PVA host showed non-uniform, coagulated, bunches of Ag nanoparticles. As prepared Ag/PVA nanocomposite film has higher thermal stability than that prepared from bulk synthesis. The antibacterial properties of Ag/PVA films against Gram-negative, *E. coli* and Gram-positive, *S. aureus* were tested by zone of inhibition method. The results demonstrated that the as synthesized Ag/PVA nanocomposite film has enhanced antibacterial efficacy compared to that generated through *in situ* synthesis without using TX-100 microemulsion under the same test condition.

6.1. Introduction

With the increased microbial resistance against numerous antibiotics and bactericides much attention has been focused on the development of effective antimicrobial agents for pharmaceutical and biomedical applications.[1-7] Ag nanoparticles have been proved effective as they exhibit excellent biocidal activity against 650 types of bacteria, viruses and fungi[8] limiting the development of resistant microbial strains[7,9,10] at exceptionally low concentrations[11] with low toxicity toward mammalian.[12] In chapter 3 highest antibacterial efficacy was reported for Ag among four metal nanoparticles studied against both Gram-negative and Gram-positive bacteria. However, controlled release and agglomeration, which can reduce efficacy of the antibacterial activity of Ag nanoparticles, have become the major problems to be resolved.[13] Entrapment of

Ag nanoparticles on various substrates and matrices can resolve these issues and ensure a sustained release of Ag.[14-16]

In this context, polymers are the first priority materials because of their flexible structures with suitable functional groups on long polymeric chains allowing incorporation and immobilization of nanoparticles thereby formation of nanocomposites.[8,17] These Ag nano/polymer composites are more advantageous since they are not directly taken up by mammalian cells and therefore they make remarkably low human toxicity.[18] Generally, there are many polymeric matrices for the synthesis of Ag/polymer antibacterial nanocomposites.[19] Poly(vinyl alcohol) (PVA) as a matrix is promising for its high surface chelation and stabilization properties.[20,21] PVA has a lot of medical applications[8] including wound dressings[22] since it is non-toxic, non-carcinogenic,[23] highly biocompatible and biodegradable owing to its hydrophilic nature. Moreover it has excellent film-forming properties.[8,20] The common approaches for the embedment of Ag nanoparticles on the PVA polymer host include either by mixing preformed nanoparticles with chains of the polymer matrix (*ex situ*) or synthesis and growth of nanoparticles inside the matrix (*in situ*).[20,24] The latter mode of synthesis involves reduction of Ag salts either by conventional reducing agents[25] or by polymer host itself at specific reaction conditions.[24,26-28] The entrapment of Ag nanoparticles on the polymer host (*in situ* or *ex situ*) affects the size and the size distribution of nanoparticles enormously.[29] *Ex situ* strategy induces agglomeration of the seeded Ag nanoparticles before their transfer to PVA host.[20,29,30] For *in situ* formation of Ag/PVA using reducing agent, the polymer can effectively protect the nanoparticles from aggregation.[25] But the casting of the film does not involve washing to eliminate unreacted Ag salts which might cause toxicity by the adsorption of ions in epidermis cells and sweat glands.[17] For *in situ* reduction and encapsulation of Ag nanoparticles in PVA by the host itself, previous studies claimed non-agglomerated uniformly distributed Ag particles in PVA with small sizes and narrow distributions. The ratio of PVA to metal is an important issue, but its role on the particle diameter and agglomeration still remains dubious.[31-33] In addition, at high temperatures, HNO_3 is produced as a byproduct.[33]

For the exploitation of the antimicrobial effect of Ag nanoparticles, good dispersion of nanoparticles on the polymer surface with sufficiently high loading is vital.[25] W/o microemulsion is promising in this regard, since it is a simple preparative route for

nanoparticles where water droplets (dispersed in continuous oil medium and stabilized by surfactants and cosurfactants) provide a compartmentalized medium to carry out chemical reactions in restricted geometries.[34,35] In this approach polymeric matrix incorporated in the core of the microemulsion has the potential to further control the size of Ag nanoparticles by chelation thereby, preventing agglomeration of nanoparticles after separation from microemulsion. Moreover the template role of microemulsion associated with the polymer host might ensure size-controlled selective precipitation of nanoparticles in specific reaction sites of PVA polymer chains to give uniform dispersion.

This work aims at investigating the influence of w/o microemulsion as a synthetic template for the preparation of Ag/PVA nanocomposite with homogenous dispersion in the matrix. Ag nanoparticles were prepared at high concentrations *in situ* in the PVA polymer matrix by chemical reduction in w/o microemulsion of TX-100/1-butanol/cyclohexane/water. Ag/PVA film was finally prepared by solution casting method after separation from the microemulsion. The antibacterial properties of the Ag/PVA films against Gram-negative, *E. coli* and Gram-positive, *S. aureus* were tested by agar diffusion method and the results were compared to that generated through *in situ* synthesis without using microemulsion under identical condition. The ultimate goal has been the development of an efficient technique to prepare Ag/PVA nanocomposite film with desirable size and distribution of nanoparticles for enhanced concurrent antibacterial activity against Gram-negative and Gram-positive bacteria for biomedical applications.

6.2. Experimental

6.2.1. Materials

All the chemicals used were of analytical grade. $AgNO_3$ (Merck), $NaBH_4$ (Acros Organics), TX-100 (Sigma Aldrich), cyclohexane (Merck), 1-butanol (Merck), PVA (MW 30000, Merck) were used without further purification. De-ionized water (conductivity: 0.055 μScm^{-1} at 25.0 °C) from HPLC grade water purification systems (BOECO, Germany) was used throughout the experiments.

6.2.2. Methods

For the preparation of 30 g PVA containing microemulsion, at first 0.87% (w/w) PVA solution was prepared by dissolving PVA in water (0.0075 g PVA in 0.864 g water) with constant magnetic stirring at 80 ^{o}C. Then TX-100 (3 g) , cyclohexane (24.9 g), 1-butanol (1.23 g) was mixed and PVA solution was added to this so that water to surfactant molar ratio becomes 10. The mixture was sonicated until an optically clear solution was obtained.

0.1 M $AgNO_3$ solution (38.5 μL) was added to PVA containing TX-100 microemulsion with initial weight ratio of Ag/PVA at 1:9 with constant stirring at room temperature. No characteristic color of Ag nanoparticles due to the surface plasmon resonance was observed. Under this experimental condition, PVA did not act as a reducing agent to reduce Ag^+ ions. Then 38.5 μL 0.2 M $NaBH_4$ solution (2:1 with respect to silver nitrate) was added to this to reduce Ag^+ ions. The color of the mixture changed from colorless to yellow instantly. Excess amount of acetone was added to the mixture and centrifuged for about 1 h. The as prepared composite was washed with acetone several times followed by dissolution in water and volume reduction to 0.5 mL at 80 ^{o}C with constant stirring. Finally, casting on a plastic petri dish at room temperature for 72 h gave brown-yellow transparent nanocomposite film, which was easily peeled off after drying at 50 ^{o}C for 2 h.

For Ag/PVA film from bulk synthesis, Ag^+ was reduced by $NaBH_4$ in 0.87% (w/w) PVA solution. The film was casted in the same manner. Pure PVA film was prepared with the same procedure without incorporation of Ag nanoparticles.

Microemulsion of TX-100 was also prepared using water instead of PVA solution and Ag nanoparticles were synthesized in this medium by the reduction of $AgNO_3$ with $NaBH_4$.

6.2.3. Characterization

Optical absorption spectra for Ag nanoparticles in TX-100 microemulsion, PVA containing TX-100 microemulsion and in PVA solution were recorded using a double beam Shimadzu UV-visible spectrophotometer, model UV-1650 PC. Rectangular quartz cells of path length 1 cm were used throughout the investigation. Average particle size and size distribution were measured using Malvern Zetasizer Nano ZS90

with a scattering angle of 90°. A He–Ne laser beam of 632.8 nm wavelength was used for the measurements. After casting the film, transmission spectra of the samples were recorded on a Shimadzu UV spectrophotometer, model UV-1800. FTIR spectra were recorded using a Perkin Elmer FT-IR/NIR spectrometer (Frontier) in the spectral wavenumber range from 4000 to 400 cm^{-1}. Morphological analysis was carried out using JEOL analytical SEM, model JSM-6490LA. The films were taken on carbon coated aluminum stubs followed by sputter coating a thin layer of platinum for the measurements at an acceleration voltage of 20 kV. Thermal properties (TGA) were studied by a Hitachi instrument (TG/DTA 7200) in the temperature range of 35–550 °C at a heating rate of 10 °C per min both under N_2 and O_2 atmospheres. In O_2 atmosphere, the samples were finally held at 550 °C for 2 h.

6.2.4. Antibacterial activity

The antibacterial properties of the films against Gram-negative, *E. coli* and Gram-positive, *S. aureus* were assessed by using the agar diffusion test[36,37] following the measurement of the zone of inhibition. Sample films (4.5 mm in diameter) were gently placed on the surface of nutrient agar plates, where bacterial broth culture (1.3×10^8 cells mL^{-1}) were swabbed uniformly across the culture plate. After 24 h incubation at 37 °C, bacterial growth was observed and the dimensions of the zones of inhibition around the samples were measured to evaluate the antibacterial performance.

6.3. Results and discussion

6.3.1. Role of PVA matrix in the core of TX-100 microemulsion

Ag nanoparticles were synthesized in TX-100 microemulsion, in PVA containing TX-100 microemulsion and in PVA solution to judge the synthetic template better suited for smaller size and narrower size distribution. UV–visible absorption spectra of Ag nanoparticles in these three media are demonstrated in Figure 6.1.

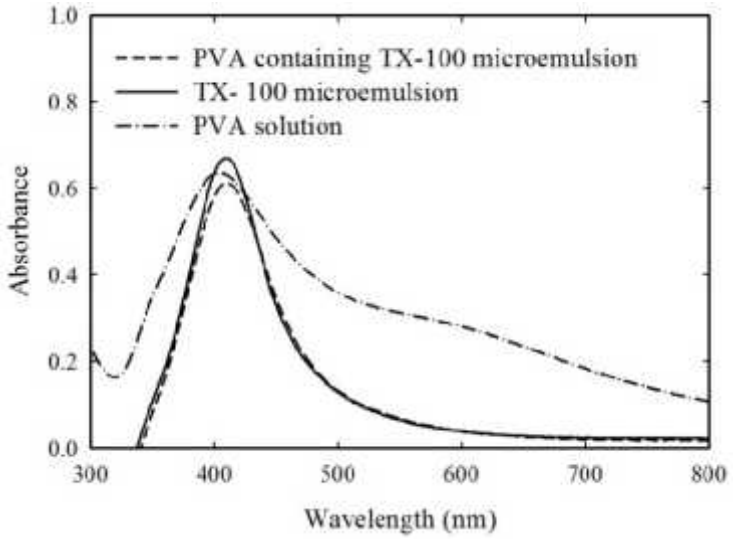

Figure 6.1. UV-visible spectra of Ag nanoparticles prepared in different media.

Sharp absorption patterns with maxima located at 405 nm were observed due to surface plasmon resonance absorption of Ag nanoparticles in TX-100 microemulsion and PVA containing TX-100 microemulsion.[25] On the other hand, a broad surface plasmon absorption band with the maxima at approximately 395 nm was obtained for Ag nanoparticles in PVA solution. The FWHM for Ag nanoparticles in TX-100 microemulsion and PVA containing TX-100 microemulsion are about 78 nm and 76 nm respectively, which are much lower than for Ag nanoparticles in PVA solution where the FWHM is of the magnitude of 113 nm. The FWHM is considered to be quite useful indicator of the particle size and its distribution within the medium and matrix[25] and in the present case, it is clear that a narrow size distribution of the Ag nanoparticles could be achieved using PVA containing microemulsion. DLS measurements further support this as the size distribution of Ag nanoparticles in PVA solution is broader compared to those in TX-100 microemulsion and PVA containing TX-100 microemulsion (Figure 6.2).

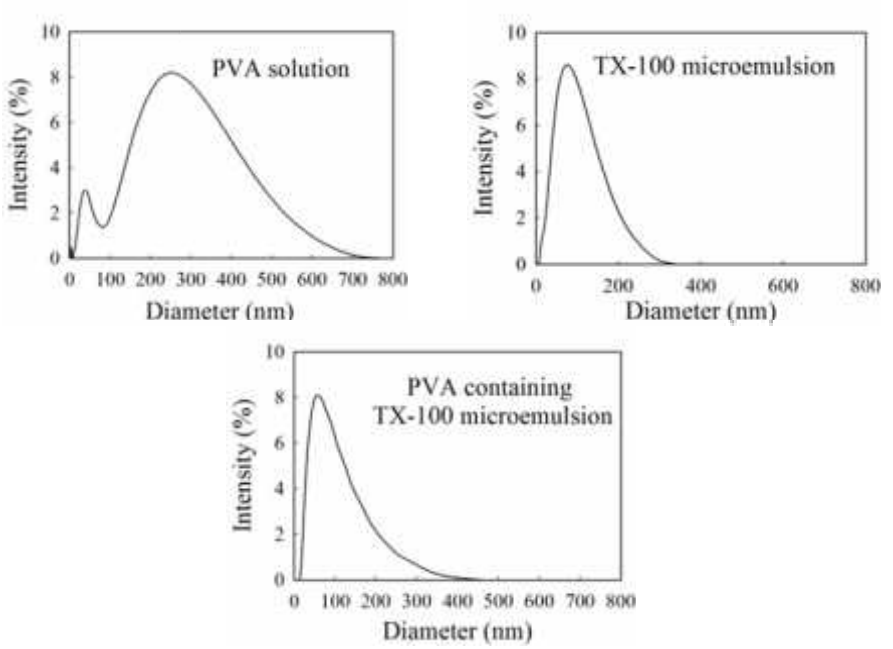

Figure 6.2. Size distributions of Ag nanoparticles prepared in different media from DLS measurements.

Prior to casting the film, Ag/PVA was separated out from microemulsion. UV-visible spectrum of Ag/PVA in water was taken to check aggregation of Ag nanoparticles. The peak shifted toward longer wavelength (415 nm) with broader FWHM (96 nm) than those for Ag nanoparticles in PVA containing microemulsion (Figure 6.3). Therefore, Ag nanoparticles became larger with broader distribution. However, the size of Ag nanoparticles obtained from TX-100 microemulsion without PVA was even larger than these. The spectrum for Ag nanoparticles after separation from TX-100 microemulsion without PVA shows absorption peak at 427 nm with FWHM of 141 nm.

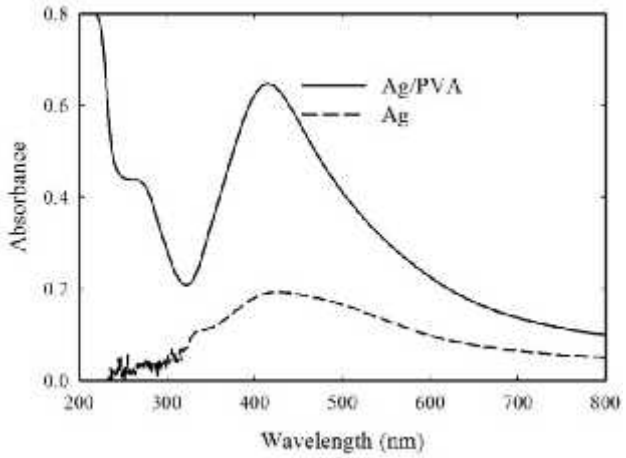

Figure 6.3. UV-visible spectra of Ag/PVA and Ag nanoparticles after separation from TX-100 microemulsion.

This was further confirmed by DLS measurements (Figure 6.4) which gave average diameter of 105 nm for Ag nanoparticles in PVA much smaller than that for Ag nanoparticles without PVA (342 nm). It is apparent that PVA protected Ag nanoparticles from agglomeration.

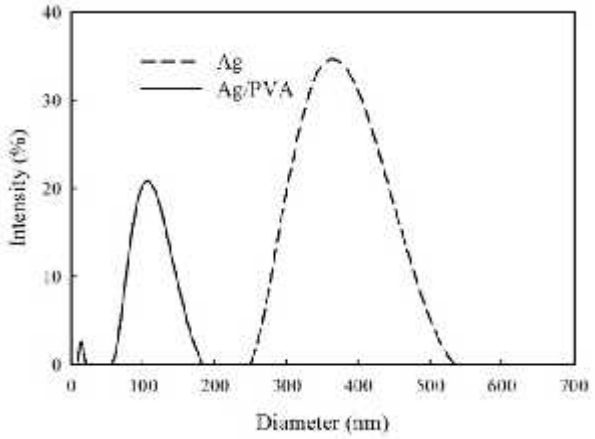

Figure 6.4. Size distributions for Ag/PVA and Ag nanoparticles after separation from TX-100 microemulsion from DLS measurements.

6.3.2. Optical and structural characterization of Ag/PVA nanocomposite film

After casting the film, optical transmittance spectra were taken (Figure 6.5) to confirm the existence of Ag nanoparticles. Colorless PVA film showed no noticeable absorption in the visible range. There was a sharp increase in transmittance from 210 to 248 nm due to the band gap of PVA polymer. A valley at 419 nm in case of Ag/PVA film can be attributed to the formation of charge transfer complexes. The surface plasmon resonance of Ag nanoparticles embedded in PVA polymer matrix resulted in the valley in the visible region in agreement with literature.[38]

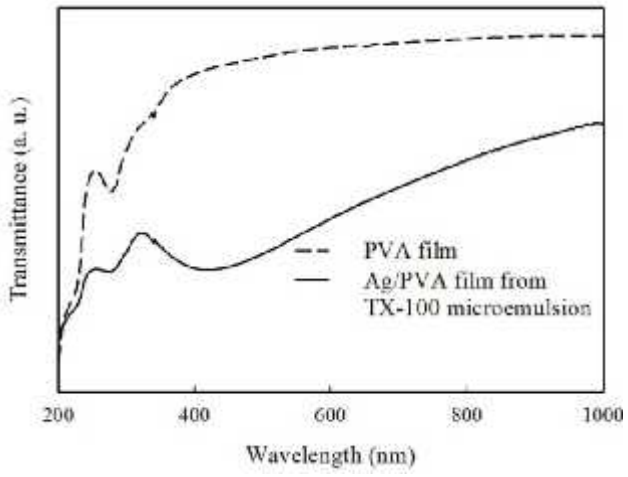

Figure 6.5. Optical transmittance spectra of PVA and Ag/PVA film using TX-100 microemulsion.

The formation of Ag/PVA composite is also supported by the FTIR spectra (Figure 6.6). In PVA, the band with minimum at 1322 cm^{-1} is attributed to the coupling of O-H in plane vibration (strong line at 1420 cm^{-1}) with C-H wagging vibrations. But in Ag/PVA nanocomposite film, a decrease in the ratio of these bands was marked. This indicates decoupling between corresponding vibrations and bonding interactions of vacant *d*-orbitals of Ag nanoparticles with non-bonding electrons available on the oxygen atoms of OH groups.[30]

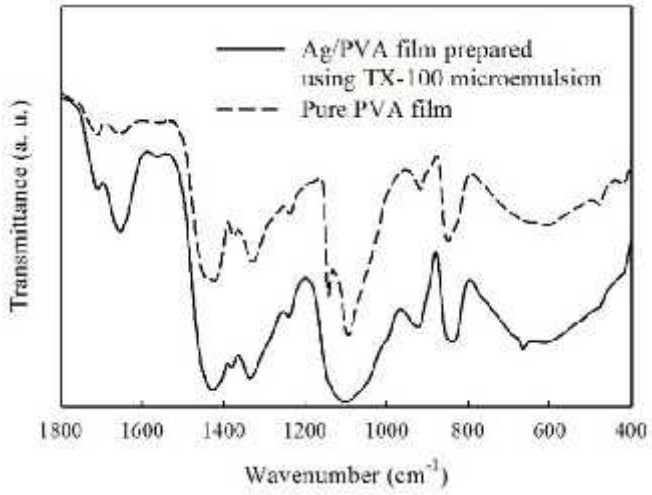

Figure 6.6. FTIR spectra of pure PVA and Ag/PVA composite films.

6.3.3. Microscopic analysis of Ag/PVA nanocomposite film

Morphological features of these composite films were analyzed by SEM (Figure 6.7). The SEM micrographs for Ag/PVA film from bulk synthesis (Figure 6.7 a, b) show spherical bunches of small but coagulated Ag nanoparticles on the PVA host where pits and cracks could also be observed. Polymers can serve as a confined medium for the synthesis (nanoreactors) to control the size and size distribution of the generated nanoparticles. Furthermore, they can stabilize and isolate the generated nanoparticles, thus preventing their aggregation.[39] Since in the present case the concentration was high (10 wt%), aggregation became highly probable and could not be avoided. The pits and cracks on the PVA film surface might originate from the unreacted species and other reaction products. In contrast, SEM micrographs of Ag/PVA composite film (Figure 6.7 c, d) prepared using TX-100 microemulsion gave uniform distribution of larger Ag nanoparticles on smooth PVA film surface. When Ag nanoparticles were prepared in PVA containing TX-100 microemulsion, confined medium of PVA molecules was further compartmentalized within the core of microemulsion droplets.

These PVA matrix containing nanoreactors resisted the coagulation of Ag nanoparticles within a curbed environment as it is evident from DLS results (Figure 6.2) which gave narrow size distribution for Ag/PVA within TX-100 microemulsion. The template role of microemulsion together with the polymer host ensured size-controlled selective precipitation of nanoparticles in specific reaction sites of PVA polymer chains to give uniform dispersion. In spite of homogeneous dispersion in the PVA matrix, the casted Ag/PVA nanocomposite film gave larger Ag nanoparticles, due possibly to the influence of higher temperature during the dissolution process of Ag/PVA after separation from microemulsion which is likely to facilitate the diffusion, migration and aggregation of smaller Ag nanoparticles through less viscous PVA solution for the formation of larger structures.

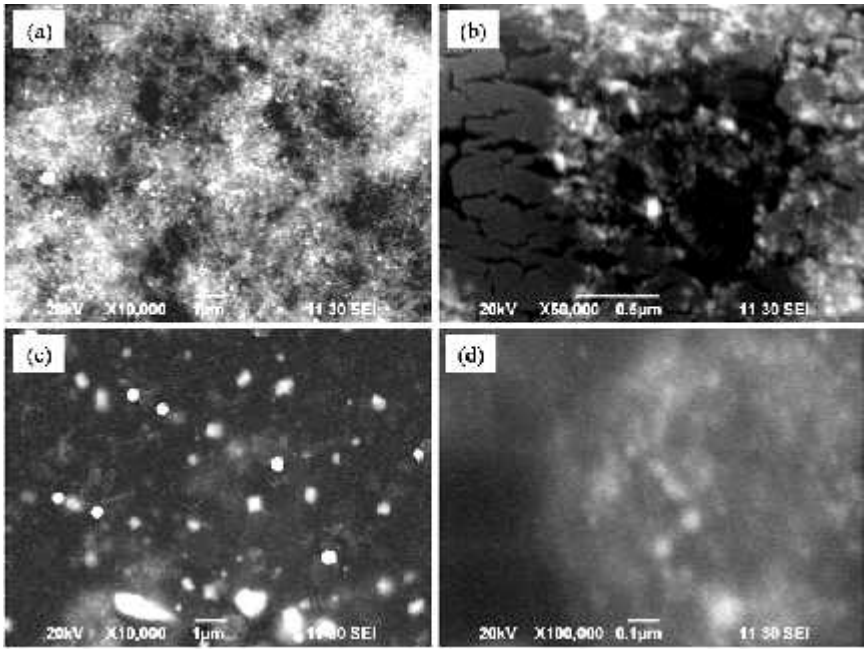

Figure 6.7. SEM images of Ag/PVA film from bulk synthesis (a, b) and Ag/PVA film prepared from TX-100 microemulsion (c, d).

6.3.4. Thermal analysis

To understand the interactions between nanoparticles and the polymer matrix, TG analyses of pure PVA and Ag/PVA nanocomposite films were performed both under N_2 and O_2 atmospheres. As shown in Figure 6.8, the onset of degradation (the intersections of the extrapolated base lines with tangents drawn at the inflection points) for the Ag/PVA composite film from TX-100 microemulsion shows an improvement in thermal stability both under N_2 and O_2 atmospheres compared to that

for pure PVA. The rate of degradation is lower and the temperature of maximal rate of degradation of the film in N_2 atmosphere is higher compared with the pure matrix (Figure 6.8(a)). Strong interaction between the well-arranged Ag nanoparticles and the –OH groups of the PVA probably hinders the initial steps involved in PVA degradation (chain stripping elimination of water)[40,41] and thus increases the energy barrier for the chain scission reactions. But the onset of degradation at a lower temperature of the Ag/PVA film obtained from bulk synthesis both in N_2 and O_2 indicates a decrease in its thermal stability. In this case, the film degrades at a higher rate at comparatively lower temperature than the pure film (Figure 6.8(a)). Spherical bunches of aggregated Ag nanoparticles are formed here and the presence of coagulated Ag nanoparticles accelerates the degradation of PVA matrix because of their high thermal conductivity.

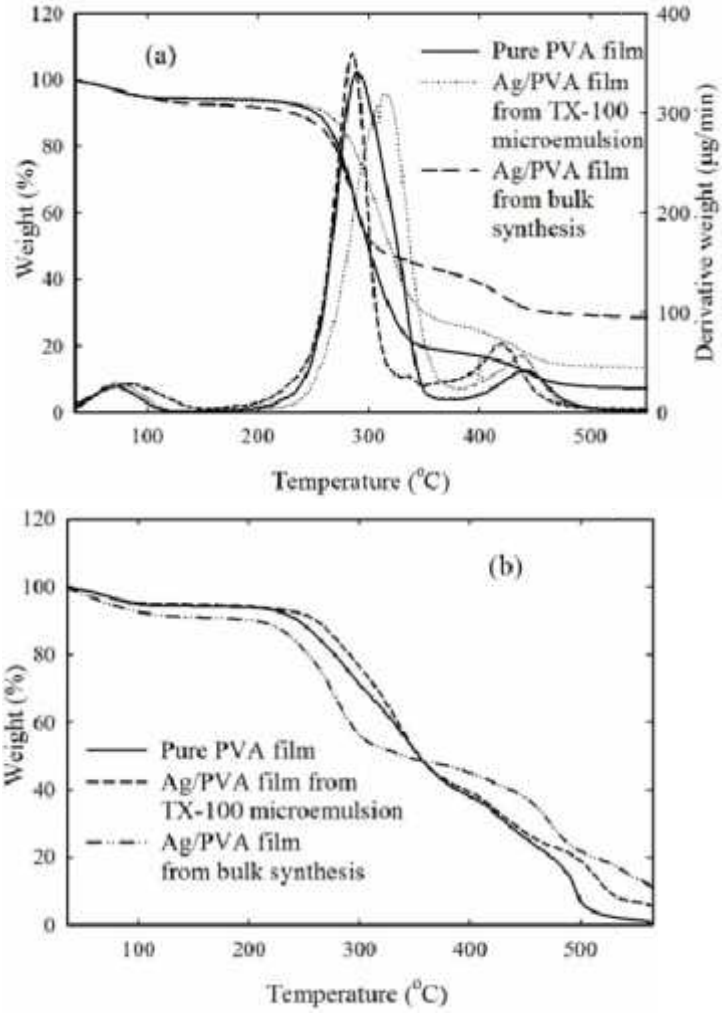

Figure 6.8. TG analysis of pure PVA film, Ag/PVA nanocomposite film from TX-100 microemulsion and from bulk synthesis in N_2 (a) and O_2 (b) atmospheres.

Figure 6.8 (b) shows that the onset of thermooxidative degradation occurred at somewhat lower temperatures compared to the degradation in N_2 atmosphere. Although thermooxidative degradation for pure PVA film was completed, residual weight at 550 ^oC after holding for 2 h for Ag/PVA film from TX-100 microemulsion and Ag/PVA nanocomposite film from bulk synthesis were 5.86% and 11.45%, respectively. This is due to the fact that prior to casting, Ag/PVA from TX-100 microemulsion was washed to eliminate unreacted salts; whereas in case of Ag/PVA film from bulk synthesis, it was casted without purification to yield large residual weight including some unreacted salts in the TG experiments.

6.3.5. Antibacterial activities

The antibacterial activities of the films were tested against *E. coli* and *S. aureus*. The experiments showed no zone of inhibition for pure PVA film which was used as a control matrix. All Ag/PVA films displayed antibacterial activity against *S. aureus* and *E. coli* (Figure 6.9). So it is clear that the antibacterial property of the films comes from Ag nanoparticles. The probable mechanism of antibacterial activity of Ag nanoparticles is discussed in chapter 3 (section 3.3.4)

Figure 6.9. Antibacterial activity test against pathogens; (A) *E. coli* (B) *S. aureus*. Samples are labeled as: (i) PVA film as control (ii) Ag/PVA film from w/o microemulsion and (iii) Ag/PVA film from aqueous synthesis.

A noticeable increase in the zones of inhibition for the film prepared using w/o microemulsion can be observed (Figure 6.10).

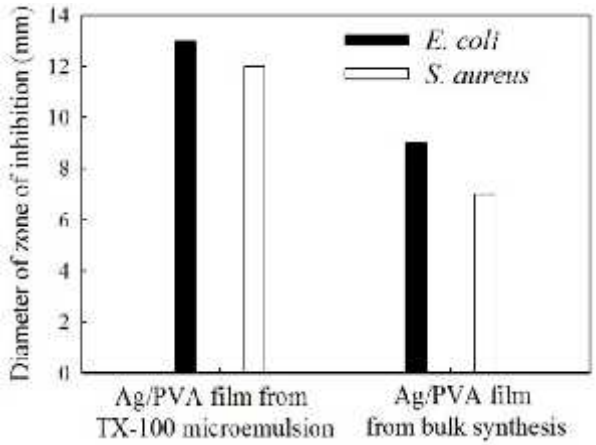

Figure 6.10. Bacterial sensitivity to Ag/PVA films prepared from microemulsion and from bulk synthesis.

The difference in antibacterial activity may be discussed in terms of the difference in the release of Ag nanoparticles from the composite films. Figure 6.11 shows the process of releasing Ag nanoparticles from PVA film surface. For Ag/PVA film from bulk synthesis, the aggregation probability of spherical bunched particles increases to reduce effective surface to volume ratio of particles which lowers the interaction of particles with the cell wall of bacteria. On the other hand, for Ag/PVA film from TX-100 microemulsion, the aggregation of uniformly and homogeneously distributed nanoparticles becomes less probable and the effective interaction of nanoparticles with bacterial cell wall to inhibit the growth of bacteria is enhanced. In brief, the higher activity of the Ag/PVA from TX-100 microemulsion film may be attributed to higher contact surface with the bacteria due to less probable aggregation of the uniformly and homogeneously distributed nanoparticles.

The observations are consistent with the observations for four metallic nanoparticles. Fe_3O_4@Ag nanoparticles and Ag/PAni composites also showed that *E. coli* is more sensitive than *S. aureus*. This has been discussed in sections 3.3.4, 4.3.4 and 5.3.6.

From the antibacterial test results it is clear that the Ag/PVA nanocomposite prepared in this work has good prospect as an antibacterial film and the use of microemulsion gives the film superior antibacterial activity to the conventionally prepared film using *in situ* technique.

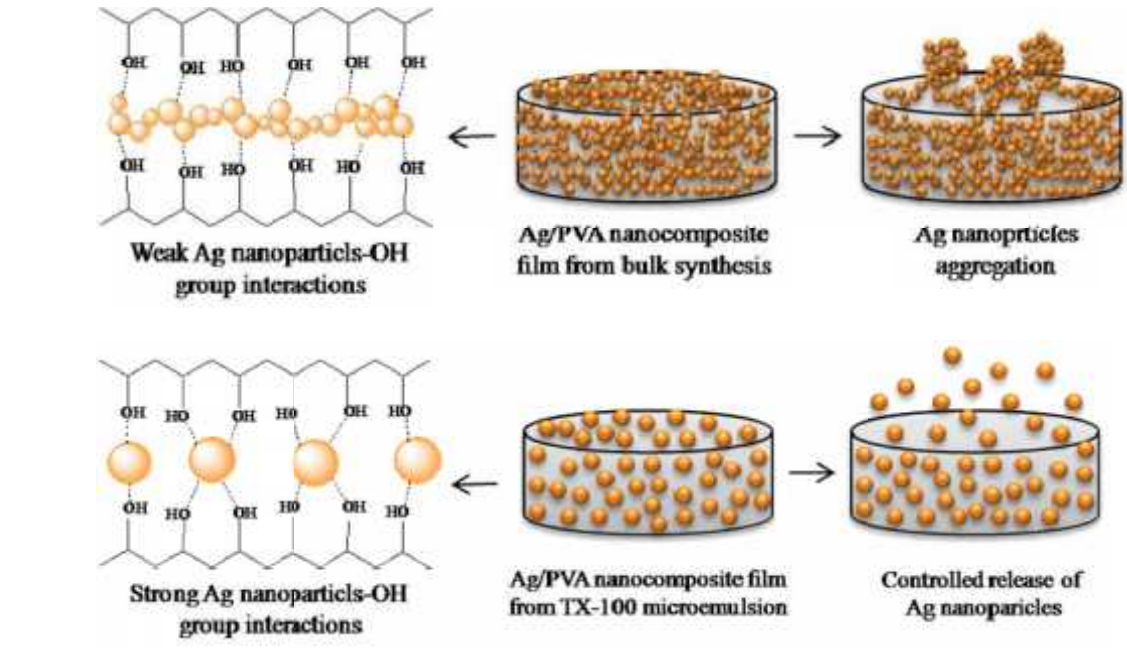

Figure 6.11. Interactions of Ag nanoparticles with PVA matrix and their release from nanocomposite films.

6.4. Conclusions

Ag nanoparticles could be prepared in PVA containing TX-100 microemulsion by reducing Ag salt with $NaBH_4$. Solution casting of a Ag/PVA nanocomposite after separation from microemulsion gave Ag/PVA nanocomposite film with uniform and homogeneous arrangement of Ag nanoparticles in the smooth PVA matrix. The composite film from bulk synthesis, on the other hand, gave spherical bunches of aggregated Ag nanoparticles with pits and cracks on the PVA film surface. Thermal stability followed the order, Ag/PVA film from TX-100 microemulsion > pure PVA film > Ag/PVA film from bulk synthesis. The Ag/PVA nanocomposite film prepared using microemulsion exhibited remarkable enhancement of antibacterial activity against *E. coli* and *S. aureus* as compared to that prepared from bulk synthesis. Thus the as-synthesized film might be a potent bactericide to reduce and eliminate the risk of infections and be used for treatment of a patient simultaneously infected by Gram-negative and Gram-positive bacteria.

References

(1) Chen, C.; Pan, F.; Zhang, S.; Hu, J.; Cao, M.; Wang, J.; Xu, H.; Zhao, X.; Lu, J. R. Antibacterial activities of short designer peptides: a link between propensity for nanostructuring and capacity for membrane destabilization. *Biomacromolecules* **2010**, *11*, 402-411.

(2) Neoh, K. G.; Kang, E. T. Combating Bacterial Colonization on Metals via Polymer Coatings: Relevance to Marine and Medical Applications. *ACS Appl. Mater. Interfaces* **2011**, *3*, 2808-2819

(3) Dong, A.; Lan, S.; Huang, J.; Wang, T.; Zhao, T.; Xiao, L.; Wang, W.; Zheng, X.; Liu, F.; Gao, G.; Chen, Y. Modifying Fe_3O_4-functionalized nanoparticles with n-halamine and their magnetic/antibacterial properties. *ACS Appl. Mater. Interfaces* **2011**, *3*, 4228-4235.

(4) Han, H.; Wu, J.; Avery, C. W.; Mizutani, M.; Jiang, X.; Kamigaito, M.; Chen, Z.; Xi, C.; Kuroda, K. Immobilization of amphiphilic polycations by catechol functionality for antimicrobial coatings. *Langmuir* **2011***, 27*, 4010-4019.

(5) Bujdák, J.; Jurečeková, J.; Bujdáková, H.; Lang, K.; Šeršeň, F. Clay mineral particles as efficient carriers of methylene blue used for antimicrobial treatment. *Environ*. *Sci*. *Technol*. **2009**, *43*, 6202-6207.

(6) Kong, H.; Song, J.; Jang, J. Photocatalytic antibacterial capabilities of TiO_2−biocidal polymer nanocomposites synthesized by a surface-initiated photopolymerization. *Environ. Sci. Technol.* **2010**, *44*, 5672-5676.

(7) Waasbergen, L. G. V.; Fajdetic I.; Fianchini M.; Dias H.V. R. Antimicrobial properties of highly fluorinated tris(pyrazolyl)borates. *J. Inorg*. *Biochem*. **2007**, *101*,1180-1183.

(8) Ghaffari-Moghaddam, M.; Eslahi, H. Synthesis, characterization and antibacterial properties of a novel nanocomposite based on polyaniline/polyvinyl alcohol/Ag. *Arabian J. Chem.* **2014**, *7*, 846-855.

(9) Morones, J. R.; Elechiguerra, J. L.; Camacho, A.; Holt, K.; Kouri, J. B.; Ramírez, J. T. Yacaman, M. J. The bactericidal effect of silver nanoparticles. *Nanotechnology* **2005**, *16*, 2346-2353.

(10) Kumar, A.; Vemula, P. K.; Ajayan, P. M.; John, G. Silver-nanoparticle-embedded antimicrobial paints based on vegetable oil. *Nat. Mater.* **2008**, *7*, 236-241.

(11) Palza, H. Antimicrobial Polymers with Metal Nanoparticles. *Int. J. Mol. Sci.* **2015**, *16*, 2099-2116.

(12) Chaloupka, K.; Malam, Y.; Seifalian, A. M. Nanosilver as a new generation of nanoproduct in biomedical applications. *Trends Biotechnol.* **2010**, *28*, 580-588.

(13) Lv, M.; Su, S.; He, Y.; Huang, Q.; Hu, W.; Li, D.; Fan, C.; Lee, S.-T. Long-term antimicrobial effect of silicon nanowires decorated with silver nanoparticles. *Adv. Mater*. **2010**, *22*, 5463-5467.

(14) Silver, S. Bacterial silver resistance: molecular biology and uses and misuses of silver compounds. *FEMS Microbiol. Rev*. **2003**, *27*, 341-353.

(15) Voccia, S.; Ignatova, M.; Jérôme, R.; Jérôme, C. Design of antibacterial surfaces by a combination of electrochemistry and controlled radical polymerization. *Langmuir* **2006**, *22*, 8607-8613.

(16) Li, Z.; Lee, D.; Sheng, X.; Cohen, R. E.; Rubner, M. F. Two-level antibacterial coating with both release-killing and contact-killing capabilities. *Langmuir* **2006**, *22*, 9820-9823.
(17) Dallas, P.; Sharma, V. K.; Zboril, R. Silver polymeric nanocomposites as advanced antimicrobial agents: Classification, synthetic paths, applications, and perspectives. *Adv. Colloid Interface Sci*. **2011**, *166*, 119-135.
(18) Song, J.; Kang, H.; Lee, C.; Hwang, S. H.; Jang, J. Aqueous synthesis of silver nanoparticle embedded cationic polymer nanofibers and their antibacterial activity. *ACS Appl. Mater*. *Interfaces* **2012**, *4*, 460-465.
(19) Dallas, P.; Tucek, J.; Jancik, D.; Kolar, M.; Panacek, A.; Zboril, R. Magnetically controllable silver nanocomposite with multifunctional phosphotriazine matrix and high antimicrobial activity. *Adv. Funct. Mater*. **2010**, *20*, 2347-2354.
(20) Abargues, R.; Marqués-Hueso, J.; Canet-Ferrer, J.; Pedrueza, E.; Valdés, J. L.; Jiménez, E.; Martínez-Pastor, J. High-resolution electron-beam patternable nanocomposite containing metal nanoparticles for plasmonics. *Nanotechnology* **2008**, *19*, 355308.
(21) Bernabò, M.; Ciardelli, F.; Pucci, A.; Ruggeri, G. Preparation and optical properties of new/metal macromolecole architectures. *Macromol. Symp*. **2008**. *270*,177-186.
(22) Galya, T.; Sedlařík, V.; Kuřitka, I.; Novotný, R.; Sedlaříková, J.; Sáha, P. Antibacterial poly(vinyl alcohol) film containing silver nanoparticles: Preparation and characterization. *J. Appl. Polym. Sci.* **2008**, *110*, 3178-3185.
(23) Valente, A. J. M.; Cruz, S. M. A.; Morán, M.C.; Murtinho, D. B.; Muniz, E. C.; Miguel, M. G. Release of DNA from cryogel PVA-DNA membranes. *eXPRESS Polym. Lett.* **2010**,*4*, 480-487.
(24) Gautam, A.; Ram, S. Preparation and thermomechanical properties of Ag-PVA nanocomposite films. *Mater. Chem. Phys.* **2010**, *119*, 266-271.
(25) Khanna, P.K.; Singh, N.; Charan, S.; Subbarao, V.V.V.S.; Gokhale, R.; Mulik, U.P. Synthesis and characterization of Ag/PVA nanocomposite by chemical reduction method. *Mater. Chem. Phys*. **2005**, *93*, 117-121.
(26) Karthikeyan, B. Spectroscopic studies on Ag–polyvinyl alcohol nanocomposite films. *Physica B* **2005**, *364*, 328-332.
(27) Porel, S.; Singh, S.; Harsha, S. S.; Rao, D. N.; Radhakrishnan, T. P.; Nanoparticle-embedded polymer: in situ synthesis, free-standing films with highly monodisperse silver nanoparticles and optical limiting. *Chem. Mater*. **2005**, *17*, 9-12.
(28) Filippo, E.; Serra, A.; Manno; D. Poly(vinyl alcohol) capped silver nanoparticles as localized surface plasmon resonance-based hydrogen peroxide sensor. *Sens. Actuators, B* **2009**, *138*, 625-630.
(29) Ananth, A. N.; Umapathy, S.; Sophia, J.; Mathavan, T.; Mangalaraj, D. On the optical and thermal properties of in situ/ex situ reduced Ag NP's/PVA composites and its role as a simple SPR-based protein sensor. *Appl*. *Nanosci*. **2011**, *1*,87-96.
(30) Mbhele, Z. H.; Salemane, M. G.; Sittert, C. G. C. E. V.; Nedeljković, J. M.; Djoković, V.; Luyt, A. S. Fabrication and characterization of silver-polyvinyl alcohol nanocomposites. *Chem. Mater*. **2003**, *15*, 5019-5024.
(31) Zhou, Y.; Yu, S. H.; Wang, C. Y.; Li, X. G.; Zhu, Y. R.; Chen, Z. Y. A novel ultraviolet irradiation photoreduction technique for the preparation of single-crystal Ag nanorods and Ag dendrites. *Adv*. *Mater*. **1999**, *11*, 850-852.

(32) Ahmadi, T. S.; Wang, Z. L.; Green, T. C.; Henglein, A.; El-Sayed, M. A. Shape-controlled synthesis of colloidal platinum nanoparticles. *Science* **1996**, *272*. 1924-1925.
(33) Gautam, A.; Tripathy, P.; Ram, S. Microstructure, topology and X-ray diffraction in Ag-metal reinforced polymer of polyvinyl alcohol of thin laminates. *J. Mater. Sci*. **2006**, *41*, 3007-3016.
(34) Ranjan, R.; Vaidya, S.; Thaplyal, P.; Qamar, M.; Ahmed, J.; Ganguli, A. K. Controlling the size, morphology, and aspect ratio of nanostructures using reverse micelles: a case study of copper oxalate monohydrate. *Langmuir* **2009**, *25*, 6469-6475.
(35) López-Quintela, M. A.; Blancoa, C. T. M. C., Rio, L. G.; Leis, J.R. Microemulsion dynamics and reactions in microemulsions. *Curr. Opin. Colloid Interface Sci*. **2004**, *9*, 264-278.
(36) Varaprasad, K., Mohan, Y. M., Vimala, K., & Raju, K. M. Synthesis and characterization of hydrogel–silver nanoparticle–curcumin composites for wound dressing and antibacterial application. *J. Appl. Polym. Sci*. **2011**, *121*, 784-796.
(37) Vimala, K.; Mohan, Y. M., Varaprasad, K., Reddy, N., Narayana Ravindra, S., Naidu, N. S. Fabrication of curcumin encapsulated chitosan–PVA silver nanocomposite films for improved antimicrobial activity. *J. Biomater. Nanobiotechnol*. **2011**, *2*, 55-64.
(38) Ghanipour M.; Dorranian D. Effect of Ag-nanoparticles doped in polyvinyl alcohol on the structural and optical properties of PVA films. *J. Nanomater*. **2013**, 1-10.
(39) Rozenberg, B. A.; Tenne, R. Polymer-assisted fabrication of nanoparticles and nanocomposites. *Prog. Polym. Sci.* **2008**, *33*, 40-112.
(40) Gilman, J. W.; VanderHart, D. L.; Kashiwagi, T. Thermal decomposition chemistry of poly(vinyl alcohol). *Fire and Polymers–II, ACS Symp. Ser*. **1995**, *599*, 161-185.
(41) Krkljěs, A. N.; Marinović-Cincovíc, M. T.; Kăcarevíc-Popovíc, Z. M.; Nedeljkovíc, J. M. Dynamic thermogravimetric degradation of gamma radiolytically synthesized Ag–PVA nanocomposites. *Thermochim. Acta* **2007,** *460*, 28-34.

7.1. General conclusions

The nature and concentration of surfactant and cosurfactant and water content have significant influence on the size and dynamics of water droplets in w/o microemulsions. Microemulsions of different surfactants give droplets of different size. The diameter of droplets depends on hydrophilicity of the surfactant. With increasing hydrophilicity of the surfactant the size of microemulsions droplets increases. Higher surfactant concentration and lower water content generates smaller microemulsion droplets. The nonionic surfactant, TX-100 can form stable w/o microemulsion without any cosurfactant at higher concentrations. But at low concentrations no microemulsion is formed without the assistance of a cosurfactant. In both cases the droplet-size of the microemulsions decreases with increasing amount of the cosurfactant. Longer chain cosurfactants give smaller microemulsion droplets with more compact and rigid interfacial film.

Size of nanoparticles of Cu, Zn, Ag and Fe prepared using these w/o microemulsions as synthetic template follow the same trend as microemulsion droplets. Thus increase in surfactant and cosurfactant concentration and the chain length of cosurfactant bring about a decrease in particle size; whereas an increase in water content causes an increase in the size of nanoparticles. But for different surfactants, the result is not consistent with the droplet size. In this case more the rigidity of interfacial film (TX-100 > CTAB > SDS), smaller is the size of nanoparticles. At high concentrations of TX-100 where microemulsions are formed without the assistance of a cosurfactant, less rigid interfacial film allows a reaction to take place. But in case of low TX-100 concentrations even with the assistance with the cosurfactant strong surfactant film barrier resists the entrance of reactants inside the microemulsion droplets and thus no nanoparticles are formed in mocroemulsions at low P_o.

The antibacterial activity of nanoparticles against *E. coli* and *S. aureas* was tested by zone of inhibition method. All the four nanoparticles have antibacterial activity against *E. coli* and *S. aureas*. Ag nanoparticles show highest antibacterial activity among the four nanoparticles. Ag and Cu nanoparticles show the potential for use as antibacterial agents with sensitivity as good as conventional antibiotics.

Functionalized nanoparticles, Fe_3O_4@Ag could also be prepared using w/o microemulsion method. FTIR spectra confirm the formation of Fe_3O_4 and UV–visible absorption spectra confirm the presence of both Fe_3O_4 and Ag. Fe_3O_4@Ag nanoparticles have pronounced antibacterial properties because of synergistic antibacterial activities of Ag and Fe_3O_4.

W/o micoemulsion method is also suitable for the preparation of polymeric nanoparticles and nanocomposites. PAni nanoparticles and Ag/PAni nanocomposite could be successfully prepared using w/o microemulsions. Both PAni and Ag/PAni nanocomposite have smaller average size, narrower size distribution but lower thermal stability compared to PAni obtained from aqueous synthesis. Ag/PAni nanocomposite prepared using w/o microemulsion method has enhanced antibacterial activity against *E. coli* and *S. aurious* compared to pure PAni synthesized from both microemulsion and aqueous system.

W/o micoemulsion method could also be used to prepare nanocomposite films. Thus Ag/PVA could be prepared using microemulsion of TX-100. As prepared Ag/PVA nanocomposite film gives uniform and homogeneous arrangement of Ag nanoparticles in the smooth PVA matrix whereas the composite film from bulk synthesis gives spherical bunches of aggregated Ag nanoparticles with pits and cracks on the PVA film surface. Thermal stability follows the order, Ag/PVA film from TX-100 microemulsion > pure PVA film > Ag/PVA film from bulk synthesis. The Ag/PVA nanocomposite film prepared using microemulsion exhibits remarkable enhancement of antibacterial activity against *E. coli* and *S. aureus* as compared to that prepared from bulk synthesis.

7.2. Outlook

The supramolecular self-assembly systems, w/o microemulsions, can influence the size of nanoparticles depending on the different parameters of the organized media. They can be versatile synthetic templates for nanoparticles with desirable dimension simply by the manipulation of size controlling parameters of microemulsion droplets-nature and concentration of surfactant and cosurfactant and water content in the preparation stage. Variation of these constituents and thereby change in the

composition of the microemulsions can tune the size of nanoreactors (droplets of microemulsions) and thus nanoparticles of tunable dimension can be prepared in these systems. As nanoparticles show size dependent properties, particles with desirable dimension can be prepared using w/o microemulsions for particular applications. These systems are cost effective and provide a very easy and convenient means to controllably synthesize a wide variety of metal nanoparticles with tunable optical, electrical, magnetic and other properties which can be used in manifold applications. As microemulsions can solubilize polar substrate in their aqueous core, they can be suitable candidate for fabricating not only metallic but also metal oxide, semiconducting and core/shell nanoparticles. For core/shell nanoparticles a wide variation in the thickness of the core and shell can be possible in these systems. Suitable surface functionalization with uniform coating of nanoparticles for task-specific applications can also be performed in these reactors. Nanoscopic polymeric particles with controlled morphology and their composites with metal nanoparticles with desirable dimension can be successfully synthesized in these stable w/o microemulsions which have many advantages such as long-term stability and outstanding optical, catalytic, electronic and magnetic properties. Even metal nano/polymer composite film can be prepared using w/o microemulsions. This methodology has advantage over other common approaches of nanocomposite film formation since the template role of microemulsion provides the uniform dispersity even at high metal content whereas conventional methods give agglomerated particles. This opens up a new route for fabrication of nanocomposite film overcoming the problem of agglomeration and nonhomogeneous distribution of metal nanoparticles throughout the film. Thus w/o microemulsions offer themselves as good templates, suitable media and ideal nanoreactors for the formation of metallic, core/shell and functionalized nanoparticles and metal/nano polymer composites and thus open a wide range of potential applications in biotechnology, optoelectronics, energy and sensing, biomedical sciences and engineering.

List of publications

1. Md. Abu Bin Hasan Susan, Shakhwat Hossain, **Ummul Khair Fatema**, Md. Yousuf Ali Mollah, M. Muhibur Rahman, "*Microemulsions as nanoreactors for preparation of nanoparticles with antibacterial activity*", Proceedings of the International Conference on Chemical Engineering **2011** ICChE, 29-30 December, Dhaka, Bangladesh, 229-233.

2. Shakhwat Hossain, **Ummul Khair Fatema**, Md. Yousuf Ali Mollah, M. Muhibur Rahman, Md. Abu Bin Hasan Susan, "*Preparation of metal nanoparticles with antibacterial activity using microemulsions as nanoreactors*", Journal of Bangladesh Chemical Society, **2012**, *25*, 71-79.

3. **Ummul Khair Fatema**, Md. Yousuf Ali Mollah, M. Muhibur Rahman, Md. Abu Bin Hasan Susan, "*Droplet sizes in water in oil microemulsions and their correlation with microemulsion variables*", in preparation.

4. **Ummul Khair Fatema**, Md. Yousuf Ali Mollah, M. Muhibur Rahman, Md. Abu Bin Hasan Susan, "*Water in oil microemulsions as size-tuned templates for the preparation of copper nanoparticles*", in preparation.

5. **Ummul Khair Fatema**, Md. Yousuf Ali Mollah, M. Muhibur Rahman, Md. Abu Bin Hasan Susan, "*Size and stability of copper nanoparticles prepared in microemulsions of different surfactant* ", in preparation.

6. **Ummul Khair Fatema**, Md. Yousuf Ali Mollah, M. Muhibur Rahman, Md. Rakibul Islam, Md. Abu Bin Hasan Susan, "*Synthesis and antibacterial activities of Ag functionalized Fe_3O_4 nanoparticles prepared using water in oil microemulsion*", in preparation.

7. **Ummul Khair Fatema**, Md. Yousuf Ali Mollah, M. Muhibur Rahman, Md. Rakibul Islam, Md. Abu Bin Hasan Susan, "*Preparation of silver/polyaniline nanocomposites using water in oil microemulsions as potent antibacterial agent*", in preparation.

8. **Ummul Khair Fatema**, Md. Yousuf Ali Mollah, M. Muhibur Rahman, Md. Rakibul Islam, Md. Abu Bin Hasan Susan, "*Silver/poly(vinyl alcohol) nanocomposite film prepared using water in oil microemulsion for antibacterial applications*", in preparation.

List of attended seminars

1. Seminar on Novel Functional Materials, organized by the Higher Education Quality Enhancement Project (HEQEP) of the University Grants Commission of Bangladesh, 12 May 2011.

2. Seminar on Synthesis and Characterization of Binary and Ternary Solid Materials, organized by the Higher Education Quality Enhancement Project (HEQEP) of the University Grants Commission of Bangladesh, 30 July 2011.

3. Seminar on Supramolecular Systems, organized by the Higher Education Quality Enhancement Project (HEQEP) of the University Grants Commission of Bangladesh, 15 November 2012.

5. Seminar on Electrochemistry for Material Science, organized by the Higher Education Quality Enhancement Project (HEQEP) of the University Grants Commission of Bangladesh, 10 December 2012.

6. Seminar on Tendam Mass Spectrometry and its Application for Analysis of Chemical Contaminats in Food Stuff, 02 June 2015, Dhaka, Bangladesh.

7. Seminar on 3D Gel Printer and Future Life Innovation, organized by the Material Chemistry Research Laboratory, Department of Chemistry, University of Dhaka, 30 August 2015.

Abstracts published as contribution in the scientific meetings

1. **Ummul Khair Fatema**, M. Muhibur Rahman, Md. Yousuf Ali Mollah, Md. Abu Bin Hasan Susan, "*Preparation and Characterization of Metallic Nanoparticles of Ag, Cu and Fe using Microemulsions as Nanoreactors*", 34th Annual Conference of Bangladesh Chemical Society, Dhaka, Bangladesh, 19-20 December, 2011 (Oral presentation)

2. **Ummul Khair Fatema**, M. Muhibur Rahman, Md. Yousuf Ali Mollah, Md. Abu Bin Hasan Susan, "*Particle Size and Stability of Copper Nanoparticles Prepared in Reverse Microemulsions*" 35th Annual Conference of Bangladesh Chemical Society, Dhaka, Bangladesh, 07-09 December, 2012 (Oral presentation)

3. **Ummul Khair Fatema**, M. Muhibur Rahman, Md. Yousuf Ali Mollah, Md. Abu Bin Hasan Susan, "*Microemulsions as Nanoreactors for Size-Controlled Synthesis of Metallic Nanoparticles for Biomedical Applications*" International Workshop on Nanotechnology, Dhaka, Bangladesh 21-23 September 2012 (Poster presentation)

4. **Ummul Khair Fatema**, M. Muhibur Rahman, Md. Yousuf Ali Mollah, Md. Abu Bin Hasan Susan, "*Role of Surfactants and Cosurfactants on Synthesis of Copper Nanoparticle in Water-in-Oil Microemulsion*" Bose Conference, Dhaka, Bangladesh, 2013 (Poster presentation)

5. **Ummul Khair Fatema**, M. Muhibur Rahman, Md. Yousuf Ali Mollah, Md. Abu Bin Hasan Susan, "*Size Controlled Synthesis of Copper Nanoparticles in Water in Oil Microemulsions*" 2nd Conference of Bangladesh Crystallographic Association, Dhaka, Bangladesh, 10 January 2015 (Oral presentation)

6. **Ummul Khair Fatema**, M. Muhibur Rahman, Md. Yousuf Ali Mollah, Md. Abu Bin Hasan Susan, "*Preparation of Silver-Poly(vinyl alcohol) Nanocomposite Film Using Water in Oil Microemulsions*" 37th Annual Conference of Bangladesh Chemical Society, Comilla, Bangladesh, 11 April 2015 (Oral presentation)

7. **Ummul Khair Fatema**, M. Muhibur Rahman, Md. Yousuf Ali Mollah, Md. Abu Bin Hasan Susan, "*Preparation of Polyaniline/Silver Nanocomposites Using Water in Oil Microemulsions as Potent Antibacterial Agent*" 2nd International Bose Conference, Dhaka, Bangladesh, 3-4 December 2015, (Oral presentation)

8. **Ummul Khair Fatema**, M. Muhibur Rahman, Md. Yousuf Ali Mollah, Md. Abu Bin Hasan Susan, *"Metal Nanoparticles and their Polymer Composites with Controllable Dimension from Water in Oil Microemulsions for Biomedical Applications*" 8th HOPE Meeting with Nobel Laureates, Tsukuba, Japan, 7-11 March, 2016 (Poster presentation)

9. **Ummul Khair Fatema**, M. Muhibur Rahman, Md. Yousuf Ali Mollah, Md. Abu Bin Hasan Susan, "*Preparation of Silver-Poly(vinyl alcohol) Nanocomposite Film using Water in Oil Microemulsions for Wound Dressing*" 16th Asian Chemical Congress, Dhaka, Bangladesh, 16-19 March, 2016 (Oral presentation)

List of workshops attended

1. Preparation and Characterization of Novel Functional Materials with Emphasis on Electrochemistry, Dhaka, Bangladesh, 12 February, 2012.

2. Black Carbon Emission from Brick Kilns in Bangladesh, Department of Chemistry, University of Dhaka, 16 November, 2014.